

# UNCLASSIFIED

AD NUMBER
AD865316
NEW LIMITATION CHANGE
TO Approved for public release, distribution unlimited
FROM Distribution authorized to U.S. Gov't. agencies and their contractors; Administrative/Operational Use; Dec 1969. Other requests shall be referred to Air Force Materials Lab., Attn: MAMC, Wright-Patterson AFB, OH 45433.
AUTHORITY
AFML ltr, 13 Sep 1972

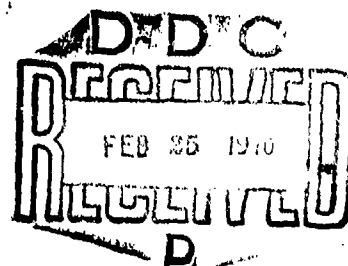
THIS PAGE IS UNCLASSIFIED

AFML-TR-69-84  
PART II. VOLUME III

**STABILITY CHARACTERIZATION OF  
REFRACTORY MATERIALS UNDER HIGH  
VELOCITY ATMOSPHERIC FLIGHT  
CONDITIONS**

**PART II. VOLUME III: FACILITIES AND TECHNIQUES  
EMPLOYED FOR HOT GAS/COLD WALL TESTS**

LARRY KAUFMAN  
HARVEY NESOR  
*ManLabs, Inc*



TECHNICAL REPORT AFML-TR-69-84, PART II, VOLUME III

DECEMBER 1969

This document is subject to special export controls and each transmittal to foreign governments or foreign nationals may be made only with prior approval of the Air Force Materials Laboratory (MAMC), Wright-Patterson Air Force Base, Ohio 45433.

Reproduced by the  
CLEARINGHOUSE  
for Federal Scientific & Technical  
Information Springfield Va. 22151

**AIR FORCE MATERIALS LABORATORY  
AIR FORCE SYSTEMS COMMAND  
WRIGHT-PATTERSON AIR FORCE BASE, OHIO**

AD 865316

## NOTICE

When Government drawings, specifications, or other data are used for any purpose other than in connection with a definitely related Government procurement operation, the United States Government thereby incurs no responsibility nor any obligation whatsoever; and the fact that the government may have formulated, furnished, or in any way supplied the said drawings, specifications, or other data, is not to be regarded by implication or otherwise as in any manner licensing the holder or any other person or corporation, or conveying any rights or permission to manufacture, use, or sell any patented invention that may in any way be related hereto.

This document is subject to special export controls and each transmittal to foreign governments or foreign nationals may be made only with prior approval of the Air Force Materials Laboratory MAMC, Wright Patterson Air Force Base, Ohio 45433.

The distribution of this report is limited for the protection of technology relating to critical materials restricted by the Export Control Act.

ACCESSION NO.	
CLASS	UNCLASSIFIED <input type="checkbox"/>
CONTROL	EXCLUDED <input checked="" type="checkbox"/>
REVIEWED	<input type="checkbox"/>
DATE REVIEWED	
REVIEWED BY	
REVIEWED DATE	
REVIEWED LOCATION	
REVIEWED COMMENTS	
DIST.	APPROV. NO. & INITIAL
2	

Copies of this report should not be returned unless return is required by security considerations, contractual obligations, or notice on a specific document.

**STABILITY CHARACTERIZATION OF  
REFRACTORY MATERIALS UNDER HIGH  
VELOCITY ATMOSPHERIC FLIGHT  
CONDITIONS**

**PART II. VOLUME III: FACILITIES AND TECHNIQUES  
EMPLOYED FOR HOT GAS/COLD WALL TESTS**

*LARRY KAUFMAN*

*HARVEY NESOR*

This document is subject to special export controls and each transmittal to foreign governments or foreign nationals may be made only with prior approval of the Air Force Materials Laboratory (MAMC), Wright-Patterson Air Force Base, Ohio 45433.


## FOREWORD

This report was prepared by ManLabs, Inc. with the assistance of the following subcontractors: Avco SSD, Wilmington, Mass. (H. Hoercher, Project Director supported by J. Recesso, R. Abate and R. Broughton) and Cornell Aeronautical Laboratory (S. Tate, D. Colosimo and K. Graves). This contract was initiated under Project 7312, "Metal Surface Deterioration and Protection", Task 731201, "Metal Surface Protection", and Project 7350, "Refractory Inorganic Nonmetallic Materials", Task Nos. 735001, "Refractory Inorganic Nonmetallic Materials: Non-graphitic", and 735002, "Refractory Inorganic Nonmetallic Materials: Graphitic", under AF33(615)-3859 and was administered by the Metals and Ceramics Divisions of the Air Force Materials Laboratory, Air Force Systems Command, with J.D. Latva, J. Krochmal and N.M. Geyer acting as project engineers.

This report covers the period from April 1966 to July 1969.

ManLabs personnel participating in this study included L. Kaufman, H. Nesor, H. Bernstein, E. Peters, J.R. Baron, G. Stepakoff, R. Pober, R. Hopper, R. Yeaton, S. Wallerstein, E. Sybicki, J. Davis, K. Meaney, K. Ross, J. Dudley, E. Offner, A. Macey, A. Silverman and A. Constantino.

The manuscript of this report was released by the authors in September 1969 for publication. This technical report has been reviewed and is approved.

  
W. G. Ramke  
Chief, Ceramics and Graphite Branch  
Metals and Ceramics Division  
Air Force Materials Laboratory

The following reports will be issued under this contract.

### Part/Volume

I-I	Summary of Results
II-I	Facilities and Techniques Employed for Characterization of Candidate Materials
II-II	Facilities and Techniques Employed for Cold Gas/Hot Wall Tests
II-III	Facilities and Techniques Employed for Hot Gas/Cold Wall Tests
III-I	Experimental Results of Low Velocity Cold Gas/Hot Wall Tests
III-II	Experimental Results of High Velocity Cold Gas/Hot Wall Tests
III-III	Experimental Results of High Velocity Hot Gas/Cold Wall Tests
IV-I	Theoretical Correlation of Material Performance with Stream Conditions
IV-II	Calculation of the General Surface Reaction Problem

## ABSTRACT

The oxidation of refractory borides, graphites and JT composites, hypereutectic carbide-graphite composites, refractory metals, coated refractory metals, metal oxide composites and iridium coated graphites in air was studied under conditions encountered during high velocity atmospheric flight and in conventional furnace tests. Elucidation of the relationship between hot gas/cold wall (HG/CW) and cold gas/hot wall (CG/HW) surface effects in terms of heat and mass transfer rates at high temperatures was a principal goal. This report deals with facilities and techniques employed for performing HG/CW tests in the Model 500, ROVERS and Ten Megawatt Arc installations at Avco and the Wave Superheater at Cornell. Stagnation pressures between 0.002 and 4.0 atm, stagnation enthalpy between 2000 and 16,000 BTU/lb, coldwall heat flux between 100 and 1500 BTU/ft<sup>2</sup>sec and exposure times between 20 and 23,000 seconds were employed. Diagnostic measurements included continuous recording of surface temperature and radiated heat flux. Color motion picture coverage was also provided. Although most of the testing was performed on flat faced right circular cylinders some hemispherical capped samples and some pipes were also tested.

Heat flux measurements were made in the Model 500 and ROVERS facilities of the variation of heat flux with radial distance across the model. Model size was varied to ascertain the effect of size on the heat flux. Stream diameter was 0.60 inches and 2.25-3.00 inches in the Model 500 and ROVERS facilities, respectively. Calorimeters with diameters of 0.125 to 0.750 inches were employed with 0.500 and 1.500 inch diameter shrouds. The Model 500 results were described by a +10% band independent of diameter. The heat flux showed a peak near a diameter of 0.375 inches.

The heat flux was independent of calorimeter radius in the ROVERS facility. The heat flux observed with a 0.500 inch diameter shroud was larger than observed with a 1.500 inch shroud. However, while the expected ratio is  $\sqrt{3}$  or 1.73, the observed ratio was about 1.20. The values obtained for the 0.500 inch diameter shrouded calorimeter were about 10% higher than the values predicted on the basis of a Fay-Riddell calculation, while the 1.500 inch shrouded calorimeter results were 50% higher than that calculated.

In-depth temperature measurements were performed in the Model 500 and ROVERS facilities. A micro-optical pyrometer was employed to measure the temperature at the base of a cavity drilled from the rear of the model to within 0.100 inch of the heated face. For oxide forming materials like ZrB<sub>2</sub> and Hf-Ta-Mo, the temperature at the in-depth station was found to range from 500° to 1900°R lower than the surface temperature.

Sixteen refractory material models were exposed to the high velocity flow of air in the Mach 6 Wave Superheater Hypersonic Tunnel. Data were taken in two 15 second tests of eight models, each at a velocity of 10<sup>4</sup> ft/sec, a stagnation pressure (at the model nose) of one atmosphere and a tunnel flow rate of 2.5 lb/sec. The stagnation enthalpy was 2200 BTU/lb while the cold wall heat flux was 600 BTU/ft<sup>2</sup>sec.

This abstract is subject to special export controls and each transmittal to foreign governments or foreign nationals may be made only with prior approval of the Air Force Materials Laboratory (MAMC), Wright-Patterson Air Force Base, Ohio 45433.

## TABLE OF CONTENTS

Section		Page
I	INTRODUCTION AND SUMMARY . . . . .	1
	A. Introduction . . . . .	1
	B. Summary . . . . .	2
II	HOT GAS/COLD WALL TESTS AT AVCO/SSD . . . . .	5
	A. Introduction . . . . .	5
	B. Testing in the Model 500 Arc . . . . .	5
	1. Description of Facilities . . . . .	5
	2. Calibration Techniques . . . . .	6
	3. Measurement of the Radial Heat Flux Distribu- tion Across the Heated Surface of Flat Face Cylinders in the Model 500 Facility . . . . .	8
	4. Measurement of Temperature Gradients through Oxide Films Formed on Samples During Arc Plasma Exposures in the Model 500 . . . . .	11
	5. Comparison of Heat Flux Measurements with Flat Faced and Hemispherical Capped Calorimeter in the Model 500 Facility . . . . .	13
	C. Testing in the ROVERS Arc . . . . .	14
	1. Description of Facilities . . . . .	14
	2. Calibration of the ROVERS Facility . . . . .	15
	3. Measurement of the Radial Heat Flux Distribu- tion across the Heated Surface of Flat Face Cylinders in the ROVERS Facility . . . . .	16
	4. Measurement of Temperature Gradients through Oxide Films Formed on Samples During Arc Plasma Exposures in the ROVERS Arc . . . . .	18
	5. Comparison of Heat Flux Measurements with Flat Faced and Hemispherical Capped Calori- meters in the ROVERS Facility . . . . .	18
	D. Testing in the Ten Megawatt Arc . . . . .	19
	1. Description of Ten Megawatt Arc Facility . . . . .	19
	2. Calibration of the 10MW Arc Facility. . . . .	20
	3. Pipe Testing in the 10MW Test Facility . . . . .	21
	4. Calibration of the 10MW Supersonic Pipe Test . . . . .	22
	(a) Determination of Gas Enthalpy . . . . .	22
	(b) Determination of Heat Flux . . . . .	23
	(c) Shear Stress and Reynolds Number . . . . .	23

## TABLE OF CONTENTS (CONT)

Section	Page
III	
HOT GAS/COLD WALL TESTS AT THE CORNELL WAVE SUPERHEATER HYPERSONIC TUNNEL . . . . .	25
A. Description of Facilities . . . . .	25
B. Description of Testing Procedures and Instrumentation . . . . .	26
C. Calculation of Surface Temperature and Heat Flux Levels for Test Models . . . . .	28
D. Experimental Evaluation of Conduction Losses for Spherical Shells . . . . .	32
REFERENCES . . . . .	34



## LIST OF ILLUSTRATIONS

Figure		Page
1	Model 500 Plasma Generator (Rear View)	37
2	Model 500 Plasma Generator Control Room	38
3	Zirconium Diboride Cylinder Prior to Exposure in the Avco-SSD Model 500 Arc Plasma Facility	39
4	Zirconium Diboride Cylinder Prior to Exposure in the Avco-SSD Model 500 Arc Plasma Facility	40
5	Zirconium Diboride Cylinder During Exposure in the Avco-SSD Model 500 Arc Plasma Facility	41
6	Basic Experimental Setup (Model 500 Plasma Generator)	42
7	Model 500 Plasma Generator (Right-Rear View)	43
8	Specimen Mounted in the Model 500 Facility	44
9	Constant Flow Water Calorimeter	45
10	Avco Calorimeter Installation - Model 500 Facility	46
11	Avco Calorimeter During Test in the Model 500	47
12	Comparison of Cold Wall Heat Fluxes to Avco Water Cooled Calorimeters Having 1/2 and 3/4 Inch Diameters Enclosed in 1-1/2 Inch Diameter Shields in the Model 500 Arc.	48
13	Stagnation Pressure Probe Mounted in Test Position in the Model 500	49
14	Stagnation Pressure Probe During Test in the Model 500	50
15	Specimen No. HfB <sub>2</sub> + SiC(A-4) A-4-24M During Test in the Model 500	51
16	Close-up View of Specimen No. HfB <sub>2</sub> + SiC(A-4) A-4-2-4M During Test in the Model 500	52
17	Cross-Sectional View of the Transient Calorimeter	53
18	Cross-Sectional View of the Steady State Calorimeter	54
19	Test Sample Being Exposed in the Model 500 Arc	55

# LIST OF ILLUSTRATIONS (CONT)

Figure		Page
20	Transient Calorimeter (0.500 inch diameter shroud) Measurement of Heat Flux in the Model 500	56
21	Transient Calorimeters, Shrouds and Conical Sections	57
22	Transient Calorimeter (0.125 inch Diameter)	58
23	Calorimeters Mounted on Remote Controlled Stings in the Model 500	59
24	Calorimeters Mounted on Remote Controlled Stings	60
25	Transient Calorimeter with 1.500 Inch Diameter Shroud During Test in the Model 500 Arc	61
26	Transient Calorimeter Measurement of Heat Flux as a Function of Time in the Model 500 Arc	62
27	Ratio of Heat Transfer Coefficients as a Function of Calorimeter Diameter and Shroud Diameter in the Model 500 Arc	63
28	Comparison of Heat Fluxes Measured with 0.500 Inch Diameter and 0.750 Inch Diameter Calorimeters in 1.500 Inch Shrouds in the Model 500 Arc	64
29	Effect of Calorimeter Diameter and Shroud Size on Heat Flux in the Model 500 Facility	65
30	Cross-Sectional View of the Model Holder for In-Depth Temperature Measurements in the Model 500 Arc	66
31	Water Cooled Model Holder and Test Sample Employed for Measurement of Internal Temperature Gradients in the Model 500 Arc	67
32	Experimental Arrangement for Measurement of Internal Temperature Gradients in the Model 500 Arc	68
33	Side View of Sample $ZrB_2(A-3)-2MC$ During Exposure in the Model 500 Arc	69
34	Post Exposure Photographs of Samples $ZrB_2(A-3)-1MC$ , 2MC, 3MC and 4MC after Testing in the Model 500 Arc	70
35	Post Exposure Photographs of Samples $Hf-Ta-Mo(I-23)-$ 1MC, 2MC, 3MC and 4MC after Testing in the Model 500 Arc	71

# LIST OF ILLUSTRATIONS (CONT)

Figure		Page
36	Time-Temperature History for Surface Temperature and In-Depth Temperature (100 mils from surface) for Sample Hf-Ta-Mo (I-23)-3MC	72
37	Arc Plasma Test $ZrB_2$ (A-3)-2MC	73
38	Arc Plasma Test Hf-20Ta-2Mo(I-23)-1MC	73
39	Hemispherical Tip Transient Calorimeter	74
40	Comparison of Heat Flux Measurements with a 0.125 Inch Diameter Calorimeter in a 0.500 Inch Diameter Hemispherical Shroud ( $q_H$ ) and a 0.500 Inch Diameter Calorimeter in a 1.500 Inch Diameter Flat Faced Shroud ( $q_{FF}$ ) in the Model 500 Facility	75
41	Sectional View of ROVERS Facility	76
42	ROVERS Arc Facility	77
43	ROVERS Arc Facility Operating (View from Control Room)	78
44	RVA Graphite Cylinder Prior to Exposure in the Avco-SSD ROVERS Facility	79
45	RVA Graphite Cylinder During Exposure in the Avco-SSD ROVERS Facility	80
46	Water Calorimeter Mounted in Test Position in ROVERS Arc	81
47	Transients Calorimeter with 3.5, 1.0 and 0.5 Inch Shields	82
48	Comparison of Cold Wall Heat Fluxes to a 3/8 Inch Diameter Transient Calorimeter in a 1/2 Inch Shroud and a 5/8 Inch Diameter Water Calorimeter in a 1-1/2 Inch Shroud in the Avco ROVERS Facility	83
49	Transient Calorimeters Mounted on Remotely Controlled Stings	84
50	Ratio of Transient Calorimeter Heat Flux to Water Calorimeter Heat Flux (0.625 inch Diameter - 1.500 inch Shroud) as a Function of Transient Calorimeter Diameter in the Low Pressure ROVERS Arc at Mach 3.2	85

# LIST OF ILLUSTRATIONS (CONT)

Figure		Page
51	Ratio of Transient Calorimeter Heat Flux to Water Calorimeter Heat Flux (0.625 Inch Diameter - 1,500 Inch Shroud) as a Function of Transient Calorimeter Diameter in the High Pressure ROVERS Arc at Mach 3.2	86
52	Comparison of Transient and Water Calorimeter Measurements of Heat Flux in the ROVERS Arc at Mach 3.2	87
53	ManLabs Hemispherical Model in Testing Position	88
54	ManLabs Specimen Being Tested with Holder for Observing Backface Temperatures	89
55	Comparison of the Ratio $q_T$ (heat flux measured with a 0.250 inch Diameter Transient Calorimeter) to $q_W$ (heat Flux measured with a 0.625 inch Water Calorimeter in a 1.50 inch Diameter Shroud)	90
56	The 1.0 and Unassembled 0.5 Inch Hemispherical Calorimeter	91
57	Comparison of Heat Flux Measurements Performed in ROVERS Arc at Mach 2.2 (Stream Diameter 0.750 Inches) Employing Flat Faced and Hemispherical Models	92
58	Overall View of the Ten Megawatt Arc Test Cell	93
59	Avco-SSD Ten Megawatt Arc Plenum Chamber and Arc Head Configuration	94
60	Schematic View of Ten Megawatt Arc Splash Test	95
61	Pre-Test View of ManLabs Test Sample in Ten Megawatt Arc	96
62	ManLabs Test Sample During Exposure in Ten Megawatt Arc Facility	97
63	Post Test View of Sample Tested in Ten Megawatt Arc Facility	98
64	Supersonic Pipe Test Configuration	99
65	Experimental Configuration for Supersonic Pipe Ablation Tests	100
66	Supersonic Pipe Holder and Test Samples Prior to Assembly	101

## LIST OF ILLUSTRATIONS (CONT)

Figure		Page
67	Ten Megawatt Arc Facility Flow Parameters	102
68	Supersonic Pipe Calorimeter Containing Two Pressure Sensors and Two Heat Flux Calorimeters	103
69	CAL Wave Superheater Rotor and Nozzle	104
70	CAL Wave Superheater Hypersonic Tunnel	105
71	Tungsten and HfC-C 15° Cone Models Tested in Cornell Wave Superheater	106
72	Details of Specimen Holders Employed in Wave Superheater Tests	107
73	Orientation of Calorimeter and Models in Wave Superheater Exposures	108
74	Calorimeter Time-Temperature History	109
75	Calculated Heat Flux as a Function of Wall Temperature for a One-Half Inch Diameter Hemispherical Cap Shell of Zirconium Diboride One-Eighth Inch Thick in the Mach 6 Test Section of the Cornell Wave Superheater	110
76	Calculated Wall Temperature as a Function of Time for a One Inch and a One-Half Inch Diameter Hemispherical Cap Shell of Zirconium Diboride One-Eighth Inch Thick in the Mach 6 Test Section of the Cornell Wave Superheater	111
77	Geometrical Definitions for Analysis of Conduction Losses Through a Hemispherical Shell	112
78	Temperature Response for Hemispherical Shells of 1020 Steel Exposed under Flux-Conductivity Conditions to Simulated Wave Superheater Tests	112

## LIST OF TABLES

Table		Page
1	Test Conditions and Heat Flux Measurements	113
2	Normalized Comparison of Radial Heat Flux Distribution in the Model 500 Facility	114
3	Summary of Test Conditions for Samples Used for Temperature Gradient Studies	115
4	Summary of In Depth Temperature Measurements	116
5	ROVERS Arc Facility - Calorimeter Data at Mach 3.2	117
6	Characteristic Operating Conditions in the CAL Wave Superheater	118
7	Heat Transfer Results	119
8	Test Conditions	120
9	Wall Temperature and Heat Flux History for the Stagnation Point of a 0.500-Inch Radius Hemispherical Nose with a Thickness of 0.125 Inch	121
10	Wall Temperature and Heat Flux History for the Stagnation Point of a 0.250-Inch Radius Hemispherical Nose with a Thickness of 0.125 Inch	122

## I. INTRODUCTION AND SUMMARY

### A. Introduction

The response of refractory materials to high temperature oxidizing conditions imposed by furnace heating has been observed to differ markedly from the behavior in arc plasma "reentry simulators."

The former evaluations are normally performed for long times at fixed temperatures and slow gas flows with well-defined solid/gas-reactant/product chemistry. The latter on the other hand are usually carried out under high velocity gas flow conditions in which the energy flux rather than the temperature is defined and significant shear forces can be encountered. Consequently, the differences in philosophy, observables, and techniques used in the "material centered" regime and the "environment centered, reentry simulation" area differ so significantly as to render correlation of material responses at high and low speeds difficult if not impossible in many cases. Under these circumstances, expeditious utilization of the vast background of information available in either area for optimum matching of existing material systems with specific missions or prediction and synthesis of advanced material systems to meet requirements of projected missions is sharply curtailed.

In order to progress toward the elimination of this gap, an integrated study of the response of refractory materials to oxidation in air over a wide range of time, gas velocity, temperature and pressure has been designed and implemented. This interdisciplinary study spans the heat flux and boundary layer-shear spectrum of conditions encountered during high-velocity atmospheric flight as well as conditions normally employed in conventional materials centered investigations. In this context, significant efforts have been directed toward elucidating the relationship between hot gas/cold wall (HG/CW) and cold gas/hot wall (CG/HW) surface effects in terms of heat and mass transfer rates at high temperatures, so that full utilization of both types of experimental data can be made.

The principal goal of this study was the coupling of the material-centered and environment-centered philosophies in order to gain a better insight into systems behavior under high-speed atmospheric flight conditions. This coupling function has been provided by an interdisciplinary panel composed of scientists representing the component philosophies. The coupling framework consists of an intimate mixture of theoretical and experimental studies specifically designed to overlap temperature/energy and pressure/velocity conditions. This overlap has provided a means for the evaluation of test techniques and the performance of specific materials systems under a wide range of flight conditions. In addition, it provides a base for developing an integrated theory or *modus operandi* capable of translating reentry systems requirements such as velocity, altitude,

configuration and lifetime into requisite materials properties as vaporization rates, oxidation kinetics, density, etc., over a wide range of conditions.

The correlation of heat flux, stagnation enthalpy, Mach No., stagnation pressure and specimen geometry with surface temperature through the utilization of thermodynamic, thermal and radiational properties of the material and environmental systems used in this study was of prime importance in defining the conditions for overlap between materials-centered and environment-centered tests.

Significant practical as well as fundamental progress along the above mentioned lines necessitated evaluation of refractory material systems which exhibit varying gradations of stability above 2700°F. Emphasis was placed on candidates for 3400° to 6000°F exploitation. Thus, borides, carbides, boride-graphite composite (JTA), JT composites, carbide-graphite composites, pyrolytic and bulk graphite, PT graphite, coated refractory metals/alloys, oxide-metal composites, oxidation resistant refractory metal alloys and iridium-coated graphites were considered. Similarly, a range of test facilities and techniques including oxygen pick-up measurements, cold sample/hot gas and hot sample/cold gas devices at low velocities, as well as different arc plasma facilities capable of covering the 50-1500 BTU/ft<sup>2</sup>sec flux range under conditions equivalent to speeds up to Mach 12 at altitudes up to 200,000 feet were employed. Stagnation pressures were used covering the range between 0.001 and 10 atmospheres. Splash and pipe tests were performed in order to evaluate the effects of aerodynamic shear. Based on the present results, this range of heat flux and stagnation enthalpy produced surface temperatures between 2000° and 6500°F. The present report describes the facilities and techniques employed for performing the HG/CW tests.

## **B. Summary**

Exposures were performed in the Model 500, ROVERS and Ten Megawatt Arc Facilities at Avco/SSD. The range of conditions employed in these tests covered stagnation pressures between 0.002 and 4.0 atm., stagnation enthalpy between 2000 and 16,000 BTU/lb, cold wall heat flux between 100 and 1500 BTU/ft<sup>2</sup>sec and exposure times between 20 and 23,000 seconds. Diagnostic measurements included continuous recording of surface temperature and radiated heat flux as well as color motion picture footage. Measurements of in-depth temperatures were reported for selected models. Although most of the testing was performed on flat faced right circular cylinders some hemispherical capped samples and some pipes were tested as well.

Characterization of the test environment was performed prior to each test by measuring stagnation pressure, stagnation enthalpy and cold wall heat flux. These measurements were performed by means of water cooled probes, energy balance measurements, and transient and steady state calorimetry. The heat flux calorimeters were of the same geometrical configuration as the test models. Measurements of surface brightness temperature at  $\lambda = 0.65$  microns were carried out employing an IDL recording pyrometer while an Eppley thermopile was used to monitor total radiated heat flux. Brightness temperatures were converted to true temperature by employing suitable emittance values, while the radiated heat flux data were employed to compute total normal emittance. Selected measurements



of surface temperature were performed by means of two color pyrometry in order to confirm the brightness temperature measurements with good results.

A series of heat flux measurements were performed in the Model 500 and ROVERS facilities using a calorimeter of fixed outer diameter to disclose the variation of heat flux with radial distance across the surface of the calorimeter. In addition, the outside diameter of the calorimeter was varied in order to ascertain the effect of overall size on the heat flux. The stream diameter was 0.60 inches and 2.25-3.00 inches in the Model 500 and ROVERS facilities respectively. Transient and steady state calorimeters were employed to measure the heat flux. These calorimeters were 0.125, 0.250, 0.375, 0.450, 0.500 and 0.750 inches in diameter. In addition, the shroud diameters were 0.500 and 1.500 inches.

The results of these calibration studies in the Model 500 showed that most of the measurements could be described by a  $\pm 10\%$  band independent of diameter. A peak was noted near a diameter corresponding to 0.375 inches. In addition, slightly lower heat flux levels were noted with the 1.500 inch shrouds than in the cases where 0.500 inch shrouds were employed. The explanation of this result is not evident in view of the 0.600 inch diameter stream.

The heat flux dependence on calorimeter radius in the ROVERS facility showed that most of the data fell within the  $\pm 10\%$  band independent of calorimeter size. As expected, the heat flux observed with a 0.500 inch diameter shroud was larger than observed with a 1.500 inch shroud. However, while the expected ratio is  $\sqrt{3}$  or 1.73, the observed ratio was about 1.20. The values obtained for the 0.500 inch diameter shrouded calorimeter were about 10% higher than the values predicted on the basis of a Fay-Riddell calculation. However, the results obtained with the 1.500 inch shrouded calorimeters were 50% higher than that calculated on the basis of Fay-Riddell. Since the stream was 2.25 to 3.00 inches in diameter in the ROVERS tests, the agreement between the computed and observed results for the 0.500 inch shroud tests is encouraging. At the same time, it is not clear why the tests of 1.500 inch shrouded calorimeters yielded such high heat flux results.

Experiments were performed in the Model 500 in order to determine the in-depth temperatures of test materials. A micro-optical pyrometer was employed to measure the temperature at the base of a cavity drilled from the rear of the model to within 0.100 inch of the heated face. For oxide forming materials like  $ZrB_2$  and Hf-Ta-Mo, the temperature at the in-depth station was found to range from 500 to 1900°R lower than the surface temperature. In order to determine the surface temperature, the heated face of the sample was continuously monitored during the test interval with a recording pyrometer operating at a wavelength of 0.65 microns. Corrections for spectral emittance allow the conversion of measured brightness temperatures into true temperatures. In some cases, a heavy oxide deposit forms on the heated surface, while the remainder of the test sample is essentially in the virgin state. Since the surface temperature is measured in the area of the oxide deposit, there is some question concerning the temperature distribution behind the deposit. A steep temperature gradient may result if the oxide layer acts as an insulator, thus restricting the flow of energy into the sample.

The current tests in the Ten Megawatt Arc Facility consisted of exhausting a supersonic arc jet onto a splash or pipe model held in graphite fixtures. Heat flux, stagnation pressure and enthalpy were determined for each exposure. Continuous measurements of surface temperature and recorded color motion pictures were also made for each test. Test time was limited to twenty seconds.

Sixteen refractory material models were exposed to the high velocity flow of air in the Mach 6 Wave Superheater Hypersonic Tunnel. Data were taken in two 15 second tests of eight models, each at a velocity of  $10^4$  ft/sec., a stagnation pressure (at the model nose) of one atmosphere, and a tunnel flow rate of 2.5 lb/sec. The models were designed to permit their surface temperature to approach the radiation/aerodynamic heating equilibrium value during each exposure to the test stream at  $q(R)^{1/2} = 90$  BTU/ft<sup>3/2</sup> sec. Temperatures in excess of 4000°R were expected from all models. The models were returned to ManLabs for post exposure analysis. All sixteen models tested were hollow hemispheric cylinders. The "elox" process was used to bore from the aft end to provide a uniform material thickness which was nominally 1/8 inch. The diameter of the bore was a nominal 1/4 inch for the thirteen 1/4 inch nose radius models and 3/4 inch for the three 1/2 inch nose radius models. The purpose of the shell or "thimble" design was to promote faster wall temperature response so as to approach the radiation equilibrium wall temperature as rapidly as possible. Eight models and a single 1/4 inch nose radius steady-heating copper calorimeter were mounted in the tunnel by a multiple sting arrangement.

The test conditions which exist in the Wave Superheater Hypersonic Tunnel are tractable throughout a test by virtue of a computer program which interprets the recorded (pressure and temperature) time histories of the supply gases. As determined by this data reduction, the test conditions are not instantaneously established but exhibit a transient of about six-tenths second duration. The transient is terminated by a twenty to thirty millisecond step change to the final test conditions. Both the stream reservoir pressure and enthalpy undergo this transient in a manner that produces a stream heating capacity during the plateau portion of the transient of 85% of the value appropriate for the steady state test conditions. The heat transfer rate to the 1/4 inch spherical nose radius calorimeter measured during the transient was about 500 BTU/ft<sup>2</sup>sec. Because this is 85% of the value for the test, the steady state value is in agreement with the intended 600 BTU/ft<sup>2</sup>sec. Calorimeters used in the Wave Superheater facility are normally expected to burn out. The gage life was greater than one second. Although the gage was too hot after the transient to obtain quantitative heat transfer data, the recorded temperature signal from the calorimeter is very smooth, precise, and clearly represents the 600 BTU/ft<sup>2</sup>sec level.

An analysis of the surface temperature response of these models allowing for convective heating and losses via radiation and conduction is presented in order to evaluate the effects of wall thickness on the temperature response of hemispherical shells.

## II. HOT GAS/COLD WALL TESTS AT AVCO/SSD

### A. Introduction

Hot Gas/Cold Wall oxidation testing was performed at Avco/SSD under the direction of H. Hoercher, J. Reccasso, R. Broughton and R. Abate were actively engaged in performing these tests. Exposures were carried out in the Model 500, ROVERS and Ten Megawatt Arc Facilities. The range of conditions employed in these tests covered stagnation pressures between 0.002 and 4.0 atm, stagnation enthalpy between 2000 and 16,000 BTU/lb, cold wall heat flux between 100 and 1500 BTU/ft<sup>2</sup>sec and exposure times between 20 seconds and 23,000 seconds. A full spectrum of diagnostic measurements including surface temperature and radiated heat flux was continuously monitored during the exposures. Complete color film coverage was reported for selected models. The following sections describe the facilities, calibration techniques for characterizing the level and distribution of stream parameters, as well as the material characterization measurements. Although most of the exposures were splash tests conducted on flat faced right circular cylinders, some testing of hemispherical capped samples and some pipe tests were carried out.

### B. Testing in the Model 500 Arc

#### 1. Description of Facilities

The Avco Model 500 Plasma Generator is employed as a heat source to evaluate the hyperthermal properties of materials. The basic parts of the arc apparatus are the anode and cathode. Air is heated to a high temperature by passing it through an electrical arc discharge between the anode and cathode. The gas is injected tangentially into a chamber and flows through the region occupied by the arc discharge, momentarily becomes part of the discharge, and then flows through a plenum or mixing chamber where initial inhomogenities in temperature and velocity are dampened. Finally, the plasma passes out of the system, into the laboratory atmosphere, through a 1/2 inch diameter subsonic exit nozzle. Material evaluations are obtained by subjecting test specimens to the precalibrated plasma at a point 1 inch downstream from the nozzle exit plane. An overall view taken from the rear of the plasma generator is presented in Figure 1. Figure 2 is a view taken from the control room showing the test cell in the background.

Figures 3 through 5 show the Model 500 holder and a ZrB<sub>2</sub> test cylinder. The water cooled copper holder shown in Figure 3 is fitted with a threaded tungsten adapter rod which fits into a 1/4 inch diameter hole recessed in the back of the specimen cylinder. Figure 4 shows the holder in the Model 500, while Figure 5 is a photograph of a subsonic exposure.

A schematic showing the basic experimental setup is presented in Figure 6. A photograph taken from the right-rear of the plasma generator is shown in Figure 7 with the recording pyrometer in the lower right and the front surface camera visible slightly above. The 35 mm ablation camera is visible on the extreme left side. The Eppley thermopile and mirror stop can be seen in the center foreground of Figure 8.

## 2. Calibration Techniques

A test environment can be characterized by values of stagnation pressure and stagnation enthalpy for suitably uniform parallel test streams of relatively large extent. In practice, the following quantities are determined by the characteristics of the stream: (a) heat flux to the surface and (b) shear stress at the surface. The calibration of the plasma then consists of the determination of these parameters.

The enthalpy of the plasma is determined from a simple energy balance using Eq. 1

$$i_e = \frac{0.948 (P_{in} - P_{loss})}{\dot{M}} = \frac{0.948 P_{net}}{\dot{M}} \quad (1)$$

where  $i_e$  = stagnation enthalpy of the plasma (BTU/lb),  $P_{in}$  = power input to arc, volts x amps (KW),  $P_{loss}$  = power loss to cooling system, determined from measurements of cooling water mass flow and temperature rise (KW),  $P_{net}$  = net power delivered to the gas (KW) and  $\dot{M}$  = gas mass flow rate (lb/sec).

With suitable empirical choice of power input to the arc, power loss to the cooling system\* and gas mass flow rate, gas (air) enthalpies can be generated over a range of 400 to 12,000 BTU/lb.

Steady-state measurements of laminar heat transfer from the plasma jet to a flat surface are made with a constant-flow water calorimeter constructed of copper. Figure 9 is a schematic of the Avco calorimeter assembly. Measured heat transfer occurs through the central circular area, the diameter of which usually matches the test specimen diameter. The 1-1/2 inch diameter water-cooled annular guard ring (shield) surrounding the sensor prevents heat transfer to the sides of the calorimeter in order to insure one-dimensional heating. Heat transfer rates to flat faced cylinders cover the range of 30 to 1300 BTU/ft<sup>2</sup>sec over the test enthalpy range noted above.

A view of the Avco calorimeter with no plasma flow is shown in Figure 10 and Figure 11, illustrating the calorimeter immersed in the plasma jet.

---

\* Power loss to the cooling system is increased by lengthening the plenum section. This results in more energy transfer to the plenum wall.

Normally, the diameter of the sensor portion of the Avco calorimeter assembly is chosen to match the test specimen diameter in order to simulate the interaction of the plasma with the specimen. However, a 3/4 inch diameter calorimeter sensor was employed in most of the ManLabs testing (1/2 inch diameter specimens) in order to be consistent with previously established test methods. Experiments have been performed in order to determine the relationship between the 3/4 inch and 1/2 inch diameter calorimeter sensors (both installed in 1-1/2 inch diameter shields) when exposed to the Model 500 plasma. As expected, due to the radial decay in jet impingement heating, the 1/2 inch diameter calorimeter yielded 14 to 37 percent higher heating rates over the heat flux range employed. The results of the experiments are presented in Figure 12.

Stagnation pressure measurements are obtained by inserting a water-cooled probe into the plasma. Impact pressure measurements taken on the arc axis at a point 1 inch downstream from the nozzle exit plane have been found to agree with arc plenum pressure measurements. A view of the pressure probe with no plasma flow is shown in Figure 13. Figure 14 shows the probe immersed in the plasma jet.

In addition to the plasma calibration, the following data is obtained in order to characterize and evaluate materials. Both profile and front surface motion pictures can be taken of the test specimen during the ablative process. The front surface motion pictures are obtained with a 16 mm Bell and Howell camera (adjustable framing rate). The silhouette photographs used for determining the specimen ablative velocity are obtained using a 35 mm Flight Research Laboratory camera (adjustable framing rate). Total radiation measurements reported were made with a single junction Eppley thermopile. Surface brightness temperature is measured with an Instrument Development Laboratories (IDL) recording pyrometer\*. If a sample is instrumented, all electrical outputs can be simultaneously recorded on magnetic tape and on a Consolidated Electro-Dynamics Corp. (CEC) oscillograph.

Initial power setting and gas mass flow rate to the arc are selected in order to generate a particular enthalpy, heat flux and jet Mach No. environment. In the case of the present testing program, the environment is selected to yield the desired specimen surface temperature.

The plasma is probed with diagnostic instruments (stagnation pressure and heat flux probes) immediately prior to insertion of the test specimen. All plasma calibration data (net power, plenum pressure and mass flow) and material characterization data (total radiation, surface temperature and front surface motion pictures) are continuously recorded throughout the test interval.

---

\* Operating at  $\lambda = 0.65\mu$ .

A test specimen is shown installed in testing position in Figure 8. Figures 15 and 16 are specimen photographs of a sample of  $\text{HfB}_2 + \text{SiC}$ (A-4) obtained during an 1830 second exposure at Mach 0.38. The stagnation pressure and enthalpy were one atmosphere and 5565 BTU/lb respectively. The one half inch diameter sample was exposed to a cold wall heat flux of 915 BTU/ft<sup>2</sup>sec and a surface temperature of 5200°F was attained. The total recession during the 1830 second exposure was 188 mils.

In addition to these measurements, two-color pyrometer measurements were performed during the course of exposures:  $\text{HfB}_2 + \text{SiC}$ (A-4)-2M, PG(B-6)-9M, BPG(B-7)-6M, JTA(D-13)-2M,  $\text{HfB}_2 + 35\% \text{SiC}$ (a-9)-6M and Si/RVC(B-8)-13M. The results agreed with the measured brightness temperatures and the average spectral emittance values at  $\lambda = 0.65\mu$ . A final check of temperature measurements was obtained by melting molybdenum (melting point = 5220°R,  $\epsilon = 0.30$  at  $\lambda = 0.65$ ) and tungsten (melting point = 6570°R,  $\epsilon = 0.41$  at  $\lambda = 0.65$ ) in nitrogen streams in both the Model 500 and ROVERS. Both sets of melting point measurements (5250° + 30°R-Model 500, 5190° + 30°R-ROVERS for molybdenum and 6850° + 110°R-Model 500, 6710° + 70°R-ROVERS for tungsten) agree well with the accepted values.

Experiments were performed in the Model 500-5 Plasma Generator Facility in order to determine heat flux distributions across the heated surface of flat faced specimens. Results are presented for five (5) transient calorimeters, diameters ranging from 0.125 to 0.500 inches, and two (2) steady-state calorimeters, 0.500 and 0.750 inch diameters. In order to test materials in the Model 500-5 Plasma Generator Facility (Model 500 Arc), a cylindrical sample having a diameter of 0.500 inch is placed into a 0.600 inch diameter subsonic jet. The heat flux to this sample is normally measured using a steady-state, water cooled calorimeter which has a diameter of 0.500 inch and is centrally located in a water cooled shroud having a diameter of 1.50 inches. The purpose of the described study is to determine the heat flux distribution across the heated surface of calorimeters having different diameters but constant shroud diameters. In this manner, heat flux distributions can be determined and applied to sample tests. In addition, the effect of shroud diameter on local heat transfer rates can be ascertained.

Transient and steady-state calorimeters were tested at two discrete levels of enthalpy and heat flux in the Model 500 Arc. The transient calorimeter assembly (Figure 17) was designed to simulate the plasma interaction with a specimen 1.00 inch long and 0.500 inch in diameter mounted on a conical sting. Hopefully, this method would provide an accurate measurement of the heat flux distribution across the front face of the test specimen. A 1.500 inch diameter shroud section was employed in those tests where it was desired to obtain the effect of a large shroud diameter on heat transfer to the calorimeter and a comparison between the transient and steady-state calorimeter shown in Figure 18. A typical test specimen of the geometry described above is presented during a test exposure in Figure 19. Figure 20 shows one of the current transient calorimeter tests. Pictorial views of the transient calorimeter assemblies are presented in Figures 21 and 22.

Heat flux measurements obtained with the steady-state, constant-flow water calorimeter are based on measurements of water mass flow rate ( $\dot{M}$ ) and temperature rise ( $\Delta T$ ). Measured heat transfer occurs through the central circular area (see Figure 18), the diameter of which is selected to coincide with the test specimen diameter. The 1.500 inch diameter water-cooled shroud surrounding the sensor insures a one-dimensional heat path to the sensor. Usually the calorimeter is exposed to the plasma jet for periods of up to 60 seconds. After a transient period of approximately 15 seconds, the coolant temperature rise ( $\Delta T$ ) reaches a constant level. Solution of the equation  $q = \dot{M} C_p \Delta T$  yields the measured heat flux rate (where  $C_p$  is the specific heat of water).

Heat flux measurements obtained with the transient calorimeter are determined by measurements of front face temperature as a function of time. The transient calorimeter consists of a cylindrical copper body instrumented with a single chromel-alumel thermocouple sensor (see Figure 17). Placement of the thermocouple sensor (hot junction) within the copper body causes the internal temperature distribution to differ from that obtained in the absence of the thermocouple. Implanting the thermocouple at a particular location (null point) in the copper body results in a device which indicates the undisturbed surface temperature (1-6)\* of the copper slug. Thermocouple outputs (time-temperature histories) were simultaneously recorded on a multi-channel CEC oscillograph and magnetic tape. The results were then digitized at the rate of 40 samples per second and fed into a computer program for solution of the one-dimensional differential equation for heat conduction:

$$\frac{\partial}{\partial x} \left( k \frac{\partial T}{\partial x} \right) = \rho C_p \frac{\partial T}{\partial x} \quad (2)$$

To insure one dimensionality, the calorimeter is insulated from the body holder in which it is installed by a small clearance (0.001 inch) along the sides and by a Mica insulator on the rear face of the calorimeter. Therefore, solution of the differential equation for heat conduction with the imposed boundary conditions allows surface heat flux to be determined as a function of time (7). Generally, the transient calorimeters were exposed to the plasma jet for periods of less than 3.5 seconds due to the high heating rates involved.

All test calorimeters were mounted on remote controlled stings to allow insertion or withdrawal from the plasma jet as required. A typical testing sequence involved a power input adjustment to yield the desired heat flux and enthalpy levels followed by a 0.500 inch diameter steady-state calorimeter measurement. The transient calorimeters were then exposed to the plasma in rapid succession followed by a measurement with the 0.750 steady-state calorimeter. In Figure 23, the calorimeters used in Tests 1 and 2 are shown mounted on the remote controlled stings. For Tests 3 through 6, the 0.250 inch and

\* Underscored numbers in parentheses indicate References given at the end of this report.

0.375 inch diameter transient calorimeters were replaced with the 0.450 and 0.500 transient calorimeters. The calorimeters used in Tests 5 and 6 are presented in Figure 24. As shown in Figure 22, the transient calorimeters are fitted with 1.500 inch diameter shrouds. A typical transient calorimeter with a 1.500 inch shroud is presented during a test in Figure 25.

A summary of the test conditions and heat flux measurements is presented in Table 1. The steady-state heat flux measurements given are the constant values that were achieved during 60 second calorimeter exposures. The transient calorimeter data was obtained by curve fitting heat flux as a function of time data points, a typical plot of which is shown in Figure 26. No data was obtained for the 0.500 inch diameter transient calorimeter without the 1.500 shroud attachment, since significant side heating occurred without the shroud and nullified the one-dimensional heating concept. After an initial transient interval (see Figure 26), the transient calorimeters indicated near constant level heat fluxes. A portion of the transient response results when the calorimeter traverses the plasma jet during insertion into testing position on the jet axis.

A plot of normalized heat flux as a function of calorimeter diameter is presented in Figure 27. There is good agreement (within 8%) at each calorimeter diameter, and the data appears to have a smooth distribution with the exception of the 0.450 inch diameter data. An apparent dip in the heat flux distribution was measured by the 0.450 transient calorimeter installed in both the 0.500 and 1.500 inch diameter shrouds. The installation of the 1.500 shroud on the 0.450 transient calorimeter produced no appreciable effect at both test conditions. As expected, the 0.500 transient calorimeter installed in the 1.500 inch diameter shroud showed excellent agreement with the 0.500 steady-state calorimeter.

The 0.750 inch diameter steady-state calorimeter indicated heat fluxes approximately 10 to 20% lower than the 0.500 steady-state calorimeter. The relationship between the 0.750 and 0.500 steady-state calorimeters is also given in Figure 28. A curve fit through the current data (stabilized arc column) indicates approximately 10% lower heat fluxes measured with the 0.750 calorimeter. This is a considerable improvement over the nonmagnetically stabilized arc data.

The general trend of the measured heat flux distribution indicates slightly higher heat fluxes with increasing transient calorimeter diameter until a maximum is reached at a diameter of 0.375 inch (see Figure 28). The data obtained with the 0.450 inch diameter transient calorimeter ranges between the 0.125 and 0.250 transient data. The 0.500 inch diameter steady-state calorimeter data falls in the range of the 0.250 and 0.375 transient data, and the minimum readings occurred with the 0.750 steady-state calorimeter. Within the range of calorimeter diameters from 0.125 to 0.500 inches, it appears that measured



heat flux is not a strong function of calorimeter or shroud diameter. Therefore, it is concluded that heat fluxes obtained with the 0.500 inch diameter steady-state calorimeter mounted in a 1.500 shroud are a valid measurement of the heat flux experienced by the front face of a 0.500 inch diameter cylindrical test specimen.

These measurements of radial heat flux distribution can be considered by normalizing the data given in Table 1 to accommodate the different stagnation enthalpy and pressure levels employed in Tests 1-6. This can be done as indicated in Table 2 since the pressure variations between tests is small and the heat flux proportional to  $i_e$  times  $(p_e)^{1/2}$ . Plotting the ratio of Averaged Normalized Flux to Average Normalized Flux for a 0.125 inch transient calorimeter in a 0.500 inch shroud yields the behavior shown in Figure 29. This representation shows that most of the results can be accommodated with a  $\pm 10\%$  band. However, a peak is noted near 0.375 inch as indicated earlier (Figure 27). The differences between results obtained with 0.500 and 1.500 inch diameter shrouds are presumably due to the finite stream diameter (0.600 inches) and the actual pressure gradients for different shroud diameters.

#### 4. Measurement of Temperature Gradients through Oxide Films Formed on Samples During Arc Plasma Exposures in the Model 500

Experiments were performed in the Model 500-5 Plasma Generator Facility in order to determine the in-depth temperature of test materials during arc plasma exposures. A micro-optical pyrometer was employed to measure the temperature at the base of a cavity drilled from the rear of the test specimen to within 0.100 inch of the heated face. The temperature at the in-depth station was found to range from 500° to 1900° R lower than the surface temperature. In order to determine the surface temperature, the heated face of the sample was continuously monitored during the test interval with a recording pyrometer operating at a wavelength of 0.65 microns. Corrections for spectral emittance allow the conversion of measured brightness temperatures into true temperatures. In some cases a heavy oxide deposit forms on the heated surface, while the remainder of the test sample is essentially in the virgin state. Since the surface temperature is measured in the area of the oxide deposit, there is some question concerning the temperature distribution behind the deposit. A steep temperature gradient may result if the oxide layer acts as an insulator, thus restricting the flow of energy into the sample. A slight separation between the oxide layer and base material could produce a significant heat blocking effect. Consequently, the objective of this study was to simultaneously measure the surface and in-depth temperature along with all of the other parameters customarily employed for material evaluation studies. Results are reported for four samples of ZrB<sub>2</sub>(A-3) and four samples of Hf-Ta-Mo(I-23).

A water cooled model holder was designed to provide a view of the rear of the test sample during the plasma exposure. The overall geometry of the new fixture is similar to that of the standard model holder employed in the ManLabs testing program. Visual access to the rear of the test sample is accomplished through a sight tube (see Figure 30) and a front surface mirror. In addition, the design provided a method to introduce a helium purge to the rear of the test sample. A photograph of the model holder with a test sample mounted in position for testing is presented in Figure 31.

The heated surface of the test sample was monitored with a recording pyrometer manufactured by Instrument Development Laboratories, Inc. (IDL). A micro-optical pyrometer was employed to measure the in-depth temperature at the base of the cavity. Both pyrometers operate at a wavelength of 0.65 microns. The micro-optical pyrometer was instrumented and calibrated to provide a continuous output record. Thus, it was possible to record both the surface and in-depth temperature as a function of time.

In order to account for the reflectivity of the front surface mirror, the micro-optical pyrometer was calibrated with the same optical arrangement employed in the specimen tests (see Figure 30). The  $34^\circ$  angle of incidence and the overall optical distances were held constant during the calibration and specimen tests. An NBS calibrated tungsten ribbon filament lamp was used to calibrate both pyrometers. A photograph of the experimental set-up is presented in Figure 32, and Figure 33 is a photograph of the side of the sample during a plasma exposure, the sample being  $\text{ZrB}_2(\text{A-3})$  in this case.

The experimental results are presented in Table 3. In Table 4, temperature and radiation data are given as a function of time. Figures 34 and 35 are post-test photographs of the samples.

It is apparent that a substantial difference exists between the temperature measurements taken at the surface and in-depth station. A spectral emittance ( $\epsilon_{0.65}$ ) of 0.57 was used for the surface temperature correction for the  $\text{ZrB}_2(\text{A-3})$  and 0.55 was used for the  $\text{Hf-Ta-Mo(I-23)}$ . Blackbody conditions ( $\epsilon_{0.65} = 1.0$ ) were assumed for the in-depth temperature for both materials.

The time-temperature history for sample  $\text{Hf-Ta-Mo(I-23)-3MC}$  is plotted in Figure 36. After an elapsed test time of 1560 seconds, a sudden increase in measured temperature and radiation occurred and was soon followed by a burn-through. An in-depth temperature of  $4280^\circ\text{R}$  and a surface temperature of  $5340^\circ\text{R}$  ( $1060^\circ\text{R}$  difference) were measured immediately prior to the increase at 1560 seconds. During the transient interval from 1560 seconds until burn-through occurred, the in-depth temperature approached the surface temperature until a final temperature difference of approximately  $550^\circ\text{R}$  was measured.

In general, the temperature at the in-depth station was found to range from 500° to 1900°R lower than the surface temperature. Melting and burn-through of the Hf-Ta-Mo material began when the in-depth temperature reached 4280°R, while the surface temperature was considerably higher. Rapid melting and burn-through of the ZrB<sub>2</sub> material occurred with a surface temperature of 6342°R, while the in-depth temperature was only 4420°R. Results of post-exposure metallography are presented in Section II, B of Part III Vol. III of this series. Figures 37 and 38 are post exposure photomicrographs through samples ZrB<sub>2</sub> (A-3)-2MC and Hf-20Ta-2Mo(I-23)-1MC showing the sighting hole and the tungsten sting.

#### 5. Comparison of Heat Flux Measurements with Flat Faced and Hemispherical Capped Calorimeter in the Model 500 Facility

Testing of hemispherical tipped specimens in the Model 500 Plasma Arc required the use of a special calorimeter to measure the stagnation point heating. The hardware employed in previous calorimetry tests (Section II-B-3) was employed with only a slight modification. Figure 39 shows a 1/8 inch diameter calorimeter. This fits into the 1/2 inch diameter shroud which has been machined to a nose radius of 0.250 inch and provides a means of directly measuring the stagnation point heat flux. A method of comparing these measured values with those obtained with the standard 1/2 inch diameter water cooled calorimeter in a 1.500 inch diameter shield is discussed below.

Changing the curvature of a "jet impingement" surface has the effect of changing the stagnation point velocity gradient  $(du/dr)_0$ , and from the general stagnation point heat transfer equation it is known that

$$q_s \approx \left( \frac{du}{dr} \right)_0^{1/2} \quad (3)$$

In their work with cold jets, Snedeker and Donaldson (8) found that the effect of surface curvature on  $(du/dr)_0$  is given approximately by the expression

$$\left( \frac{du}{dr} \right)_0 \approx \frac{V_c}{r_{0.5}} \left[ 1.13 + 1.08 \frac{r_{0.5}}{r_s} \right] \quad (4)$$

where

- $r_{0.5}$  = the radial distance at which the velocity is one half the centerline velocity
- $V_c$  = the centerline velocity
- $r_s$  = radius of curvature of the impingement surface

This equation was derived from tests conducted in a fully developed cold jet where  $-0.6 < r_{0.5}/r_s < 0.6$ , the negative values arising for concave surfaces. If it is assumed that this expression holds for the Model 500 arc jet then the ratio of stagnation and a flat faced calorimeter is as follows:

$$\frac{q_H}{q_{FF}} = \frac{\left(\frac{du}{dr}\right)_{CH}^{1/2}}{\left(\frac{du}{dr}\right)_{CFF}^{1/2}} = \frac{\left(\frac{V_c}{r_{0.5}}\right)^{1/2} [1.13 + 1.08 \frac{r_{0.5}}{r_{sH}}]^{1/2}}{\left(\frac{V_c}{r_{0.5}}\right)^{1/2} [1.13 + 1.08 \frac{r_{0.5}}{r_{sFF}}]^{1/2}} \quad (5)$$

so that

$$\frac{q_H}{q_{FF}} = \left[ \frac{1.13 + 1.08 \left(\frac{r_{0.5}}{r_{sH}}\right)}{1.13} \right]^{1/2} \quad (6)$$

Since the tests were conducted at a distance of only 1 inch from the nozzle exit, little mixing with the ambient fluid could occur and of necessity  $r_{0.5}$  must be of the order of one nozzle radius or 0.250 inch. Using this value

$$\frac{q_H}{q_{FF}} = 1.40 \quad (7)$$

This analysis is largely over simplified and the given ratio of 1.40 is by no means an absolute value. However, it does present an explanation for the large differences in heat flux values measured with hemispherical and flat faced calorimeters. Figure 40 shows the experimental data where the actual ratio of  $q_H/q_{FF}$  ranges from 1.38 to 1.50.

### C. Testing in the ROVERS Arc

#### 1. Description of Facilities

The Avco/SSD ROVERS facility can be employed for simulation of reentry or a hyperthermal environment in the laboratory. It is capable of simultaneously producing radiative and/or convective heating in a low pressure environment. The facility, shown schematically in Figure 41 and pictorially in Figure 42, consists of two types of heaters. An electric arc gas heater, with a supersonic nozzle, produces the convective heating. It is powered by up to four kw rectifiers. The radiative heating is produced by four argon gas-arc imaging lamps. Each lamp is powered by two 40 kw power sources, and the lamps can be operated at pressures up to 400 psia. These two

heating sources are positioned as schematically shown in Figure 41. The test specimen is mounted inside of a double walled water cooled tank which is 6 feet in diameter and 16 feet in length. The tank is evacuated by a 33,000 ft<sup>3</sup>/min vacuum system (at 10<sup>-1</sup> torr) to simulate the low pressure, high altitude environment. There are model injectors, probes and sample injectors, as called out in Figure 41, for positioning models, calorimeters, or probes into the jet stream. Although there are several types of tests that can be performed with one or both modes of heating, only the convective (splash) test will be discussed. Other test configuration details can be found in the Avco Arc Test Capabilities Manual (9).

The electric arc heater consists of a thoriated tungsten or modified tungsten cathode, a water cooled copper anode, and a series of water cooled nozzles with different throat and exit diameters for several Mach number levels. The design of the unit is based on a constricted arc configuration (10). Nitrogen tangentially injected is used for arc operation to prevent oxidation of the tungsten cathode and to hold contamination of the exit jet (with cathode material) to less than a few parts per million. Oxygen is injected into the arc plenum chamber to produce a simulated air jet. This oxygen injection into the arc plenum makes it possible to systematically change the chemical composition of the exhaust impinging upon the test specimen. In addition, a variety of gases singly or in combination could be used as the working gas. The convective heater is usually operated with simulated air over a range of enthalpies from 3500 to 20,000 BTU/lb, and at model surface pressures from 1 to 220 mm of Hg. With the assortment of nozzle flow conditions, heat flux values from 10 to 1200 BTU/ft<sup>2</sup>sec can be achieved using synthetic air.

Figure 43 shows the arc operating in the test chamber. Photographs of the test cylinders and holder stings as well as the holder test assembly prior to and during exposure are shown in Figures 44 and 45.

## 2. Calibration of the ROVERS\* Facility

In the present program, the hyperthermal environments to which the test specimens are subjected are characterized by the free stream average enthalpy and stagnation pressure and cold wall heat flux measured at the test specimen surface. At present, this type of calibration procedure appears to be the most applicable and least ambiguous technique. The stagnation enthalpy of the free stream of the ROVERS Arc is usually estimated from a simple over-all system energy balance. The enthalpy is obtained by subtracting arc-head cooling power from the electrical power input and dividing the difference by the gas mass flow rate. The stagnation pressure is measured using a copper (water cooled) conical nosed pressure probe having a 0.125 inch diameter port opening. The arc plenum and static tank pressures are measured using wall pressure taps feeding into calibrated transducers or gauges.

For tests in the ROVERS, the average heat flux to the specimen surface is measured using a combination of null point transient calorimeters and water calorimeters (11).

---

\*Radiation Orbital Vehicle Reentry Simulator

Figure 46 shows a typical water calorimeter. The centrally located  $5/8$ " diameter calorimeter is thermally insulated from the  $1-1/2$  inch diameter water cooled shroud. Although this calorimeter is a steady-state device and consequently does not have instantaneous response, it has been found to be reliable, accurate, and reproducible. Used in conjunction with the water calorimeter is the transient "null point" calorimeter. The transient calorimeter with varying diameter shrouds is shown in Figure 47. Calorimeters employing both these methods of measuring heat flux have been used and have been found to give results that are reasonably consistent providing the geometry of the holder is not drastically changed. For the case at hand, the sample is a  $1/2$  inch diameter right hand cylinder. Two calorimeters to measure heat flux to this sample configuration were built and tested; namely, a  $3/8$  inch diameter transient null point calorimeter having a  $1/2$  inch diameter copper shroud and a  $5/8$  inch diameter water cooled calorimeter with a  $1-1/2$  inch diameter shroud. Figure 48 presents a comparison of the results. From Figure 48 it is evident that both calorimeters give consistent heat flux values for the same flow environment. For the tests conducted in the ROVERS facility, the reported heat flux data is for the water calorimeter ( $5/8$  diameter) using a  $1-1/2$  inch water cooled shroud. The surface brightness temperature of the specimen is measured using a manual pyrometer. This monochromatic pyrometer employs a disappearing filament technique and a 0.65 micron filter. These brightness temperatures are corrected to true surface temperatures using known or assumed spectral (0.65 micron) emittance values.

The total energy radiated from the surface of the specimen is measured with a single junction, water cooled Eppley thermopile. The technique is discussed in Reference (12). Basically, it is required that the image of the specimen envelops the detector. With small diameter specimens special care and alignment is necessary to obtain the proper focusing on the detector.

### 3. Measurement of the Radial Heat Flux Distribution Across the Heated Surface of Flat Face Cylinders in the ROVERS Facility

In the current program, cylindrical samples of nominal 0.500 inch diameter were tested in the ROVERS Arc Facility. These tests were conducted with both the low pressure (3.0 inch exit nozzle) and the high pressure (2.25 inch exit nozzle) arcs. The standard instrument for measuring the heat flux to the specimen is a steady state water calorimeter. The calorimeter diameter is 0.625 inches with a 1.500 inch diameter shroud to prevent side heating and insure that the measured flux is only that seen by the front face. Because of the difference in the configuration of the calorimeter and the specimens, the following study was performed to see if the flux measured by this calorimeter is the same as that seen by the smaller diameter test specimens.

Transient calorimeters of different sizes (0.125, 0.250, 0.375 and 0.450 inch diameters) were tested using shroud diameters of 0.500 and 1.500 inches and the measured heat flux was compared to that measured with the water calorimeter. A complete description of the hardware used for these tests is given in Reference (13). The transient calorimeter assemblies were mounted on remotely controlled stings, as shown in Figure 49.

This allowed the consecutive testing of three transient calorimeters and the water calorimeter also shown in Figure 49 which could be rotated in and out of the jet stream.

A complete list of the heat flux data generated is presented in Table 5 along with the arc test conditions. The low and high pressure arc data are plotted in Figures 50 and 51, respectively, where the transient calorimeter results are normalized with the values measured with the water calorimeter. It is evident from these plots that there is very little change in the measured heat flux with an increase in the diameter of the calorimeter sensor size. It is also evident, however, that the size of the shroud has a definite effect on the level of flux measured. The flux levels measured with the 0.500 inch shroud are approximately 10% higher than the water calorimeter data, while the results using the 1.500 inch shroud are approximately 10% lower. These differences were seen in both the low and high pressure arc data. The comparison of all the transient and steady state calorimeter data in Figure 52 shows nearly all the points falling within 10% of the equality line. On this basis, it appears that for a given configuration (overall diameter of test specimen or calorimeter shroud) the diameter of the calorimeter sensing element has little effect on the heat flux measured in the ROVERS Arc tests in both the low and high pressure arc heads.

These measurements of radial heat flux distribution provide some unusual results. Reference to Table 5 and Figures 50 and 51 shows that the flux measured by means of a transient calorimeter in a 1.500 inch diameter shroud was 90% of that measured by using a water calorimeter having a 1.500 inch diameter shroud. This result is insensitive to changes in the diameter of the transient calorimeter between 0.125 and 0.450 inches. Since the diameter of the ROVERS stream is 2.25 to 3.00 inches, it was expected that the heat flux to a calorimeter with a 0.500 inch diameter shroud would be  $\sqrt{3}$  times larger than the heat flux to a calorimeter with a 1.500 inch shroud. This expected behavior is based on fundamental boundary layer scaling. Reference to Figures 50 and 51, however, show that the ratio of fluxes measured with 0.500 inch and 1.500 inch shrouds is about 1.20 rather than 1.73.

If the data shown in Table 5 are used to compute the heat fluxes for tests 1-8 based on calculated stagnation pressures of 0.015 and 0.175 for the low and high pressure tests with a factor of 2.5 to convert geometrical radius to effective radius\*, the results indicate that the flux measured with a transient calorimeter in a 0.500 inch shroud is about 10% higher than the Fay-Riddell values. The flux measured with a transient calorimeter in a 1.50 shroud is about 50% higher than the Fay-Riddell value. Thus, the smaller shroud results in values which are closer to Fay-Riddell as expected. However, the reason for the large discrepancy observed with the large shrouds (higher measured heat flux) is not apparent.

---

\* Effective radius refers to the equivalent stagnation point radius of curvature to attain the same surface pressure gradient and is approximated as equal to 2.5 times the geometrical radius of the flat face cylinder.

4. Measurement of Temperature Gradients through Oxide Films Formed on Samples During Arc Plasma Exposures in the ROVERS Arc

The in-depth temperatures of specimens have been measured in the ROVERS test facility in a manner similar to that employed in the Model 500 Arc discussed in Section II-B-4. A micro-optical manual pyrometer was used to measure the temperature at the base of a flat-bottom, 100 mil diameter cavity drilled in the rear of the test specimen. These holes were either 100 or 400 mils from the initial front surface of the flat-faced or hemispherical specimen. The base of the cavity was observed with a set-up similar to that shown in the reference, but a water-cooled, conical shield was utilized to protect the mirror from the hot gases. No helium purge was used as in the reference. Figure 53 shows the test set-up; the model is in the test position. Figure 54 shows a specimen being tested.

The manual pyrometer was calibrated twice using a new and a used mirror with a pyrex window. For calibrating, the equipment was arranged similar to that in the test set-up, but no set angle of incidence was held as in the reference. No difference was found in the results when either mirror was used, and the mirror-window combination showed about a 3 percent decrease in temperature.

5. Comparison of Heat Flux Measurements with Flat Faced and Hemispherical Capped Calorimeters in the ROVERS Facility

Flat faced and hemispherical capped models were tested in the ROVERS Arc facility at stagnation pressures between 0.1 and 0.2 atmospheres. For the flat-faced specimens the standard water calorimeter was used. However, for comparison a transient calorimeter, which was mounted inside a shroud to match the specimen shroud diameter, was also used. In order to measure the stagnation point heat flux to the hemispherical specimens, a transient calorimeter in a hemispherical shroud to match the specimen shape was used. The calorimeter design, was essentially that described in Section II-B-5, where each model shape is described separately.

To achieve the 0.1 to 0.2 atmosphere impact pressures a Mach 2.2 nozzle was utilized with a 0.5 inch diameter throat and a 0.75 inch exit diameter. This nozzle produced a jet considerably smaller in diameter and flow conditions distinctly different from those with the Mach 3.2 nozzle.

As indicated earlier (Section II-C-2 and Table 5), there was a difference in the heat flux measured by a 0.25 inch flat-faced transient calorimeter in a 0.5 and a 1.5 inch diameter shroud when subjected to a Mach 3.2 low pressure jet. Figure 55 shows the results when a similar calorimeter was placed in a 0.5, 1.0 and 1.5 inch diameter shroud. The results were compared by normalizing with results of the 0.625 inch diameter water calorimeter in the 1.5 inch diameter shroud and plotted



versus transient calorimeter shroud diameter. Also shown are the values for the Mach 3.2 jet. Although the jets physically appear different, the Mach 2.2 nozzle results were about 10 percent higher than those obtained with the Mach 3.2 nozzle and this can be attributed to the higher model pressure for the Mach 2.2 condition.

The 0.5 and 1.0 inch hemispherical models employed a 0.125 inch transient calorimeter at the stagnation point. A pictorial view is shown in Figure 56; the 0.5 inch calorimeter is shown disassembled. Since the calorimeters were flat, they were fabricated to blend with the hemispherical shroud and avoid non-uniformities on the sensing surface.

The results obtained with these calorimeters are shown in Figure 57. The different radii calorimeters gave about the same values when the Mach 2.2 nozzle was used. The theoretical  $q\sqrt{r}$  relationship of

$$q_{0.5}/q_{1.0} = 1.42 \quad (8)$$

was not expected because the jet diameter and model size were about the same. If this were the case, the velocity gradient at the stagnation point would be similar for the two calorimeter model sizes with the smaller diameter model having a slightly higher velocity gradient and therefore a slightly higher heat flux. In all cases the hemispherical calorimeters experienced significantly higher heat fluxes than the flat-faced water-cooled calorimeters.

#### D. TESTING IN THE TEN MEGAWATT ARC

##### 1. Description of Ten Megawatt Arc Facility

The Avco Ten Megawatt Arc Facility (10MW Arc) is employed as a high pressure, enthalpy heat source to evaluate the high temperature properties of materials. The 10MW Arc Facility consists basically of a 4 inch diameter spherical plenum chamber, into which four individual arc heads exhaust radially. The heated air mixes in the plenum and exits in a direction perpendicular to the plane of the arcs. Using this heat source and various exhaust nozzles a variety of tests can be conducted simulating a wide range of environments. For the current tests, a supersonic arc jet was exhausted directly onto a specimen retained in a graphite holder. Figure 58 presents an overall view of the 10MW Arc test cell while Figure 59 and 60 present interior views of a conical specimen splash test. The splash sample in the 10MW Arc is arranged so that the arc-heated gases splash against the sample (see Figures 61 and 62). In all cases, a Mach 2, 1.278 inch diameter exit nozzle was employed. Material evaluations were obtained at two specimen locations of 1 and 1.5 inches respectively such that variations in heat flux at constant gas enthalpy could be obtained.

## 2. Calibration of the 10MW Arc Facility

As shown in Figure 61, the test model is essentially a flat disc upon which a finite diameter supersonic jet impinges. When a model is tested in a finite diameter supersonic free jet, a shock interaction will occur at the intersection of the bow or attached shock and the free boundary such as shown in Figure 62. For purposes of material evaluation the sample is centrally located in the graphite holder such as shown in the post test view of Sample  $ZrB_2(A-3)HF-6$ , shown in Figure 63. Consequently, for a first order approximation, the sample is subjected to a one dimensional heating environment. To define this environment, the heat flux was measured using an Avco null point transient calorimeter of 3/8 inch diameter held in a 1.125 inch diameter copper flat-faced holder. The outside diameter of the graphite sample holder was 1.25 inches. The sample diameter was either 0.875 or 0.500 inches. Consequently, the heat flux as measured using the 3/8 inch diameter calorimeter probably is slightly higher than existed on the larger diameter specimens.

In addition to the heat flux, the gas enthalpy is determined for each test run. In the 10MW Arc a sonic throat technique is utilized to measure this quantity. The measurements required are the sonic-throat diameter, gas mass flow and stagnation pressure. The gas mass flow is preset by means of sonic flow orifices located upstream of the arc unit so that the gas mass flow is constant. A Fischer-Porter flowmeter is used to measure the gas mass flow prior to passing into the arc heads. The stagnation pressure is measured in the plenum chamber by means of a standard pressure transducer whose electrical output is recorded on a CEC oscillograph. At present, arc current and voltage are also recorded continuously on the CEC oscillograph. The total test time is determined from timing lines on the oscillograph. The start of a test is taken when the recorded pressure and current traces respond (approximately 0.01 second). The end of a test is taken when the arc current is terminated. The procedure used to determine the gas enthalpy is used for both calorimeter and sample tests.

In addition to defining the test environment (heat flux, enthalpy and 10MW Arc flow parameters) measurements of the sample's behavior in the supersonic stream were also recorded. These included front surface motion pictures taken with a 16mm Bell and Howell camera, surface brightness temperature using a recording Therm-dot pyrometer (operating at a wavelength of  $0.8\mu$ ) and sample physical dimensions (length and mass).

Prior to sample tests, heat flux and enthalpy levels are determined that will yield the desired specimen surface temperature. Once these parameters are determined, the samples are tested, and are then followed by additional heat flux measurements. These data are recorded and reported in the tables presenting the test results.

The test time for each of these samples was limited to a maximum of 20 seconds because of the limitations of the graphite holder which ablated rapidly and in many cases cracked and exposed the sides of the samples.

### 3. Pipe Testing in the 10MW Test Facility

The purpose of this phase of the program was to examine experimentally the performance of candidate materials in high shear, turbulent flow steady-state heating environments. In particular, conditions were restricted to a vehicle surface area beyond the sonic point where turbulent boundary layer flow prevails over the major heating period.

The Avco Ten Megawatt Arc (10MW) was utilized in this series of experiments. The specimens were machined into a pipe configuration as shown in Figure 64. A supersonic, arc heated air stream creates a high shear, turbulent flow environment within the pipe. The following data are to be obtained from each test:

- a) Overall weight loss and pipe diameter change.
- b) Surface temperature history, and
- c) High speed color films of the heated surface.

All supersonic pipe specimens for these tests were machined in two pieces which were housed in an uncooled copper sleeve, as shown in Figure 64. The upstream end is butted directly against the 10MW sonic nozzle and the downstream or exit end is retained by a stainless steel plate. O-rings are used in three locations, as shown, to prevent any gas leakage through joints. The downstream section is regarded as the test section. The purpose of the upstream section is to allow damping of flow irregularities and weak shock waves arising from the supersonic expansion processes in the pipe. Since the pipe geometry inevitably changes during ablation or oxidation such disturbances are unavoidable.

Heat transfer and pressure surveys were made for non-ablated pipe shapes to determine the pressure and heat flux distribution which exists along the downstream surface. Nominal pipe test conditions were as follows:

<u>Condition</u>	<u>Heat Flux</u> <u>BTU/ft<sup>2</sup> sec</u>	<u>Gas</u> <u>Enthalpy</u> <u>BTU/lb</u>	<u>Shear</u> <u>Stress</u> <u>lb/ft<sup>2</sup></u>
A	500	3700	40
B	600	7200	20

Figure 65 shows an overall schematic view of the 10MW supersonic pipe test configuration. The supersonic configuration differs from the subsonic test in that the pipe sample is placed downstream of the sonic throat as shown in Figure 64. The advantages of the supersonic configuration are as follows:

1. The sample surface can be observed. As a result, direct measurements of surface brightness temperature and radiation, as well as motion pictures, can be taken of the ablating surface.
2. The effect of ablation products on arc-operating parameters is eliminated because disturbances cannot be propagated upstream in a supersonic flowfield.
3. Failure of the specimen cannot influence the operation of the arc. In the sonic configuration, a pipe failure can result in serious damage to the arc components.
4. In utilizing a supersonic pipe configuration, a greater variability of arc and flow parameters is possible.
5. The flow outside the boundary layer is low supersonic providing a close approximation to local flow conditions in the region of maximum shear on a high-performance reentry vehicle.

A typical circular, supersonic-pipe sample is shown in Figure 66. The inner diameter of the pipe sample can be varied from 1/2 to 1-1/4 inches, depending upon the desired test condition. As shown in Figure 65 the circular, supersonic pipe can be divided into a transition section and a test section. Although nonuniform flow occurs in the first section, measurements are made only on the downstream portion of the pipe sample. The samples can be instrumented with thermocouples. Data obtained for each test specimen include weight loss, inner-diameter change, surface radiation and brightness temperature, internal temperature histories, and high-speed color films of the ablating surface. For those cases where steady-state ablation is achieved, the heat of ablation can be computed.

#### 4. Calibration of the 10MW Supersonic Pipe Test

##### (a) Determination of Gas Enthalpy

Figure 67 presents a typical curve of gas enthalpy versus a sonic-throat mass flow rate parameter (assuming equilibrium gas conditions) derived by use of isentropic flow relationships. The measurements required for any turbulent pipe test (sample or calorimeter) are the sonic-throat diameter, gas mass flow and stagnation pressure. The gas mass flow in the 10-megawatt is preset by means of sonic flow orifices located upstream of the arc unit so that the gas mass flow is constant. A Fischer-Porter flowmeter is used to measure the gas mass flow prior to passing into the arc heads. The stagnation pressure is measured in the plenum chamber by means of a standard pressure

transducer whose electrical output is recorded on a CEC oscillograph. At present, arc current and voltage are also recorded continuously on the CEC oscillograph. The total test time is determined from timing lines on the oscillogram. The start of a test is taken when the recorded pressure and current traces respond (approximately 0.01 second). The end of a test is taken when the arc current is terminated. The procedure used to determine the gas enthalpy is used for both calorimeter and sample tests.

#### (b) Determination of Heat Flux

The cold-wall heat flux to the turbulent pipe at any given operating condition is determined by use of a copper turbulent pipe calorimeter. At each test condition calorimeter tests are made before and after the sample tests. The calorimeter test consists of placing an uncooled solid copper pipe section (Figure 68) where the sample is normally located. The lengths and inside diameters of the copper pipe and ablative samples are identical. The copper pipe is instrumented with two (2) transient insulated copper calorimeter plugs. A description of the theory of the transient copper calorimeters has been reported previously (Reference 14). An average value of heat flux as determined by the two calorimeters is used to represent the heat transfer rate to the pipe.

#### (c) Shear Stress and Reynolds Number

In addition to the heat flux and other flow parameters which are recorded for a pipe test, the shear stress and Reynolds number are also calculated and reported with the other pertinent data. The shear stress ( $\tau$ ) is assumed to be given by the Reynolds analogy, that is:

$$\tau = \frac{qu}{H}$$

The method used to determine the cold-wall heat flux  $q$  and gas enthalpy  $H$  were given previously. The gas velocity  $u$  is determined by use of isentropic flow relationships assuming a ratio of specific heats of 1.2 for the appropriate pipe to throat area ratio.

The Reynolds number ( $N_{Re}$ ) is defined as follows:

$$N_{Re} = \frac{\rho u x}{\mu} = \frac{\left(\frac{\dot{m}}{A}\right) x}{\mu}$$

The viscosity of air at the arc operating conditions is determined from Reference 15. The length ( $x$ ) employed in computation of the Reynolds number is the distance from the plenum chamber exit plane to the mid-plane of the pipe section, i. e.,  $x = 7.5$  inches. In addition to these

calculated parameters, motion pictures and optical pyrometer histories of the heated pipe surface are obtained in the course of the test as typically shown in Figure 65. As is noted in Figure 65 only the downstream portion of the sample can be observed.

### III. HOT GAS/COLD WALL TESTS AT THE CORNELL WAVE SUPERHEATER HYPERSONIC TUNNEL

#### A. Description of Facilities

Testing in the Cornell Wave Superheater was performed under the direction of S. Tate, D. Colosimo and K. Graves. The Wave Superheater offers the possibility of exposing samples at very high velocity for short times. The heat flux levels can be varied by changing the position of the specimen relative to the nozzle. In this manner variable heat flux/temperature levels can be attained. Multiple-sample runs can be made using samples in the size range programmed. CAL\* furnished data on gas enthalpy, heat flux, surface temperature, stagnation pressure as well as colored motion pictures of the test samples. Test samples were returned to ManLabs for post-mortem metallography.

The Wave Superheater facility is shown schematically in Figures 69 and 70. The Wave Superheater rotor has 288 quasi-rectangular tubes, 0.55 inch wide, 1.43 inches high, and 66 inches long. The tube mid-heights lie on a 2.5 foot radius about the rotor axis. The rotor structure is designed for a tangential velocity of 700 feet per second at the tube center. The rotor can be preheated to a maximum temperature of 700° F to minimize thermal stresses and temperature attenuations during its operation. This pre-heat temperature is 100° F less than the equilibrium tube wall temperature that is to be maintained during the operation.

For any desired test condition obtainable, the test duration is limited only by the gas and heat storage capacities of the facility. Helium driver gas is stored at 2000 psi in high-pressure vessels having a capacity of 375,000 standard cubic feet. The helium driver flow is regulated by means of a fast response throttle valve that controls the pressure at which the helium enters the pebble furnaces. The selected pressure is determined by the desired shock strength that is to be generated within the Wave Superheater tubes. The driver helium is preheated up to 2160° R in two electrically energized aluminum oxide pebble furnaces, each of which is 7.5 feet in diameter, and 12 feet high. The helium driver gas flows from the furnace through a specially insulated pipe to the driver nozzle. The charge air is stored in high-pressure vessels having a capacity of 26,000 standard cubic feet, and is throttled to a constant 600 psi at the inlet to a third pebble furnace. This heater is similar to the driver heaters. The air leaves this heater at temperatures up to 2000° R and flows through another insulated pipe to the charge air nozzle. A control valve reduces the charge air pressure to some desired value before entry to the rotor by means of a choked, metering nozzle. Helium coolant is stored at 1750 psi in high-pressure vessels having a capacity of 180,000 standard cubic feet and is throttle-controlled before it enters the coolant nozzle. Helium is also used as the prime gas. It is stored at 2000 psi and is heated up to 1260° R in a small capacity heater after which it is throttled to near one atmosphere at the prime nozzle. To aid in operational flexibility, additional

---

\* Cornell Aeronautical Laboratory

high-pressure vessels having a capacity of 200,000 standard cubic feet are available.

As much as 70 pounds per second of helium may be required for driver, coolant, and prime gases for Wave Superheater operation. Helium is not expendable at this rate, and therefore it must be recovered and purified. Rather than collect the drive gas in nozzles at all peripheral stations which might otherwise be left open, it is more convenient and effective to completely enclose the rotor and nozzles. The reclamation nozzle protects the enclosure (shroud) and the rotor within from exposure to that part (20 pounds per second) of the helium drive gas which is at the highest temperature and pressure. The gases collected by the shroud and by the reclamation nozzle are cooled separately in aluminum oxide pebble beds. The flows are then merged and transported to a 150,000 cubic foot internal diaphragm storage tank. The tank diaphragm is collapsed before a run and expands during a run to receive all of the reclaimable gases at atmospheric pressure. After a run, the captured helium is separated from the air in a liquid nitrogen heat exchanger and is compressed and stored in the high-pressure tank farm for reuse.

Figure 71 shows the results of a high-pressure high flux test comparing tungsten and C-HfC at 50 atmospheres and 4800 BTU/ft<sup>2</sup> sec. This test was performed for Aerospace Corp. in the CAL Wave Superheater. Characteristic operating conditions shown in Table 6 indicates that for a model having a 0.01 ft radius (0.12 inch) the flux level at Mach 2 and 60 atm. stagnation pressure is 8000 BTU/ft<sup>2</sup> sec, and 1000 BTU/ft<sup>2</sup> sec in a Mach 6 one atmosphere test.

#### B. Description of Testing Procedures and Instrumentation

Sixteen refractory material models were exposed to the high velocity flow of air in the Mach 6 Wave Superheater Hypersonic Tunnel. Data were taken in two 15 second tests of eight models, each at a velocity of 10<sup>4</sup> ft/sec., a stagnation pressure (at the model nose) of one atmosphere, and a tunnel flow rate of 2.5 lb/sec. The models were designed to permit their surface temperature to approach the radiation/aerodynamic heating equilibrium value during each exposure to the test stream at  $q(R)^{1/2} = 90$  BTU/ft<sup>3/2</sup> sec. Temperatures in excess of 4000°R were expected from all models. The models were returned to ManLabs for post exposure analysis. All sixteen models tested were hollow hemispheric cylinders. The "elox" process was used to bore from the aft end to provide a uniform material thickness which was nominally 1/8 inch. The diameter of the bore was a nominal 1/4 inch for the thirteen 1/4 inch nose radius models and 3/4 inch for the three 1/2 inch nose radius models. The purpose of the shell or "thimble" design was to promote faster wall temperature response so as to approach the radiation equilibrium wall temperature as rapidly as possible. A sketch showing the typical model features and the typical attachment to their stings is presented in Figure 72. Eight models and a single 1/4 inch nose radius steady-heating copper calorimeter were mounted in the tunnel by a multiple sting arrangement as shown in Figure 73.



The models were not, in themselves, instrumented. The calorimeter had one chromel/alumel thermocouple welded to the back face of the thermal element. The models were observed individually by miniature radiometers. The design of these radiometers is a derivative of the Aerophysics Lab of the Johns Hopkins University (16). In addition to individual model radiometers, one ManLabs Milletron two-color pyrometer and one microphotographic camera (Photosonics #4) were arranged to observe the stagnation point of the model on sting number one. Two Photosonics cameras, #2 and #3, were arranged to observe all models from the right (pilot's view) during both runs. To obtain test conditions, the normal complex of Wave Superheater cycle instrumentation data were recorded as well as the tunnel throat and nozzle exit static pressure, and the test section cabin pressures. All data were recorded on EFB or ERB 16 mm film and a CEC optical galvanometer paper recorder.

The test conditions which exist in the Wave Superheater Hyper-sonic Tunnel are tractable throughout a test by virtue of a computer program (17) which interprets the recorded (pressure and temperature) time histories of the supply gases. As determined by this data reduction, the test conditions are not instantaneously established but exhibit a transient of about six-tenths second duration. The transient is terminated by a twenty to thirty millisecond step change to the final test conditions. Both the stream reservoir pressure and enthalpy undergo this transient in a manner that produces a stream heating capacity during the plateau portion of the transient of 85% of the value appropriate for the steady state test conditions. The heat transfer rate to the 1/4 inch radius spherical nose calorimeter measured during the transient, presented in Table 7 is about 500 BTU/ft<sup>2</sup>sec. Because this is 85% of the test value, the steady state is implied to agree with the intended 600 BTU/ft<sup>2</sup>sec. Calorimeters used in the Wave Superheater facility are normally expected to burn out. For the two oxidation tests, the calorimeter temperatures are presented in Figure 74. The gage life was greater than one second. Although the gage is too hot after the transient to obtain quantitative heat transfer data, the recorded temperature signal from the calorimeter is very smooth, precise and clearly represents the 500 BTU/ft<sup>2</sup>sec. At t = 0.80 seconds, the temperature departs from its earlier track to one of higher rise rate. This point seems to be the termination of the transient.

The heat transfer data reduction for the steady calorimeters is determined by:

$$q = \rho C_p \delta \frac{\Delta T}{\Delta t} \quad (9)$$

where  $\rho$ ,  $\delta$ , and  $C_p$  are the density (559 lb/ft<sup>3</sup>), depth (0.125 inch) and specific heat of the copper gage element which is a function of temperature. Because the recorded temperature represents the back surface, it is necessary to obtain the wall or front surface temperature in order to obtain the cold wall heat transfer rate. The temperature distribution within the gage element is given, for a linearly decreasing heat transfer rate from ( $q_w$ ) at the front face to zero at the back face by:

$$\frac{dT}{dx} = \frac{q_w}{k} \left( \frac{x}{\delta} - 1 \right) \quad 0 < x < \delta \quad (10)$$

The front face temperature ( $T_w$ ) can be obtained from the back face temperature ( $T_b$ ) and the integration of Eq. (10) so that:

$$T_w = T_b + \frac{\delta q_w}{2k} \quad (11)$$

where  $q_w$  is taken from Eq. 9 and  $k$  is the gage conductivity. The cold wall heating rate ( $q_{cw}$ ) is then obtained by:

$$q_{cw} = q_w \frac{(i_e - i_{cw})}{(i_e - i_w)} \quad (12)$$

where  $i_{cw} = 118 \text{ BTU/lb}$ ,  $i_w = C_{pg}T_w$  and  $C_{pg}$  is the gas specific heat at constant pressure. Air at the calorimeter wall temperature has a specific heat of  $0.24 \text{ BTU/lb}^\circ\text{F}$ . The data ( $q_w$ ,  $T_w$ ,  $q_{cw}$ ) is tabulated in Table 7. Fay-Riddell stagnation heat transfer rate has been simplified by plotting the curve of  $q_w (R/P_e)^{1/2}$  vs.  $(i_e - i_w)$ . This curve, nearly straight, is very closely approximated by:

$$q_w (R/P_e)^{1/2} = 0.863 \times 10^{-3} (i_e - i_w) \text{ BTU/ft}^{1/2} \text{ sec lbs}^{1/2} \quad (13)$$

The use of Eq. 13 provides a value for  $i_e$  which can be compared to the Cycle Analysis (17) results ( $i_e$ ) to provide the desired test condition validation. Corrections due to flow starting transient are established by these techniques and applied appropriately to data that is obtained during the transient.

These data (Eqs. 9, 11, 12 and 13) including the transient corrections are presented in Table 8. The test conditions for both tests are presented in Table 9.

#### C. Calculation of Surface Temperatures and Heat Flux Levels for Test Models

A transient heat flux calculation of model surface temperature was performed using the Fay and Riddell (18) heat transfer relation

$$qR^{1/2} = 0.94(\rho\mu)_w^{0.1}(\rho\mu)_e^{0.4}(2P_e\rho_e^{-1}(1-P_\infty P_e^{-1}))^{1/4}(i_e - i_w) \quad (14)$$

where  $q$  is the heat flux to the body,  $R$  is the hemispherical radius at the stagnation point,  $P$ ,  $\rho$ ,  $\mu$  and  $i$  are pressure, density, viscosity and enthalpy respectively, and the subscripts  $w$ ,  $e$  and  $\infty$  refer respectively to the wall, to the stagnation point after the shock and to the test stream static values. The heat input was assumed to occur to a semi-infinite slab allowing for radiation from the face according to Eq. 15.

$$q_r = -\epsilon \sigma T^4 \quad (15)$$

where  $\epsilon$  is the total hemispherical emittance,  $T$  is the wall temperature ( $^{\circ}\text{R}$ ) and  $\sigma$  is  $0.47 \times 10^{-12} \text{ BTU/ft}^2 \text{ sec } ^{\circ}\text{R}^4$ . Eq. 16 gives the net heat flux,  $q_n$

$$q_n = q + q_r \quad (16)$$

which is used in the solution of the one dimensional unsteady heat diffusion equation for a finite slab and results in (19) Eq. 17.

$$T = q_n [4t/\pi \rho c_p k]^{1/2} f[\Theta] \quad (17)$$

Here  $T$  is the surface temperature,  $t$  is the time and  $\rho$ ,  $c_p$  and  $k$  are the density, specific heat and thermal conductivity of the slab respectively. The Fourier modulus  $\Theta$  is defined in terms of the slab thickness  $\delta$  by

$$\Theta = kt/\rho c_p \delta^2 \quad (18)$$

and

$$f[\Theta] = \pi^{1/2} \sum_{n=0}^{\infty} \text{ierfc} \left[ \frac{(2n+1) + x/\delta}{2\Theta^{1/2}} \right] + \text{ierfc} \left[ \frac{(2n+1) - x/\delta}{2\Theta^{1/2}} \right] \quad (19)$$

where  $x$  is the distance measured from the back of the slab and  $\text{ierfc}$  is the complementary integral error function

$$\text{ierfc} y = \int_y^{\infty} \text{erfc} \lambda \, d\lambda = \pi^{-1/2} e^{-y^2} - y \text{erfc} y$$

Eqs. 17-19 reduce to

$$T \approx 2q_n [t/\pi \rho c_p k]^{1/2} \quad \text{for } \Theta < 1 \quad (20)$$

$$T \approx 2q_n t/\pi^{1/2} \rho c_p \delta \quad \text{for } \Theta > 1 \quad (21)$$

Since  $q_n$  is a function of  $T$  which in turn depends upon  $t$ , Eqs. 14 and 16 were evaluated by assuming that the viscosity of air is given by Eq. 22

$$\mu_w = 1.18 \times 10^{-5} (i_w/118)^{0.624} \text{ lbs/ft sec} \quad (22)$$

where  $i_w$  is in BTU/lb. Thus Eq. 14 becomes

$$qR^{1/2} = 0.059T^{-0.038} (i_e - i_w) \text{ BTU/ft}^2\text{sec} \quad (23)$$

when  $P_e = 1$  atm. These relations, along with values of  $i_w[T]$  obtained from Hansen (20) were employed to numerically compute the time dependence of the surface temperature and the net heat flux for  $ZrB_2$  shown in Figures 75 and 76 and in Tables 9 and 10. The values of  $\epsilon$ ,  $c_p$ ,  $\rho$  and  $k$  employed in these calculations are based on published data for  $ZrB_2$  (21, 22, 23). The calculations are presented for a one inch and a one half inch hemispherical cap shell of  $ZrB_2$  having a thickness  $\delta$  equal to 0.125 inches.

The foregoing discussion considers radiation equilibrium at the surface of the model without including the effects of conduction losses. Figure 77 is the basis for an analysis of the relative importance of conduction and aerodynamic heating for a given model. Specifically, if the aerodynamic heating is given by Eq. 24 as:

$$q[\theta] = q \cos \theta \quad (24)$$

where  $q$  is the heat flux at the stagnation point and  $q[\theta]$  is the corresponding local heat flux at a point on the hemispherical surface as shown in Figure 77, the elemental area consisting of a circumferential ring  $r_o d\theta$  wide and  $r_o \sin \theta$  in radius receives an energy per unit time,  $dQ_{Aero}$ , given by:

$$dQ_{Aero} = (q \cos \theta) (2\pi r_o \sin \theta) (r_o d\theta) \quad (25)$$

The total heat input to the spherical cap due to aerodynamic heating is then:

$$Q_{Aero} = \pi r_o^2 q \int_0^\theta \sin 2\theta d\theta = 0.5\pi r_o^2 q (1 - \cos 2\theta) \quad (26)$$

Conduction through the cross section of the shell at station  $\theta$  is:

$$Q_{Cond} = k(dT/ds) (2\pi(r_o + r_i)/2)(\sin \theta) (r_o - r_i) \quad (27)$$

where  $k$  is the thermal conductivity and  $T$  is the temperature which is assumed uniform through the shell thickness  $(r_o - r_i)$ .

Thus, the relative importance of the aerodynamic heating and conduction losses is:

$$R = Q_{\text{Cond}}/Q_{\text{Aero}} = 2k(dT/ds) \sin \theta (1 - \cos 2\theta)^{-1} q^{-1} r_o^{-1/2} \text{ times } (1 - (r_i/r_o)^2) r_o^{-1/2} \quad (28)$$

Eq. 28 permits definition of the individual and combined effects of model size and shell thickness. When  $R$  is less than unity conduction is of less importance and when  $R$  is greater than unity conduction is dominant. Using nominal values of  $r_o = 1/4$  and  $1/2$  inches and shell thickness equal to  $1/8$  inch for the shells leads to ratios  $r_i/r_o = 0.50$  and  $0.75$  for the small and the large models respectively. Eq. 28 yields:

$$R_S/R_L = 1.4 \quad (29)$$

if  $r_i/r_o$  were the same for both large and small models, designated by subscript  $S$  and  $L$  in Eq. 29.

If the outer radii were identical then

$$R_S/R_L = 1.7 \quad (30)$$

for the ratios  $r_i/r_o$  for the small and large models. Substitution of  $r_o = 1/4$  and  $1/2$  inches (for the small and large models) with a shell thickness equal to  $1/8$  inch into Eq. 28 yields:

$$(R_S/R_L) = 2.4 \quad (31)$$

Thus, Eqs. 29 and 30 indicate that a small model or a relatively thicker shell each imply larger conduction effects. Eq. 31 shows that in the current tests, the smaller model would be expected to experience larger relative conduction losses than the larger model. Eq. 28 suggests that the shell thickness of the small and large models should have been chosen equal to 43 mils and 125 mils respectively in order to insure equivalent conduction effects, whatever they may be.

In order to consider the magnitude of the conduction effects for the small model in the case at hand, consider  $q = 650 \text{ BTU/ft}^2\text{sec}$ ,  $r_o = 0.02085 \text{ ft}$ ,  $(1 - (r_i/r_o)^2) = 0.75$  and  $k = 0.010 \text{ BTU/ft sec}^\circ\text{R}$ . The latter

values are an overestimate by a factor of two for the KT-SiC case in order to conservatively evaluate the conduction effect. For these values, Eq. 28 yields:

$$R_S = 1.11 \times 10^{-3} (dT/d\theta) \sin \theta (1 - \cos 2\theta)^{-1} \quad (32)$$

Assuming a linear temperature gradient which implies that  $dT/d\theta = 3000^\circ\text{R}/0.5\pi$  radians, corresponding to a linear gradient from the stagnation point to the shoulder, which is quite conservative, affords the following:

$\theta$ degrees	$R_S$
1	60.6
5	12.2
10	6.1
45	1.5
90	1.0

With temperature gradients which are one tenth of the above (i.e.,  $dT/d\theta = 191^\circ\text{R}/\text{radians}$ ) conduction appears to be important for  $\theta$  less than 5 degrees. Additional reductions would arise for smaller values of thermal conductivity. As a consequence, these results suggest that the magnitude of the conduction losses relative to aerodynamic heating is significant over a small sector of the shell in the vicinity of the stagnation point. As a consequence, this analysis suggests that the losses due to conduction should be small compared to the aerodynamic heating effects.

#### D. Experimental Evaluation of Conduction Losses for Spherical Shells

In order to obtain an experimental assessment of the relative conduction losses for spherical shells, one inch and one half inch diameter models having a wall thickness of 1/8 inch were fabricated from SAE1020 steel. This material was employed since its thermal conductivity is approximately one third that of KT-SiC(E-14) at temperatures between  $500^\circ$  and  $2000^\circ\text{R}$ . Characteristic values are shown below.

<u>T</u> <u>°R</u>	<u>SAE1020 (24)</u>	<u>KT-SiC (25)</u>	<u>Hf-20Ta-2Mo (26)</u>
500	0.0084	0.029	0.0025
600	0.0083	0.027	0.0025
800	0.0080	0.024	0.0026
1000	0.0075	0.021	0.0028
1200	0.0069	0.017	0.0029
1400	0.0063	0.014	0.0030
1600	0.0058	0.012	0.0031
1800	0.0053	0.009	0.0033
2000	0.0047	0.007	0.0035

The thermal conductivity of Hf-20Ta-2Mo(I-23) is based on recent measurements (26). For this case, there is no simple relation between the thermal conductivity of SAE1020 and Hf-20Ta-2Mo. Reference to Eq. 28 shows that if the ratio of  $k/q$  is maintained at the same level in a simulation of the test,  $R$  can be evaluated.

Accordingly, models were exposed in an oxyacetylene torch situated in the Wave Superheater Hypersonic Tunnel for convenience in utilizing the required test equipment. Separate copper calorimeters were employed to determine cold wall heat flux. Heat fluxes of 150 BTU/ft<sup>2</sup>sec and 220 BTU/ft<sup>2</sup>sec were applied to the one inch and one-half inch diameter models, respectively. Thermocouples which were spring mounted in contact with the inner wall directly behind the stagnation point were employed to measure the thermal response of the models. The results are shown in Figure 78. The results indicate that the larger model reached 1900°F in 11.4 seconds; the smaller models reached 1900°F in 13.8 ± 1.0 seconds. At shorter times, the rise rate for the smaller models is greater than for the larger models as expected. At longer times, the larger model does heat up more rapidly than the smaller model does. However, it is surprising that the cross-over occurs at low temperatures near 600°F where the magnitudes of  $dT/d\theta$  are smaller than the values assumed in the foregoing calculation. Finally, it should be noted that the  $k/q$  matching is partially satisfied for KT-SiC but not satisfactory for Hf-20Ta-2Mo.

## REFERENCES

1. Beck, J. V. and H. Hurwicz, Study of Thermal Discontinuities and Associated Temperature Disturbances in a Solid Subject to a Surface Heat Flux, Part I, Effect of Thermocouple Cavity Near Heat Sink Surface on Sink Temperature Distribution and Its Measurement, Avco RAD-TR-9-59-5 (20 February 1959).
2. Beck, J. V. and H. Hurwicz, Study of Thermal Discontinuities and Associated Temperature Disturbances in a Solid Subject to a Surface Heat Flux, Part II, Effect of Cavities Located in the Interior of Heat Sinks on Sink Temperature Distribution and Its Material Specifications, Avco RAD-TR-9-59-14 (28 April 1959).
3. Beck, J. V., Study of Thermal Discontinuities and Associated Temperature Disturbances in Solid Subject to a Surface Heat Flux, Part III, Effect of Sensors in Low Conductivity Material Upon Temperature Distribution and Its Measurements, Avco RAD-TR-9(7)-59-26, (12 October 1959).
4. Beck, J. V., Correction of Transient Thermocouple Temperature Measurements in Heat Conducting Solids, Part I, Procedures of Thermocouple Temperature Correction in Solids Possessing Constant Thermal Properties, Avco RAD-TR-60-38, Part I (8 February 1961).
5. Beck, J. V., Correction of Transient Thermocouple Temperature Measurements in Heat Conducting Solids, Part II, The Calculation of Transient Heat Fluxes Using the Inverse Convolution, Avco RAD-TR-6-60-38, Part II (30 March 1961).
6. Beck, J. V., Correction of Transient Thermocouple Temperature Measurements in Heat Conducting Solids, Part III, Certain Correction Kernels for Temperature Measurements in Low Conductivity Materials, Avco RAD-TR-7-60-38, Part III, 21 July 1961.
7. Beck, J. V. and Wolfe, H., Digital Program to Calculate Surface Heat Fluxes from Internal Temperatures in Heat-Conducting Bodies, Avco RAD-TR-62-27, August 1962.
8. Snedecker, R. S. and Donaldson, C. duP., Experiments on Free and Impinging Underexpanded Jets from a Convergent Nozzle Aeronautical Research Associates of Princeton, ARAP Report 63, September 1964.
9. Avco Arc Test Capabilities, Avco Space Systems Division, AVSSD-0265-66-CA, November 1966.
10. Avco/RAD, Theoretical and Experimental Investigation of Arc Plasma-Generator Technology, Avco/RAD-SR-61-26 (February 1961).



# REFERENCES (CONT)

11. Beck, J. V. and Wolfe, H., Digital Program to Calculate Surface Heat Fluxes from Internal Temperatures in Heat-Conducting Bodies, Avco/RAD-TR-62-27, (August 1962).
12. Carnavale, E. and Recesso, J. V., Absolute Measurements of Radiation from Ablating Surfaces, Avco/RAD-TM-59-62 (1959).
13. Abate, R. E., Heat Flux Measurements - Model 500-5 Plasma Generator Facility, R720-TR-68-22, February 6, 1968.
14. O'Connor, T. T. and Morgida, J. V., Null Point Transient Calorimeter Theoretical Concepts and Experimental Results, ISA Preprint No. 16.5-2-66, October 1966.
15. Zlotnick, M., Transport Coefficients of Air to 8000°K, Avco/RAD-TR-58-12, 1958.
16. Akridge, J. M., Keller, C. A., and Hill, M. L., "Patent Disclosure of a Photovoltaic Pyrometer", APL/JHU BFR 64-8.
17. Tate, S. E., "Wave Superheater Cycle Analysis", CAL Memo WS-300-6, February 1967.
18. Fay, J. A. and Riddell, F. R., J. Aeronautical Sciences (1958) 25, 73.
19. Kurzrock, J. W., "Selection of Surface Thermometers for Measuring Heat Flux", Cornell Aeronautical Laboratory Report No. 124, February 1963.
20. Hansen, C. G., "Approximation for the Thermodynamic and Transport Properties of High Temperature Air", NASA Technical Report No. R-50 (1959).
21. Kaufman, L. and Clougherty, E. V., "Investigation of Boride Compounds for Very High Temperature Applications", RTD-TDR-63-4096 Part III, March 1966.
22. Kaufman, L. and Clougherty, E. V., "Investigation of Boride Compounds for Very High Temperature Applications", RTD-TDR-63-4096 Part I, December 1963.
23. Kaufman, L. and Clougherty, E. V., "Investigation of Boride Compounds for Very High Temperature Applications", RTD-TDR-63-4096 Part II, February 1965.
24. Smithells, C. J., Metals Reference Book, Third Ed. Vol. 2 (1962) 705 Butterworths, Washington, D. C.
25. Lynch, J. F., Ruderer, C. G. and Duckworth, W. H., "Engineering Properties of Ceramics", AFML-TR-66-52, June 1966.
26. Denman, G. L., Air Force Materials Laboratory, Dayton, Ohio, March 1968, Private Communication.

#### REFERENCES (CONT)

27. Kendall, E.G., Slaughter, J.I. and Riley, W.C. "A New Class of Hypereutectic Carbide Composites", Aerospace Corp., El Segundo, California. Report SSD-TR-65-78, June (1965).

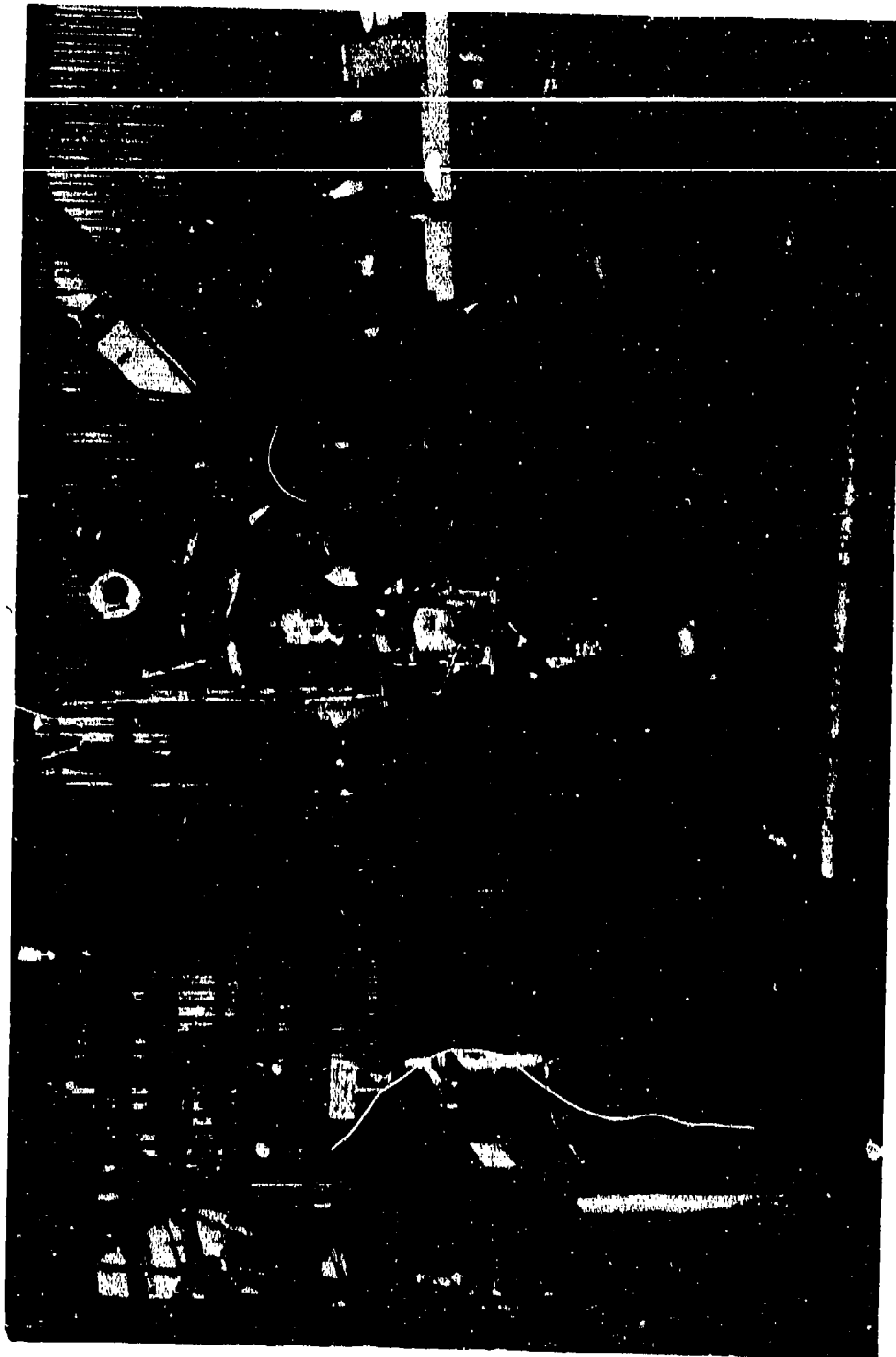


Figure 1. Model 500 Plasma Generator (Rear View) (#18146B).

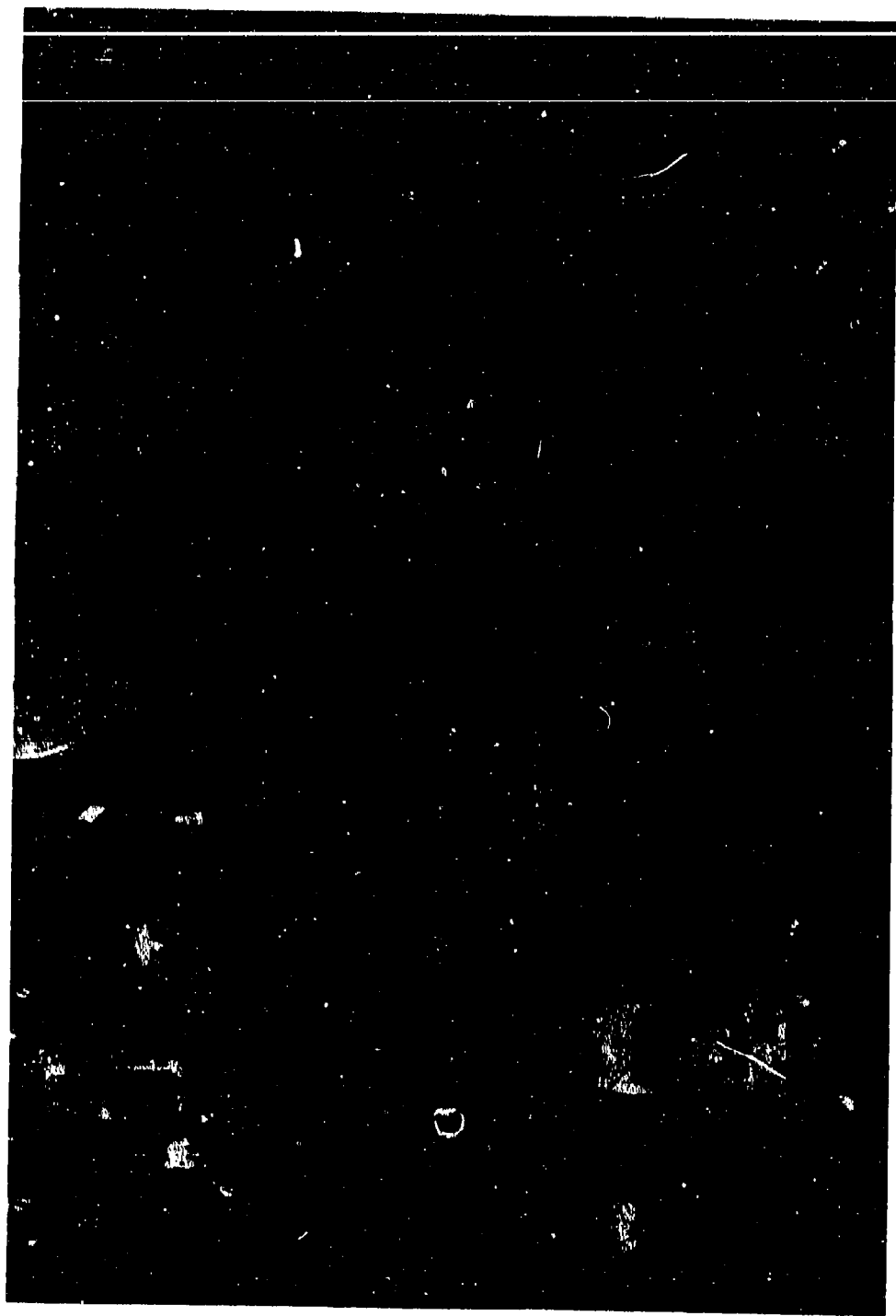


Figure 2. Model 500 Plasma Generator Control Room (#18146G).

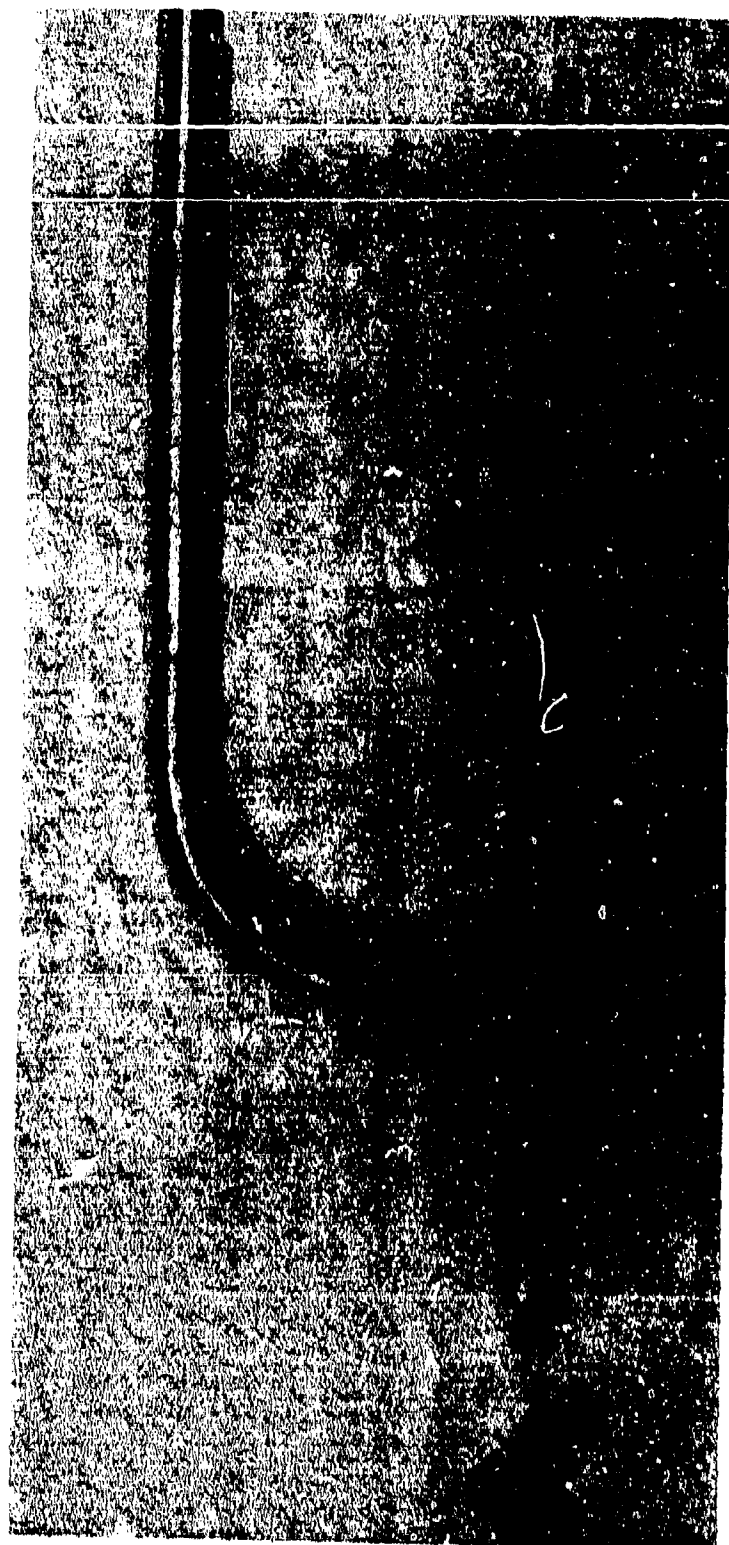


Figure 3. Zirconium Diboride Cylinder Prior to Exposure in the Avco-SSD Model 500 Arc Plasma Facility.

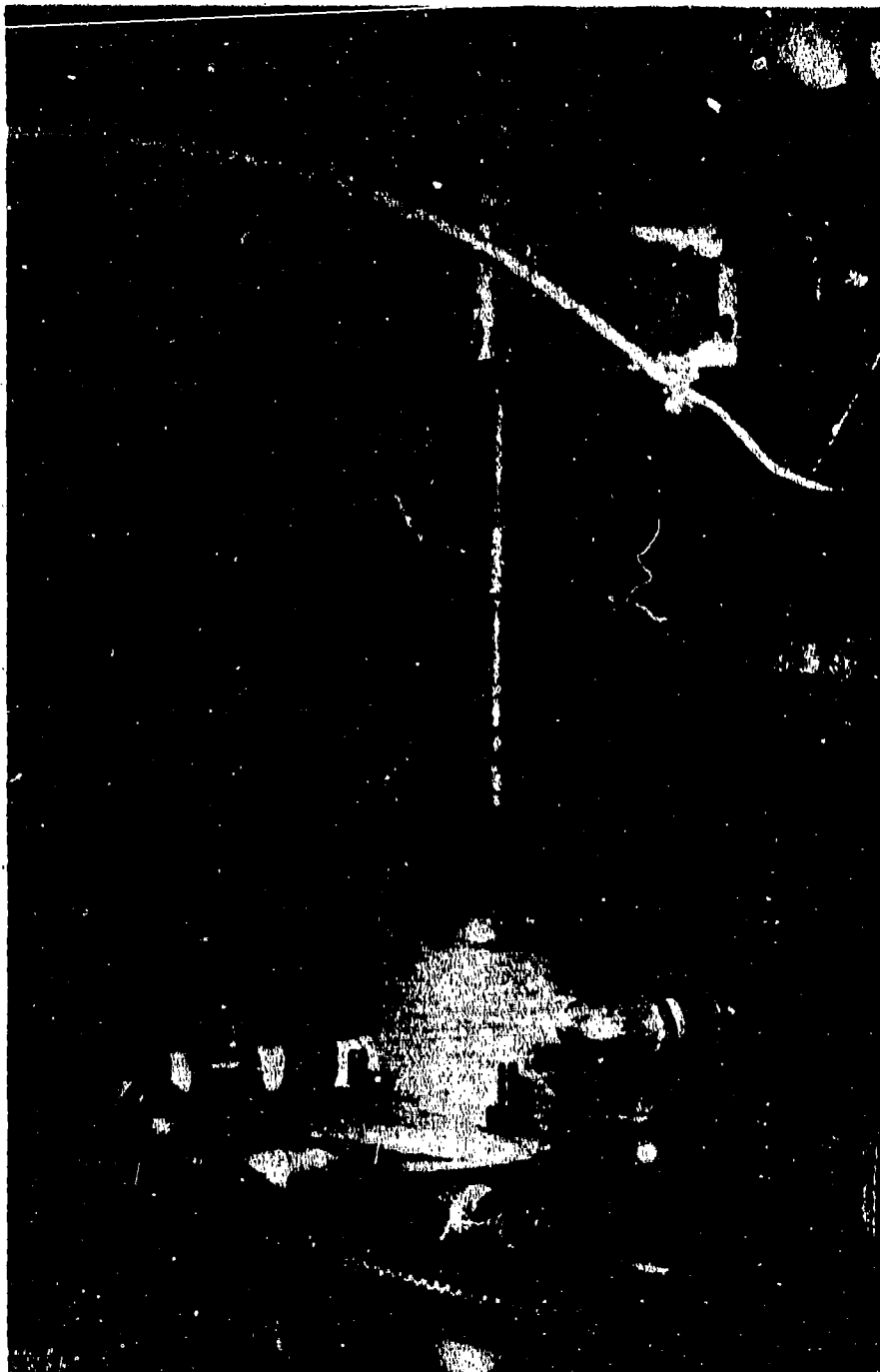


Figure 4. Zirconium Diboride Cylinder Prior to Exposure in the Avco-SSD Model 500 Arc Plasma Facility.

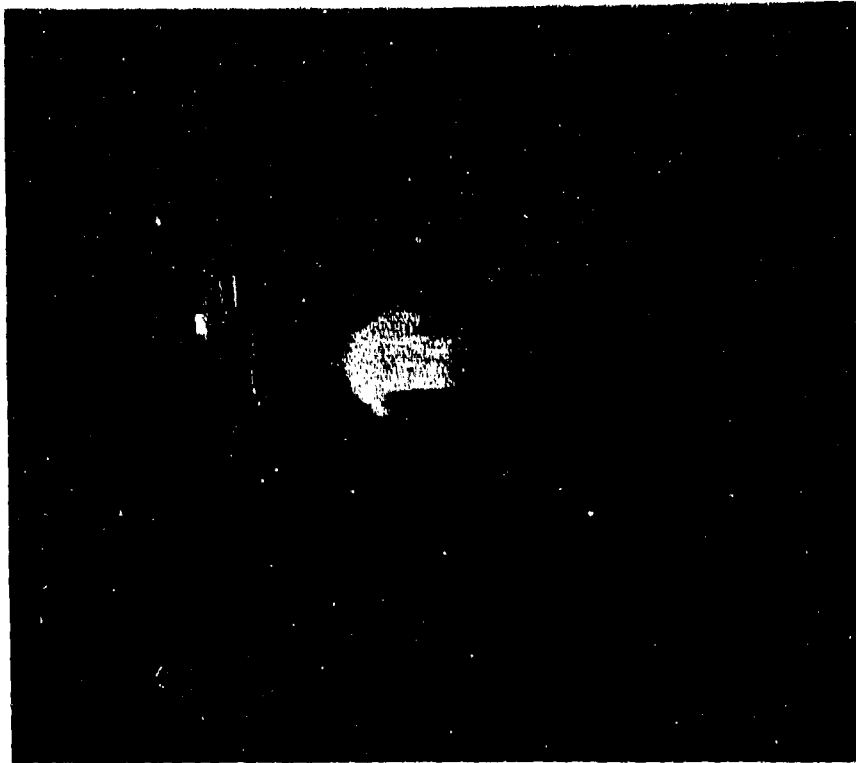


Figure 5. Zirconium Diboride Cylinder During Exposure in the Avco-SSD Model 500 Arc Plasma Facility.

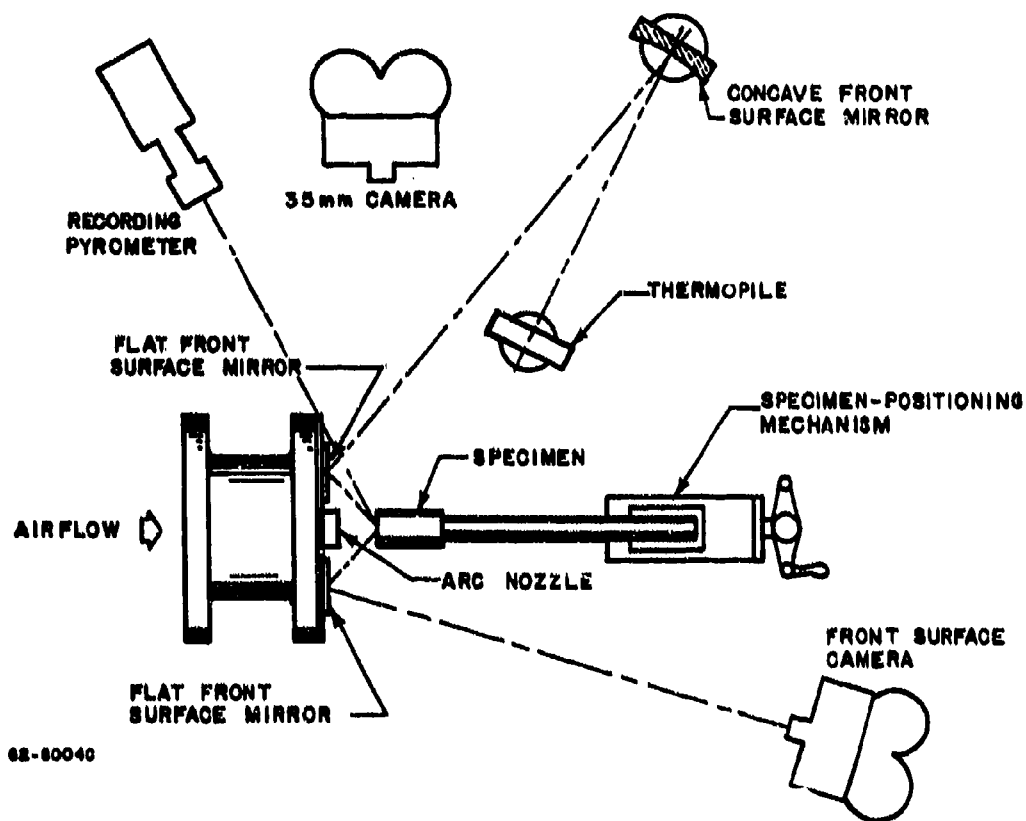


Figure 6. Basic Experimental Setup (Model 500 Plasma Generator)





Figure 7. Model 500 Plasma Generator (Right-Rear View) (#18146A).

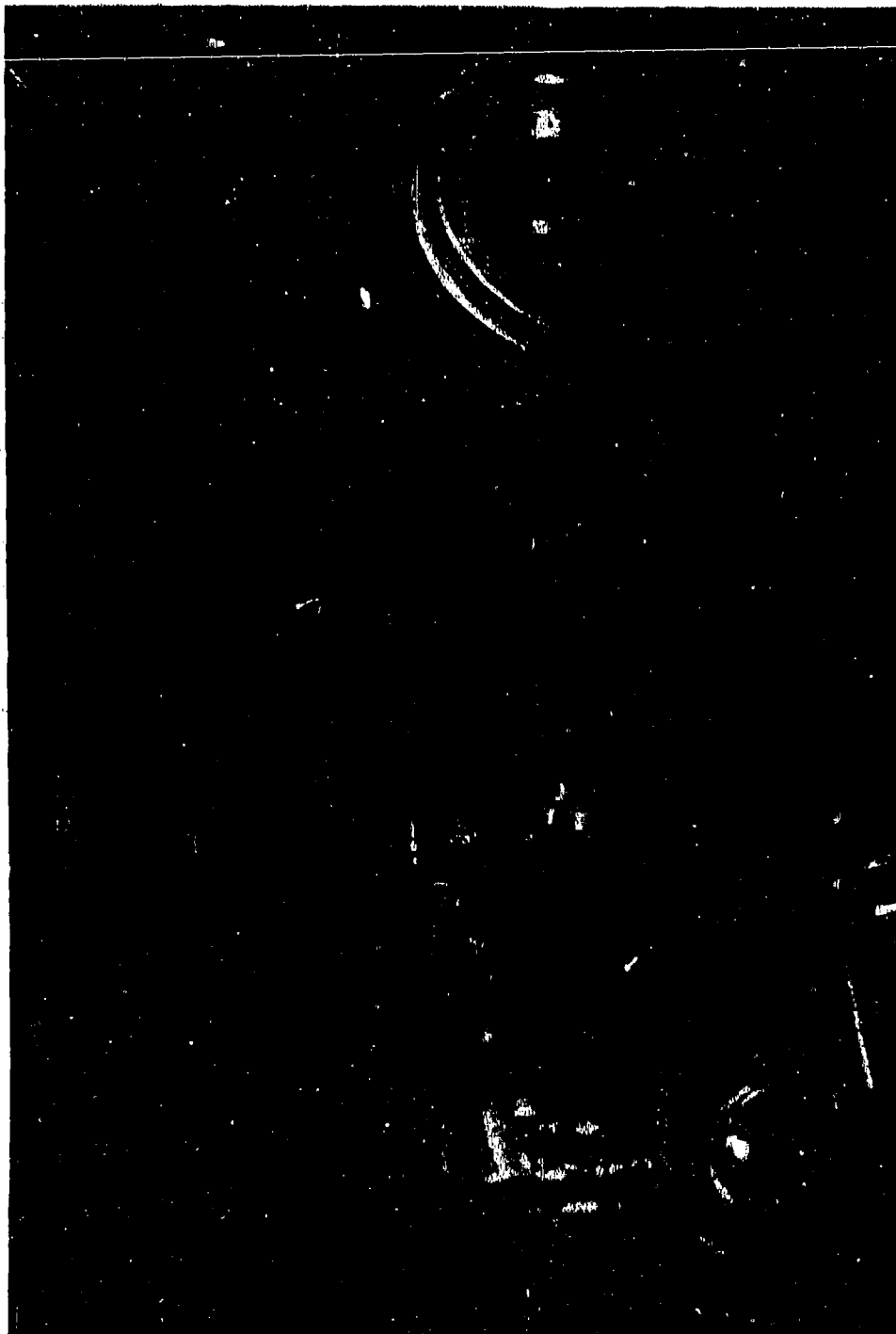


Figure 8. Specimen Mounted in the Model 500 Facility (#18146C).

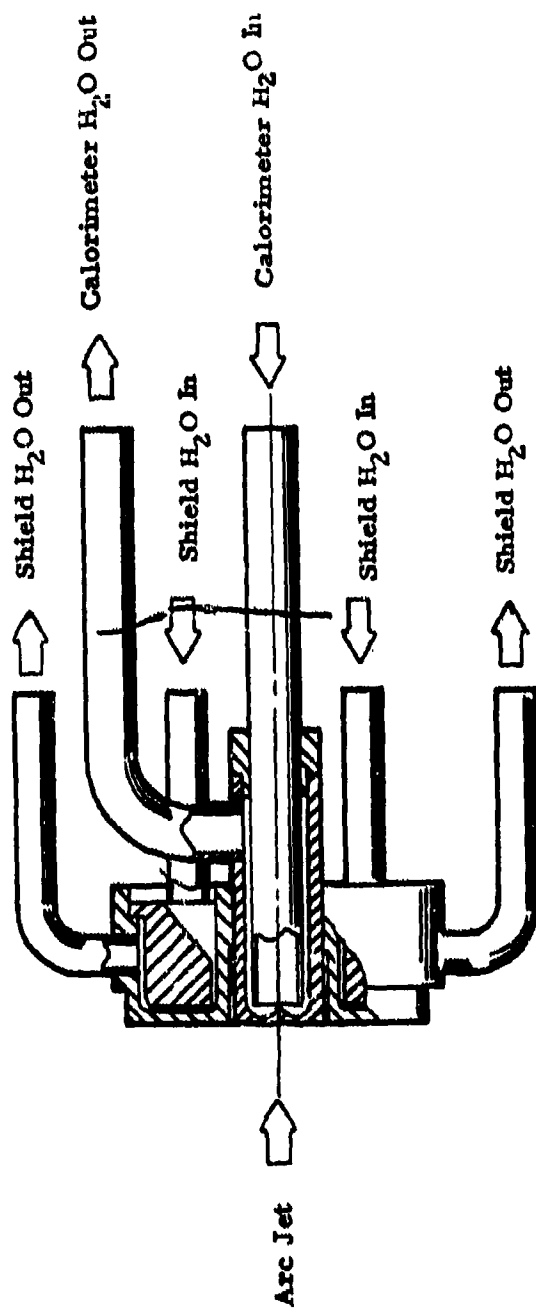


Figure 9. Constant Flow Water Calorimeter



Figure 10. Avco Calorimeter Installation - Model 500 Facility (#19146D).



Figure 11. Avco Calorimeter During Test in the Model 500 (#181461).

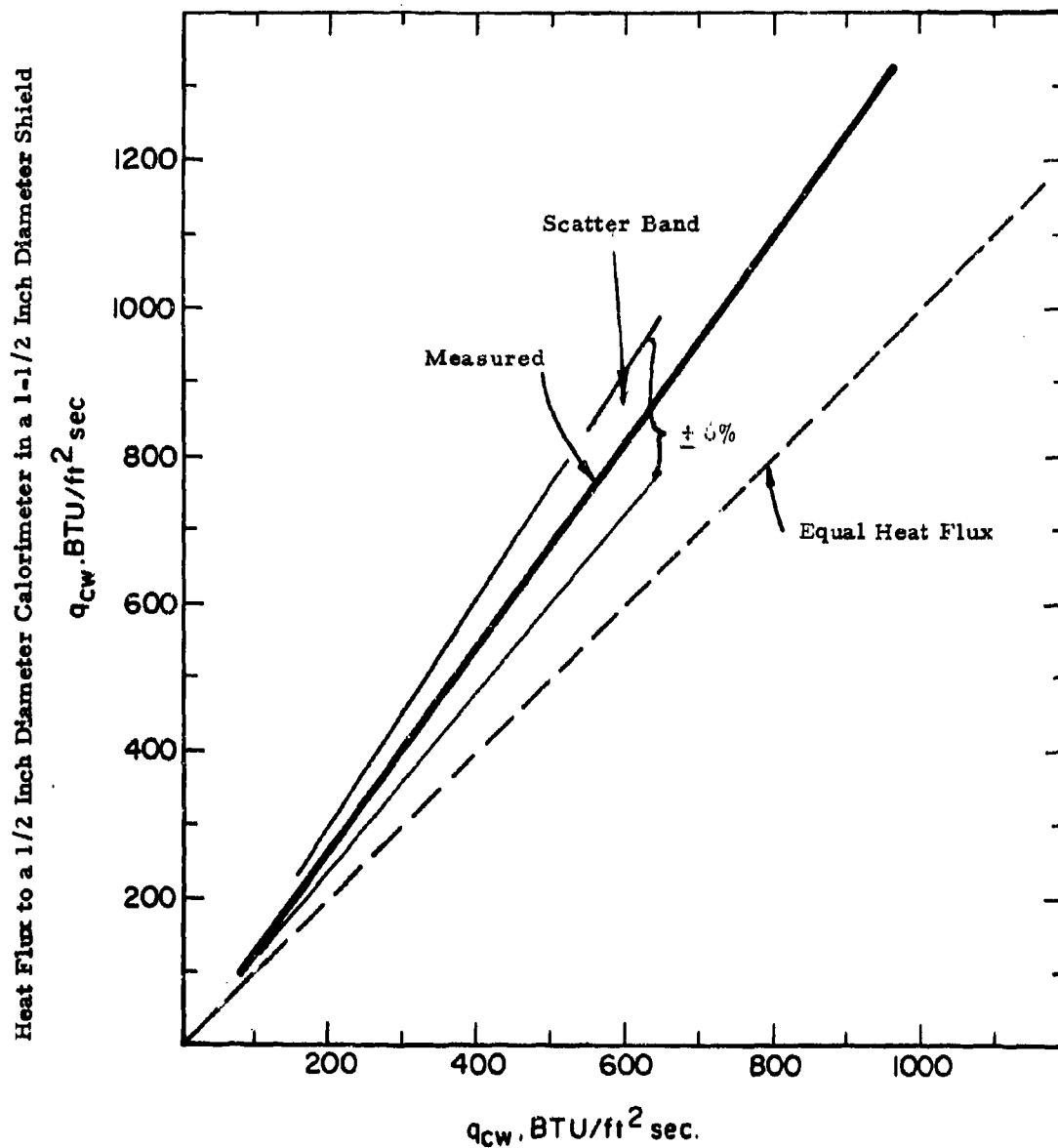


Figure 12. Comparison of Cold Wall Heat Fluxes to Avco Water Cooled Calorimeters Having 1/2 and 3/4 Inch Diameters Enclosed in 1-1/2 Inch Diameter Shields in the Model 500 Arc.

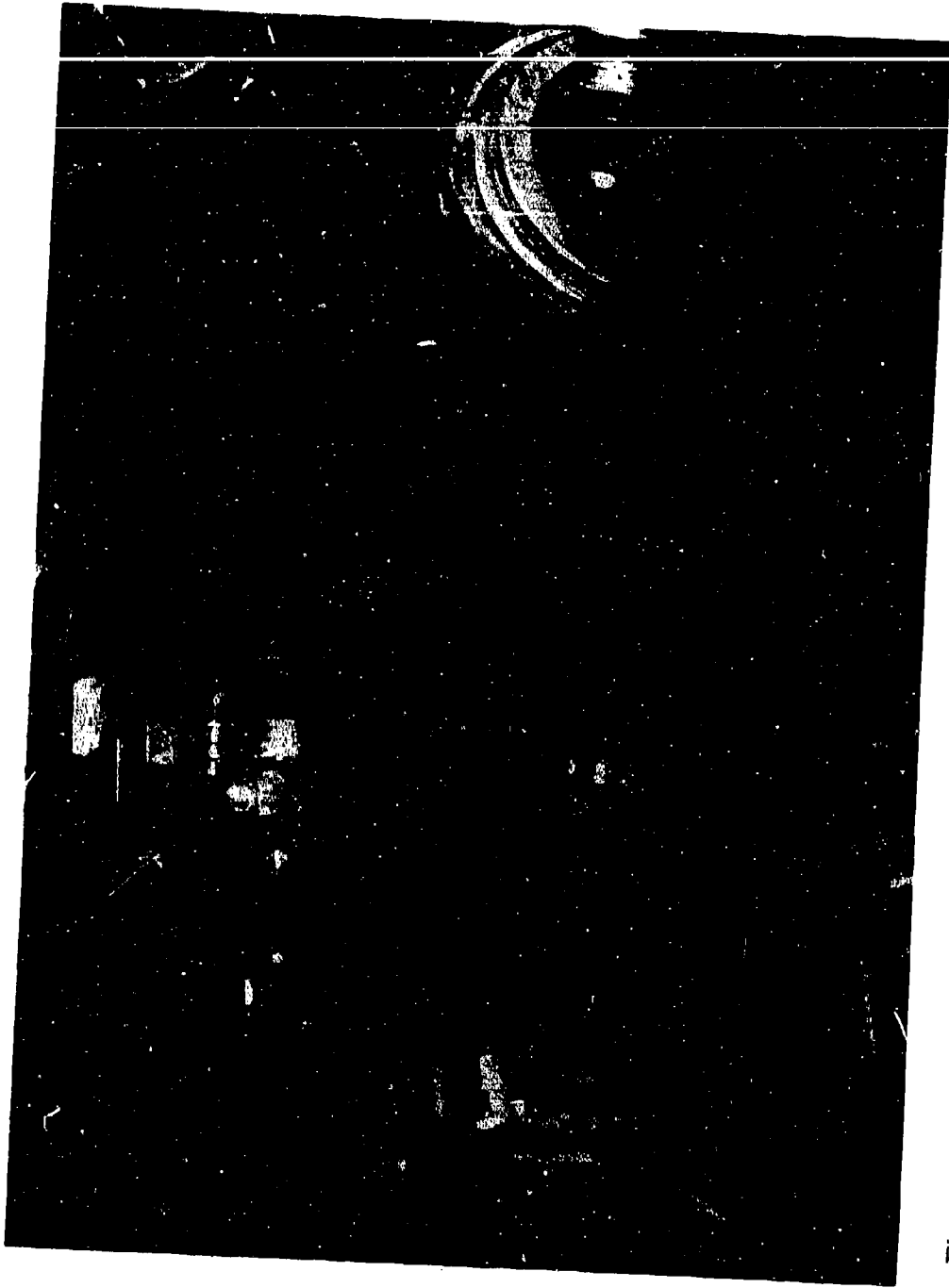


Figure 13. Stagnation Pressure Probe Mounted in Test Position in the Model 500 (#18146E).



Figure 14. Stagnation Pressure Probe During Test in the Model 500 (#18146H).



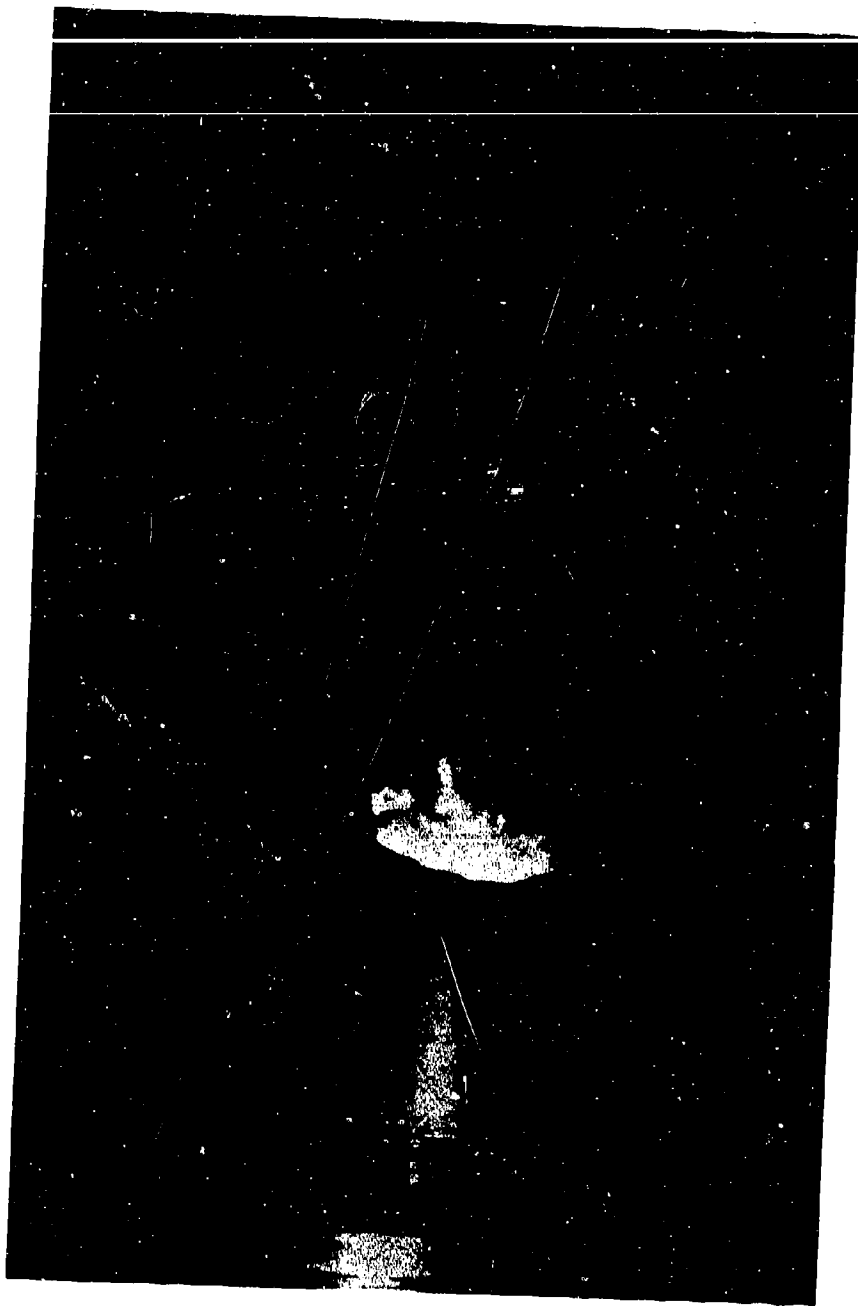


Figure 15. Specimen No.  $\text{HfB}_2 + \text{SiC(A-4)A-4-24M}$  During Test in the Model 500 (#18146J).

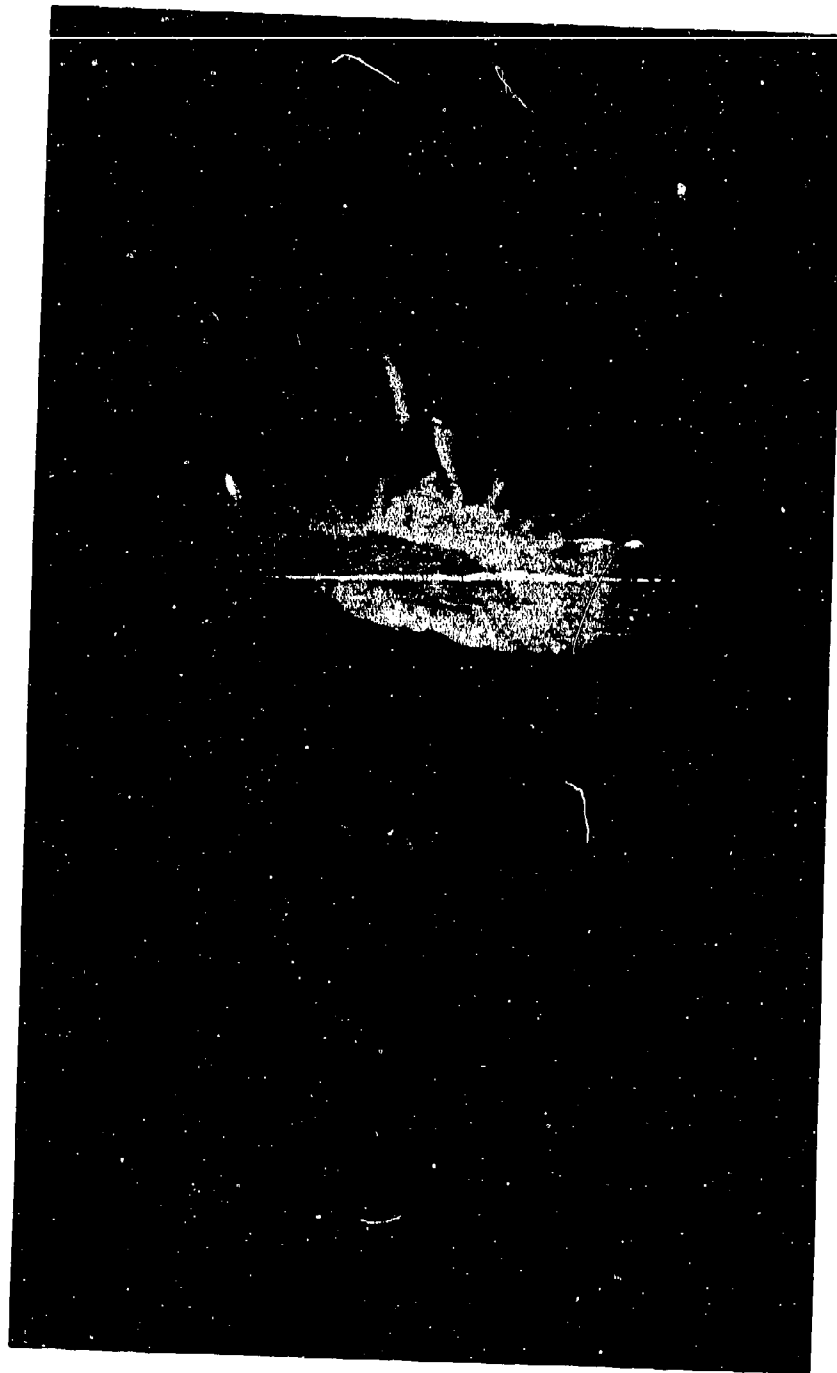
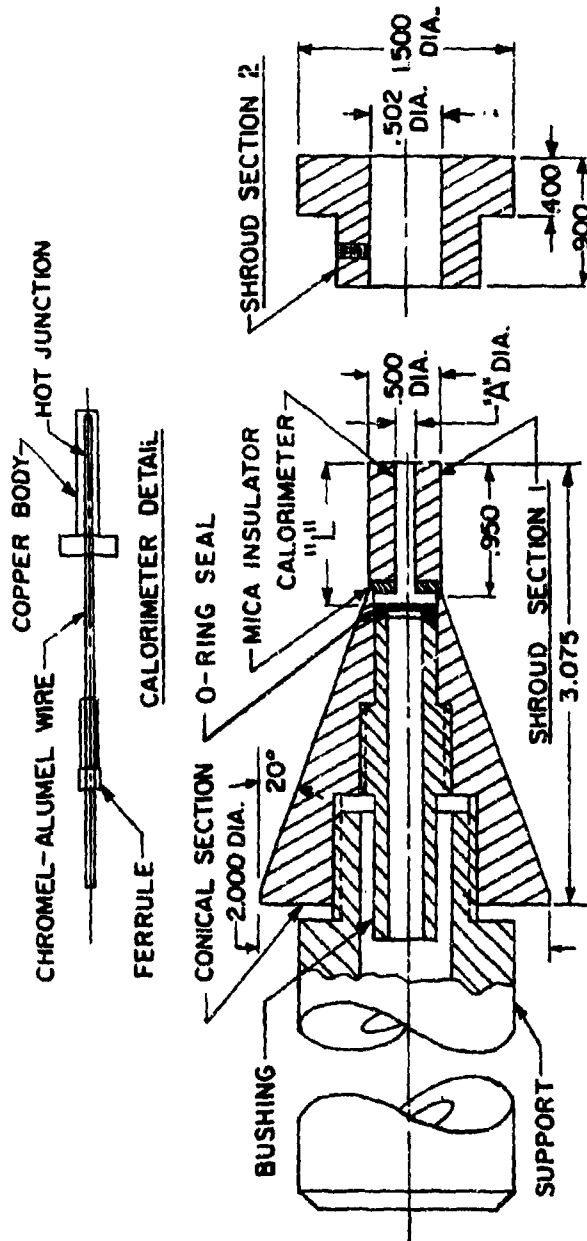


Figure 16. Close-up View of Specimen No.  $\text{HfB}_2$  +  $\text{SiC(A-4)A-4-2-4M}$  During Test in the Model 500 (#18146K).



A"	CALORIMETER DIA	L"	SHROUD SECTION EMPLOYED					
			TEST NO. 1	TEST NO. 2	TEST NO. 3	TEST NO. 4	TEST NO. 5	TEST NO. 6
.125		1.000						
.250		1.500						
.375		1.500						
.450		1.500						
.500		1.500						

Figure 17. Cross-sectional View of the Transient Calorimeter.

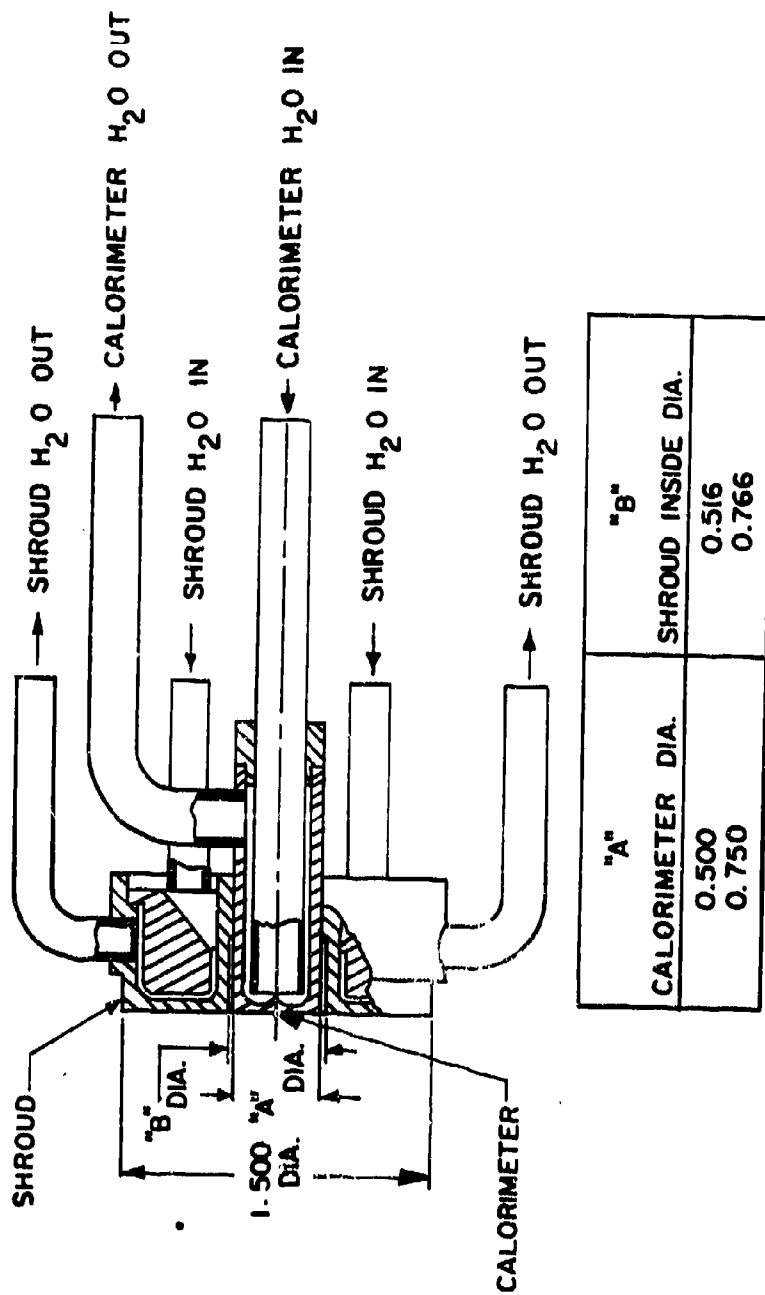


Figure 18. Cross-sectional View of the Steady State Calorimeter



Figure 19. Test Sample Being Exposed in the Model 500 Arc



Figure 20. Transient Calorimeter (0.500 inch diameter shroud) Measurement of Heat Flux in the Model 500.

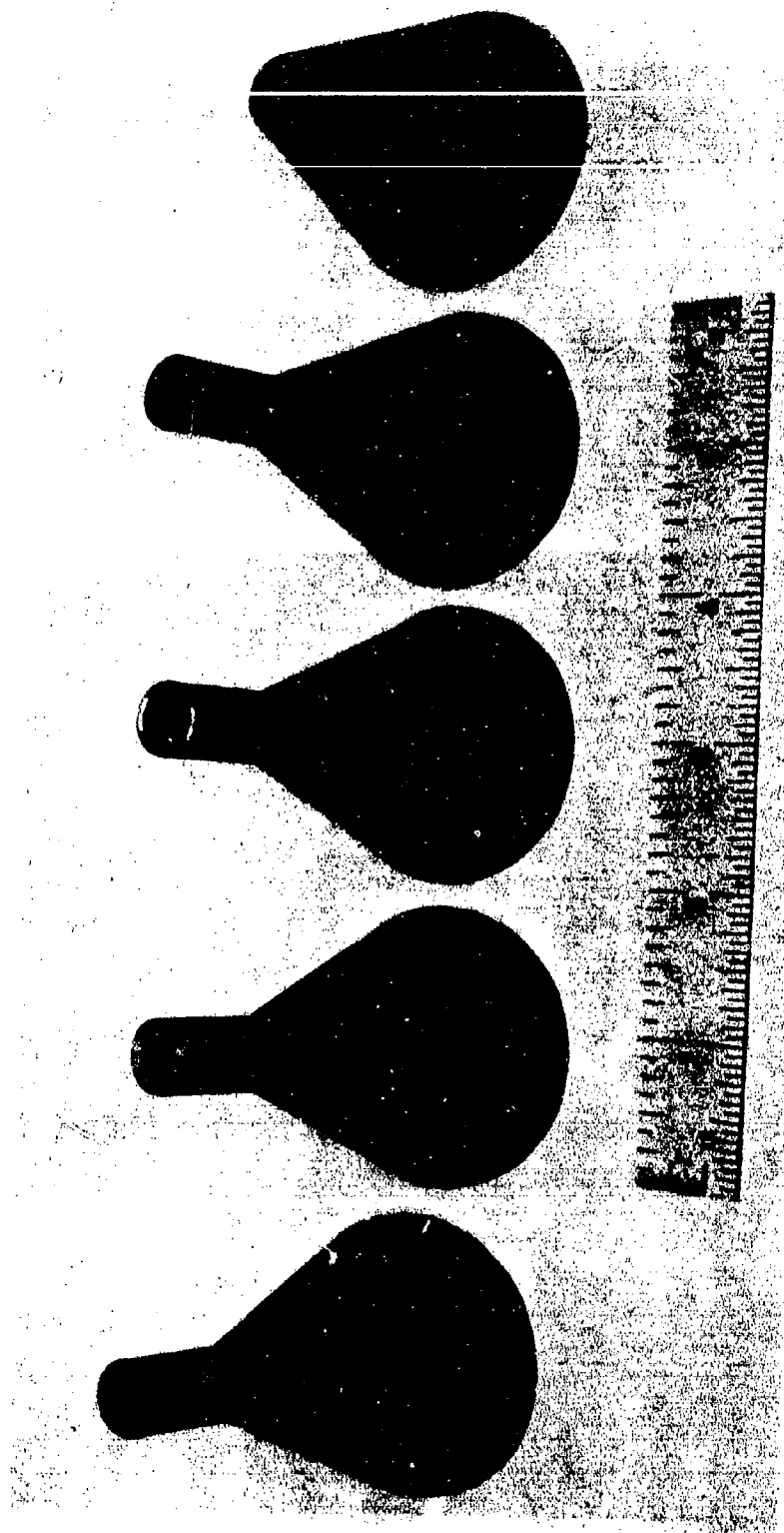


Figure 21. Transient Calorimeters, Shrouds and Conical Sections.

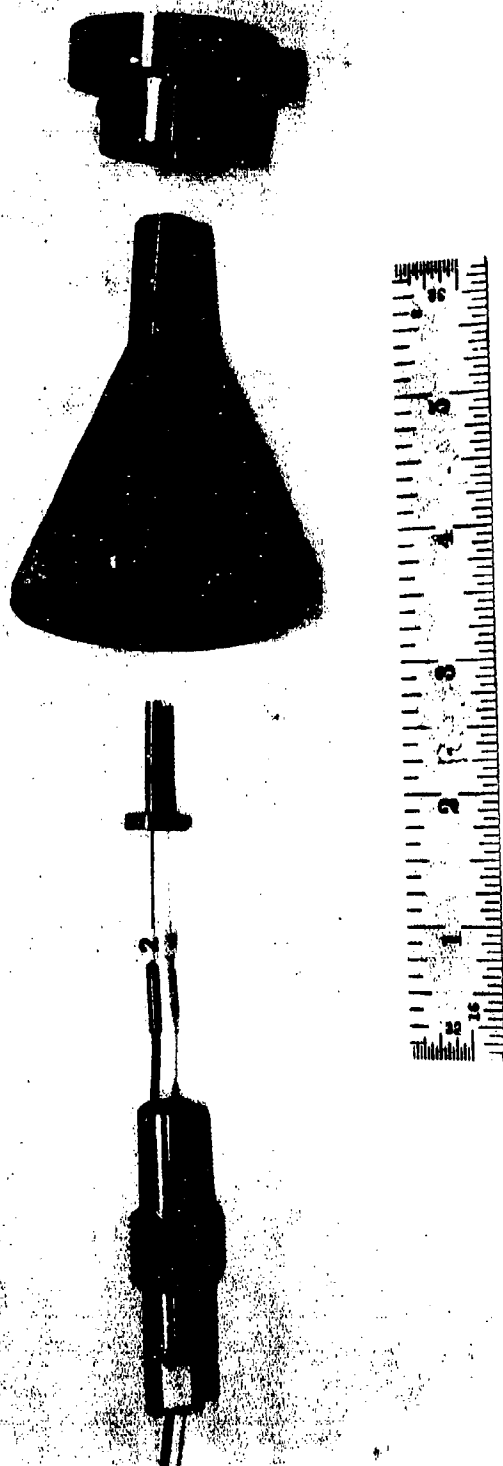


Figure 22. Transient Calorimeter (0.125 inch Diameter)



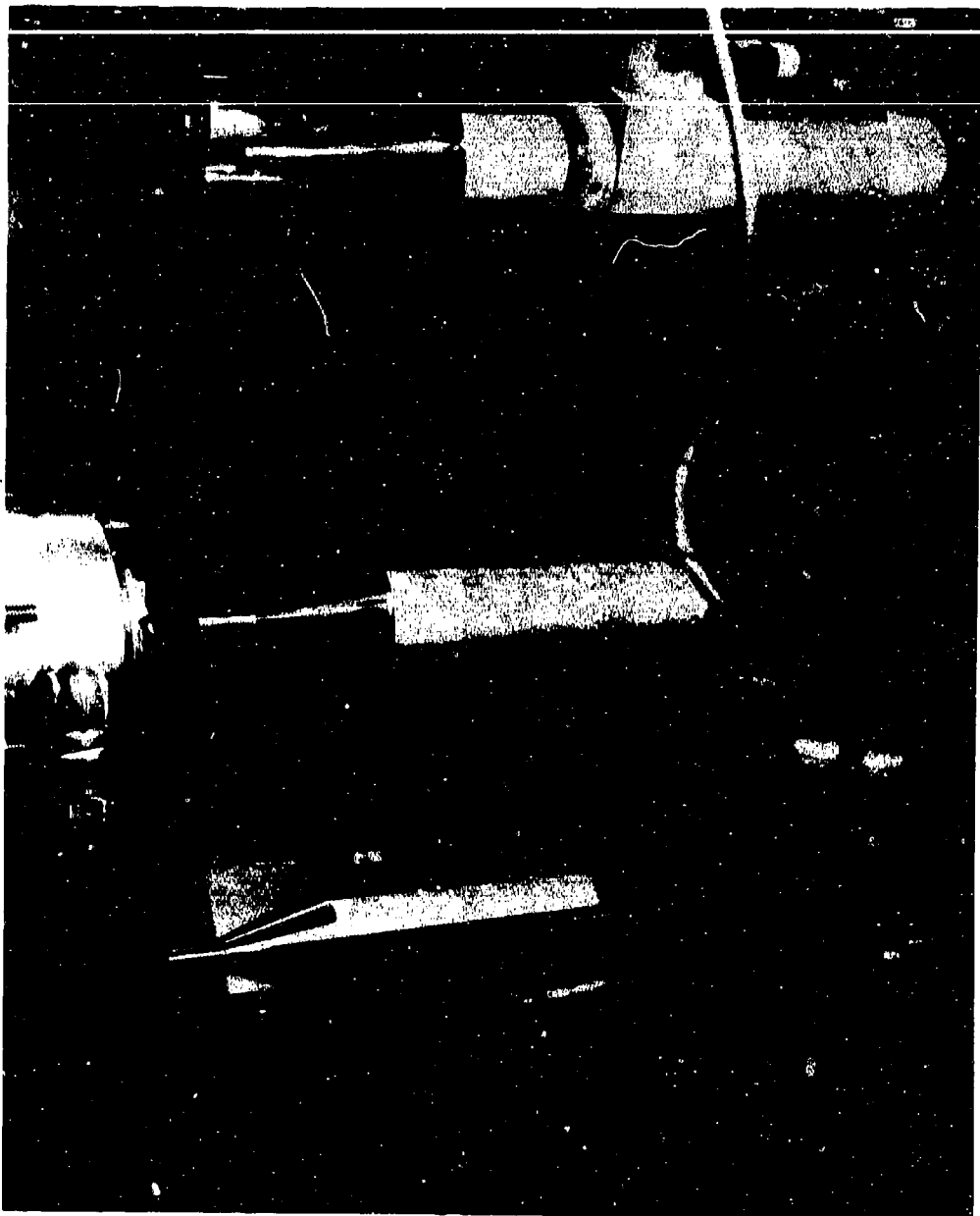


Figure 23. Calorimeters Mounted on Remote Controlled Stings in the Model 500 Arc.

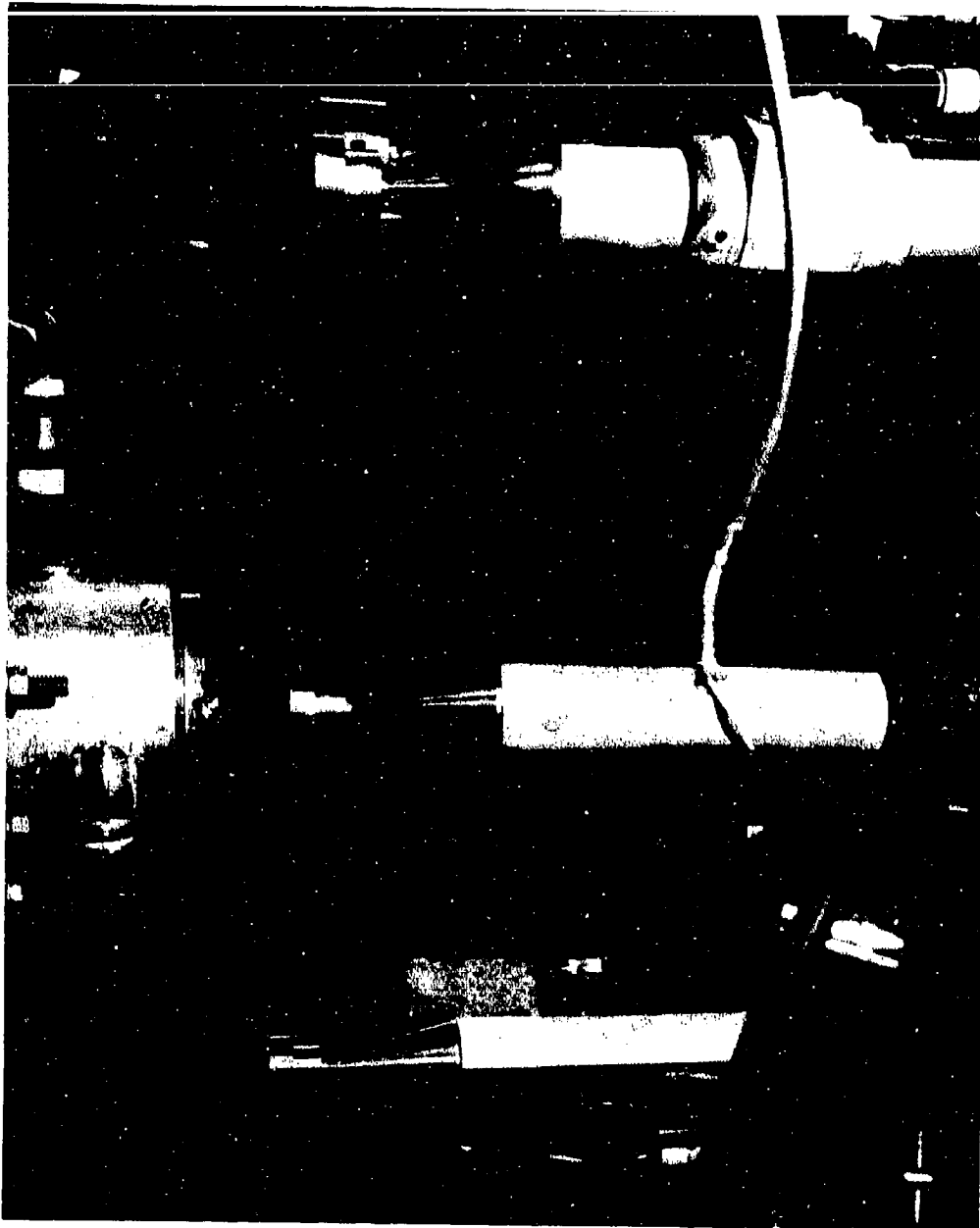


Figure 24. Calorimeters Mounted on Remote Controlled Stings. Transient Calorimeters Installed in 1.500 inch shrouds in the Model 500 Arc.

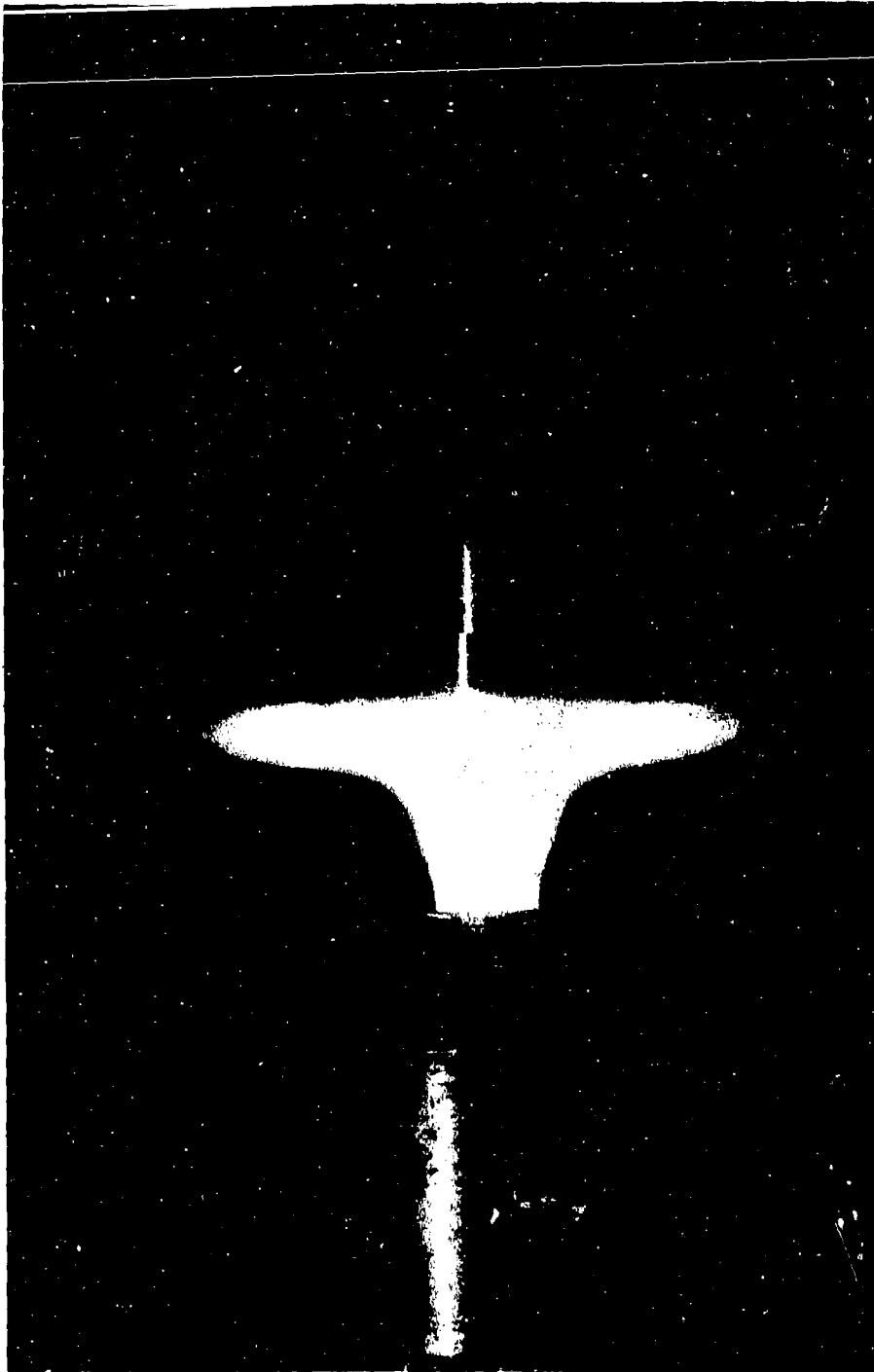


Figure 25. Transient Calorimeter with 1.500 Inch Diameter Shroud During Test in the Model  
500 Arc.

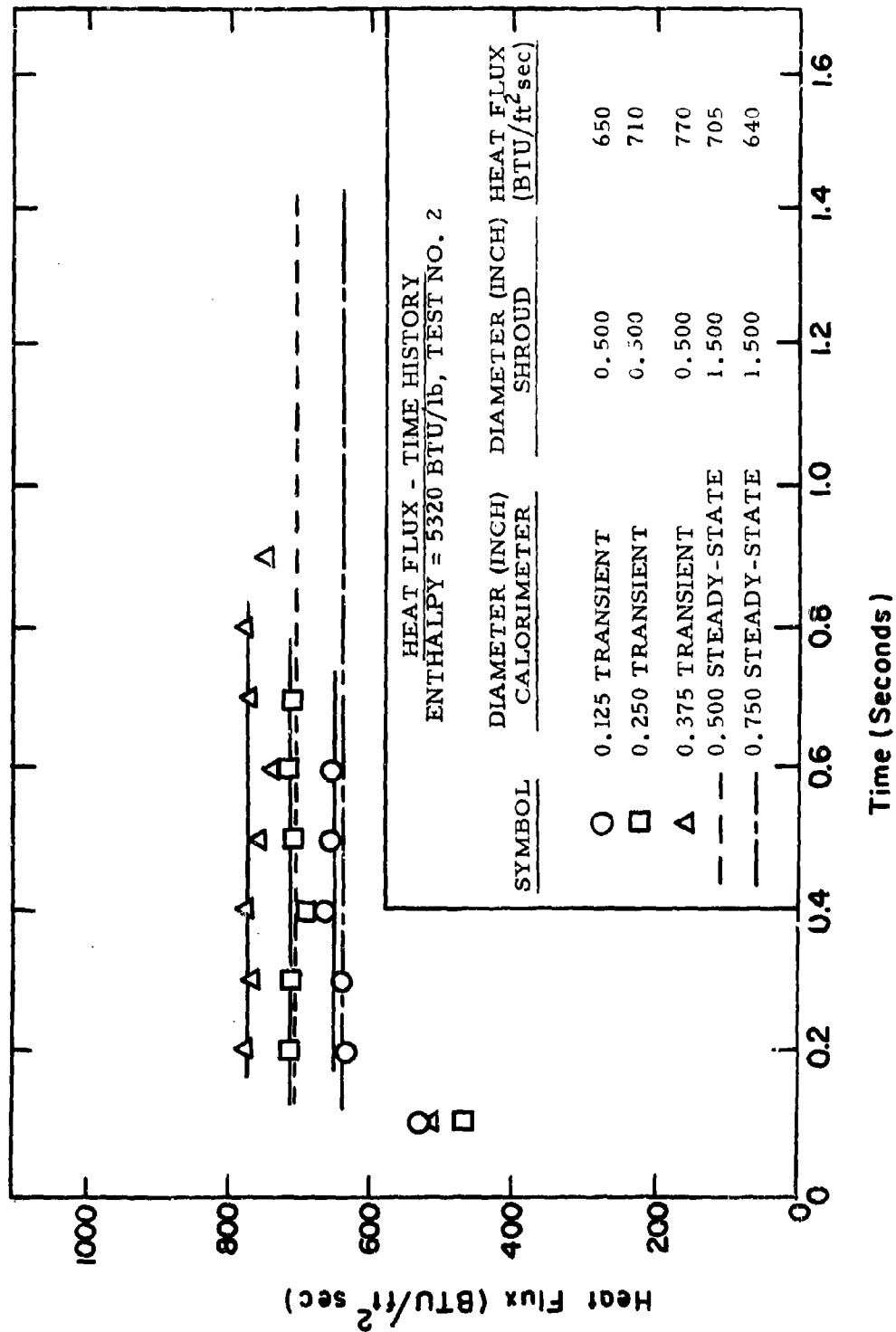


Figure 26. Transient Calorimeter Measurement of Heat Flux as a Function of Time in the Model 500 Arc.

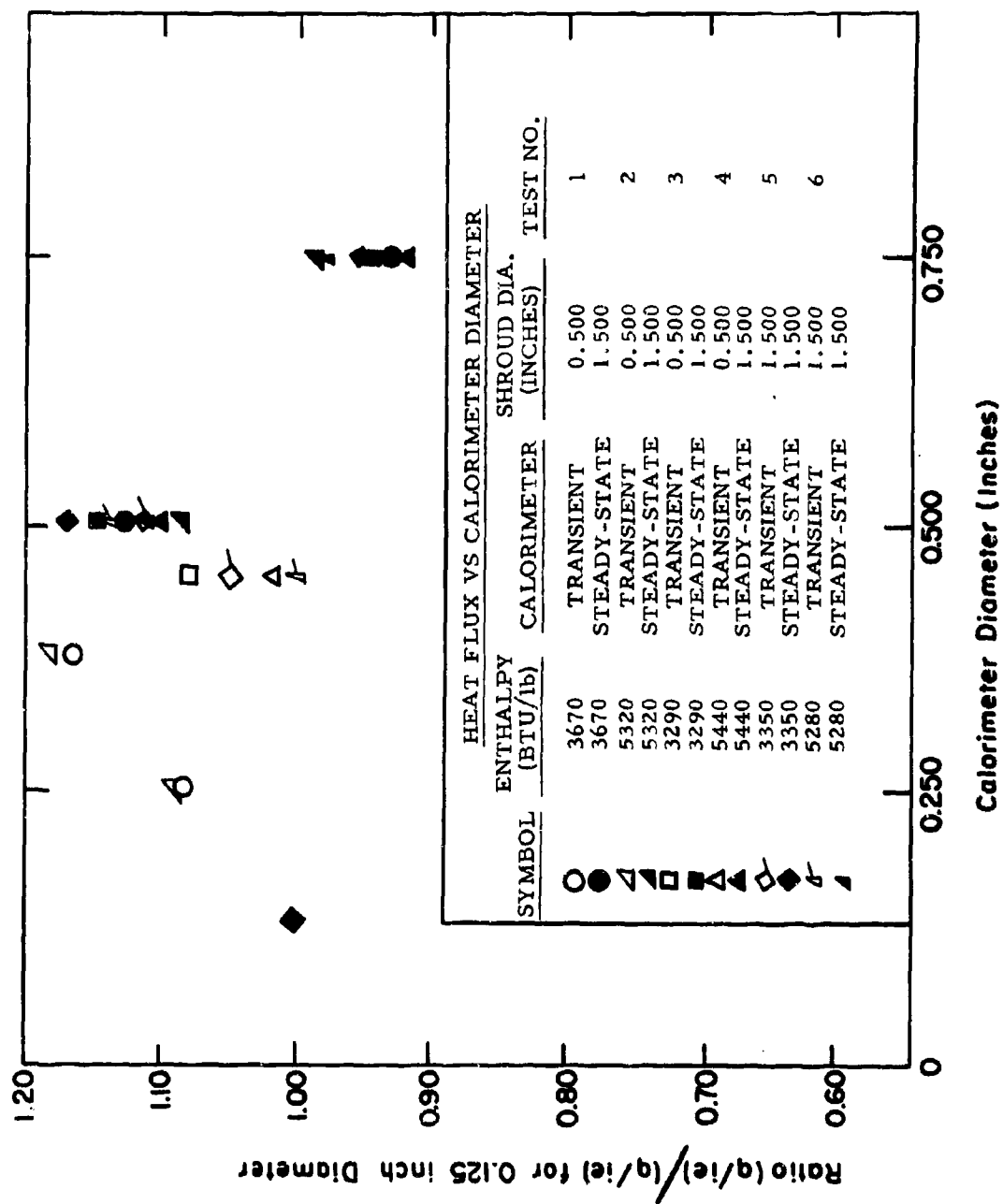


Figure 27. Ratio of Heat Transfer Coefficients as a Function of Calorimeter Diameter and Shroud Diameter in the Model 500 Arc.

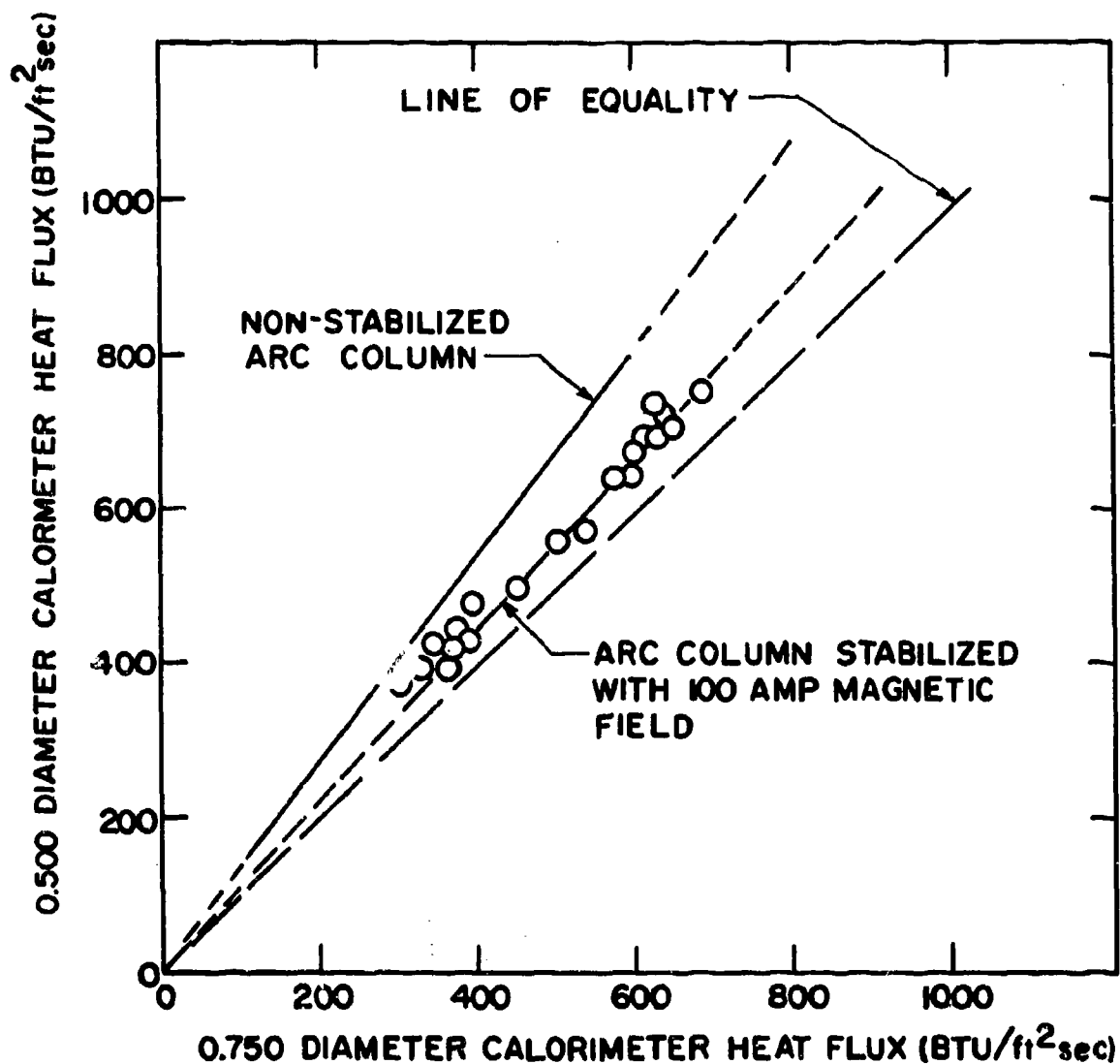


Figure 28. Comparison of Heat Fluxes Measured With 0.500 Inch Diameter and 0.750 Inch Diameter Calorimeters in 1.500 Inch Shrouds in the Model 500 Arc.

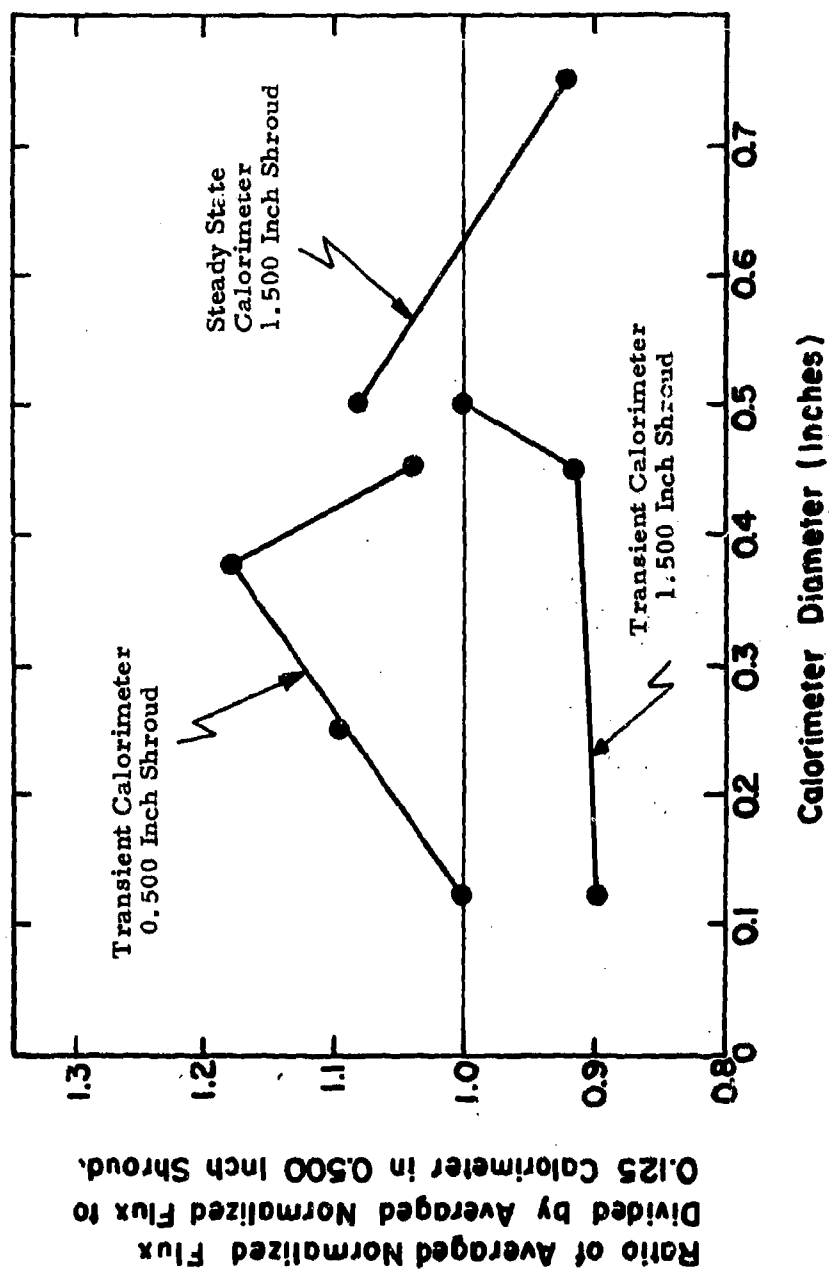


Figure 29. Effect of Calorimeter Diameter and Shroud Size on Heat Flux in the Model 500 Facility.

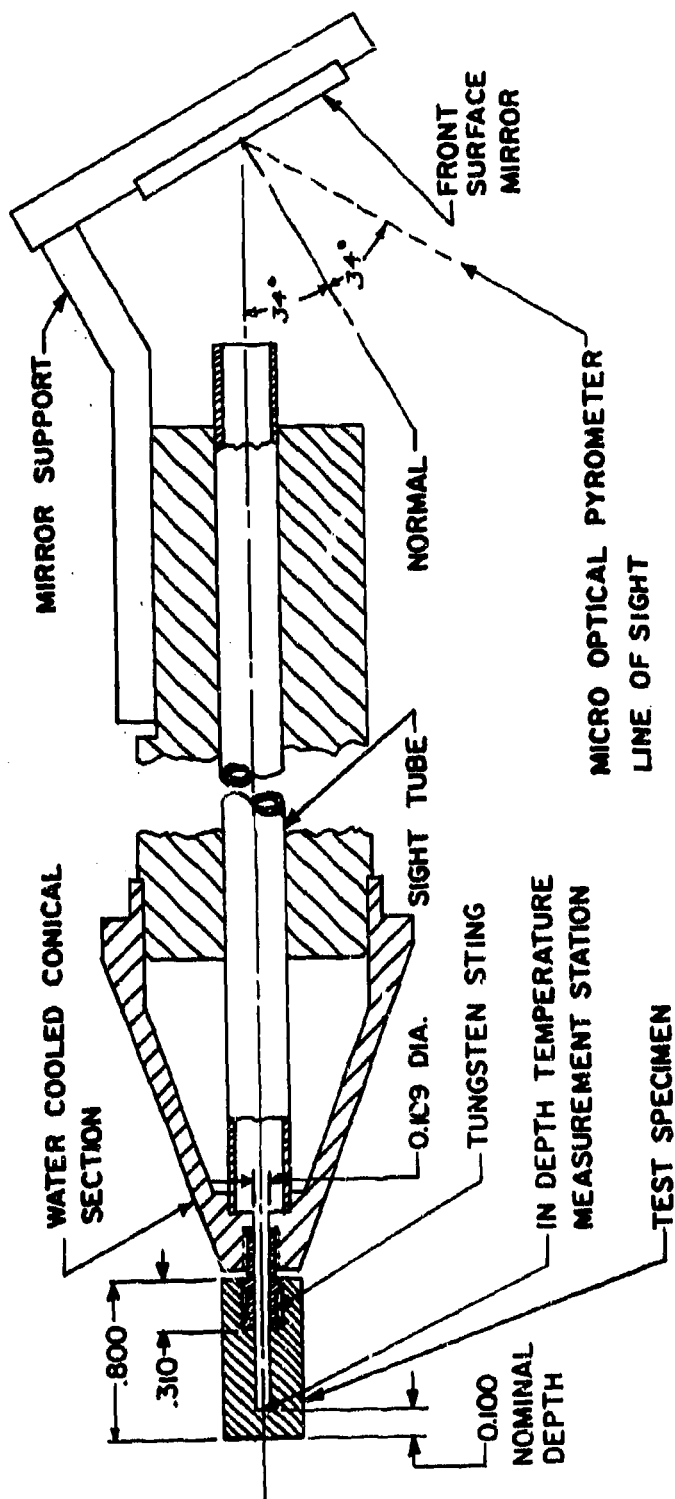


Figure 30. Cross-Sectional View of the Model Holder for In-Depth Temperature Measurements in the Model 500 Arc.



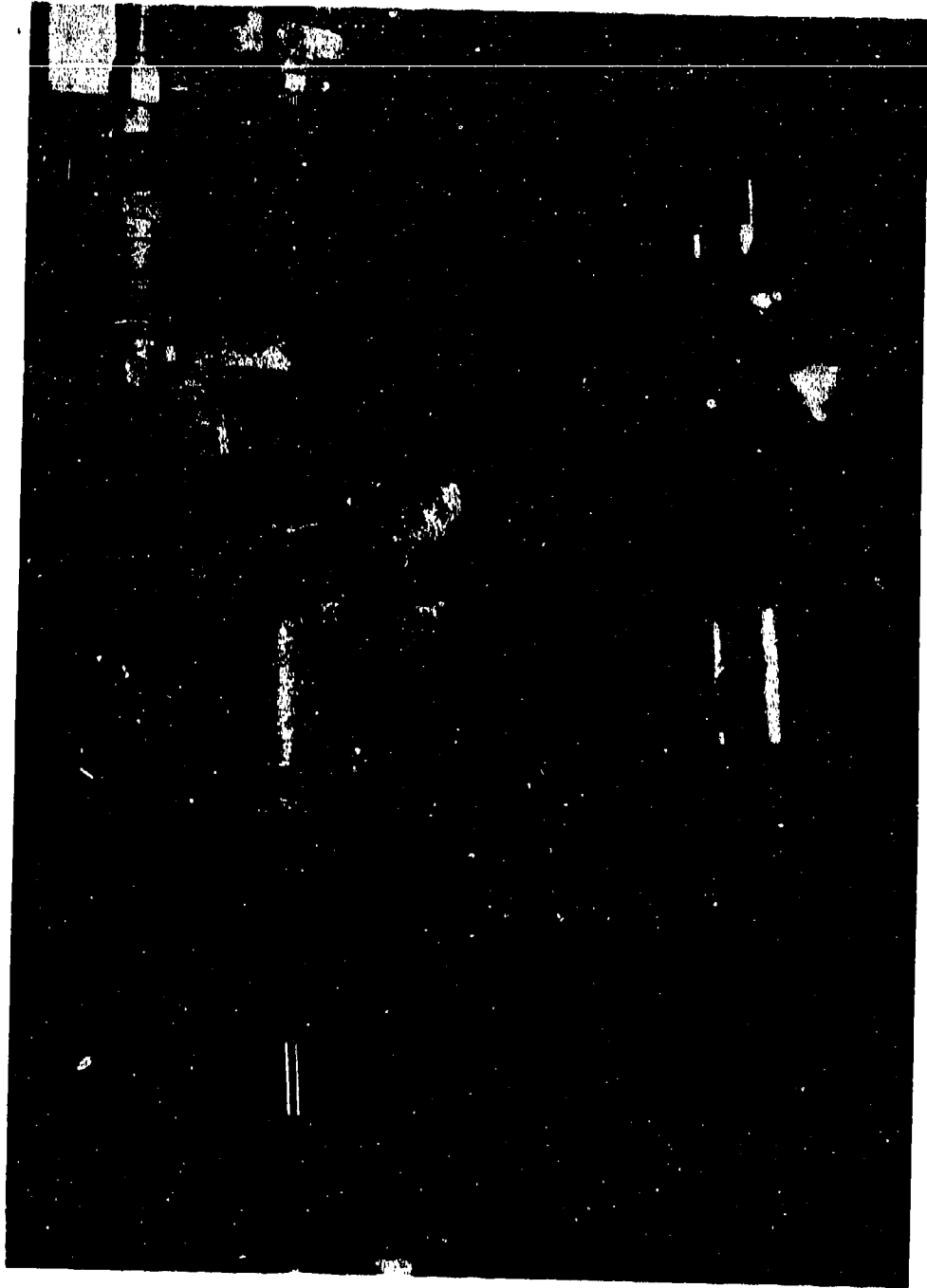


Figure 31. Water Cooled Model Holder and Test Sample Employed for Measurement of Internal Temperature Gradients in the Model 500 Arc.

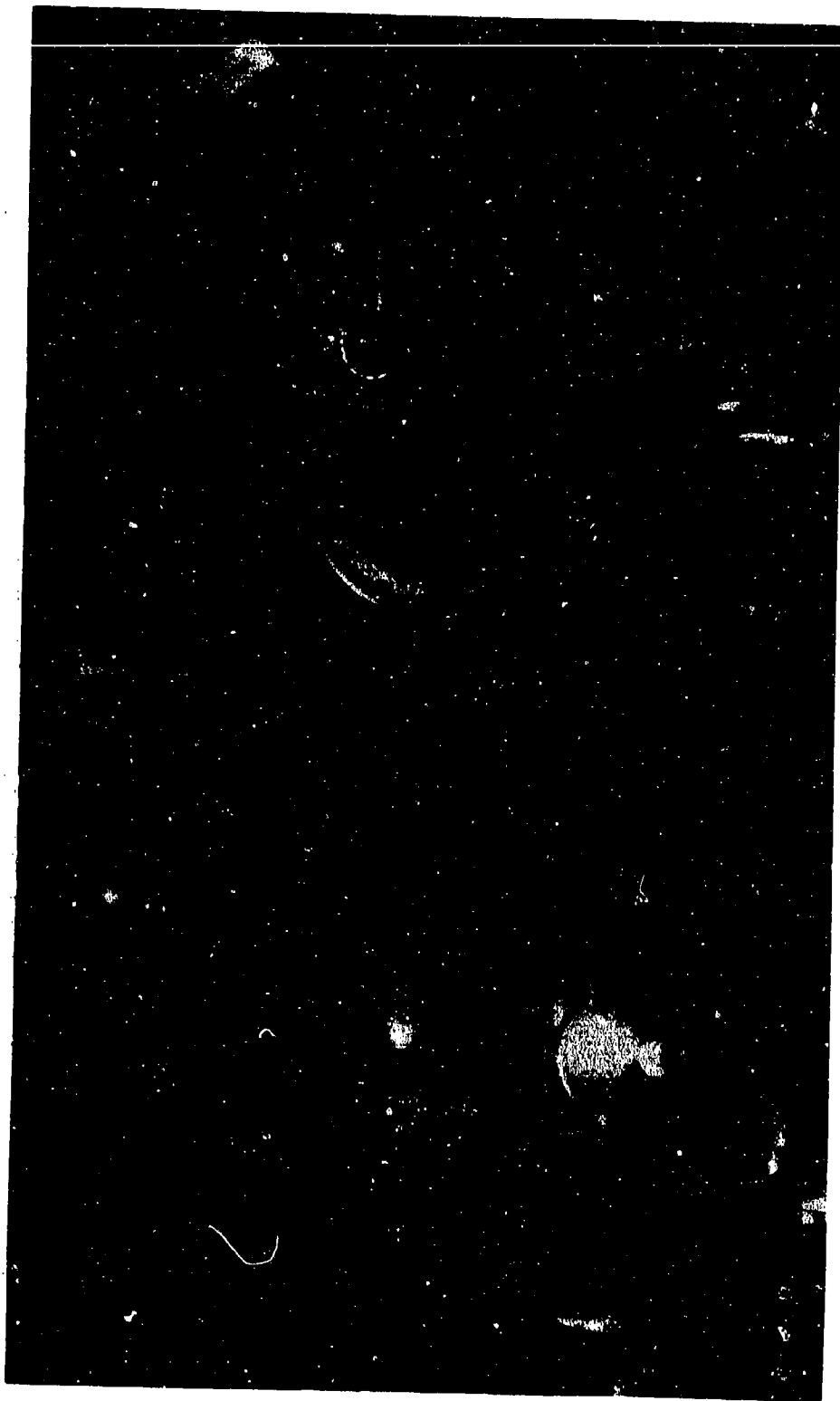


Figure 32. Experimental Arrangement for Measurement of Internal Temperature Gradients in the Model 500 Arc.



Side View of Sample  $\text{ZrB}_2$  (A-3)-2MC During Exposure in the  
Model 500 Arc.

Figure 33.

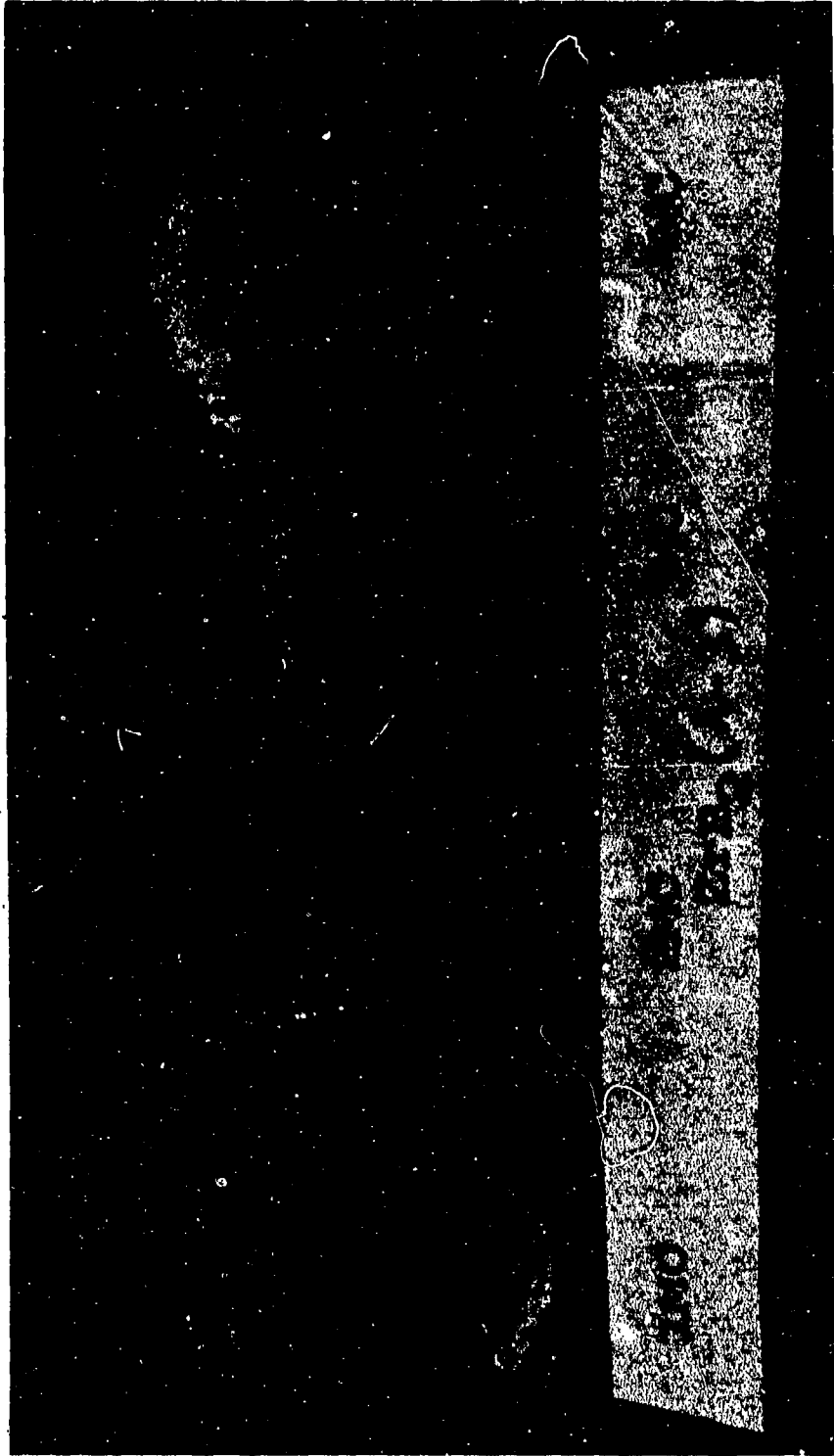


Figure 34. Post Exposure Photographs of Samples  $ZrB_2$  (A-3)-1MC, 2MC, 3MC and 4MC after Testing in the Model 500 Arc.

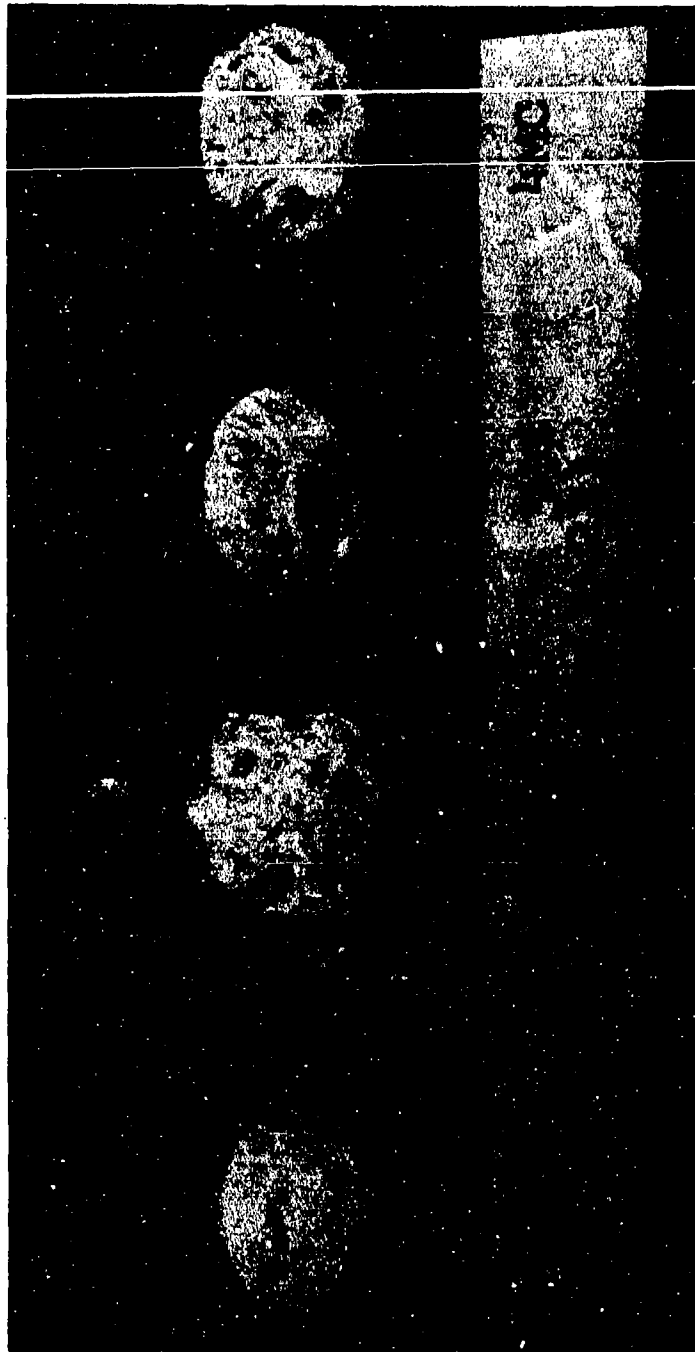


Figure 35. Post Exposure Photographs of Samples Hf-Ta-Mo(1-23) - 1MC, 2MC, 3MC and 4MC after Testing in the Model 500 Arc.

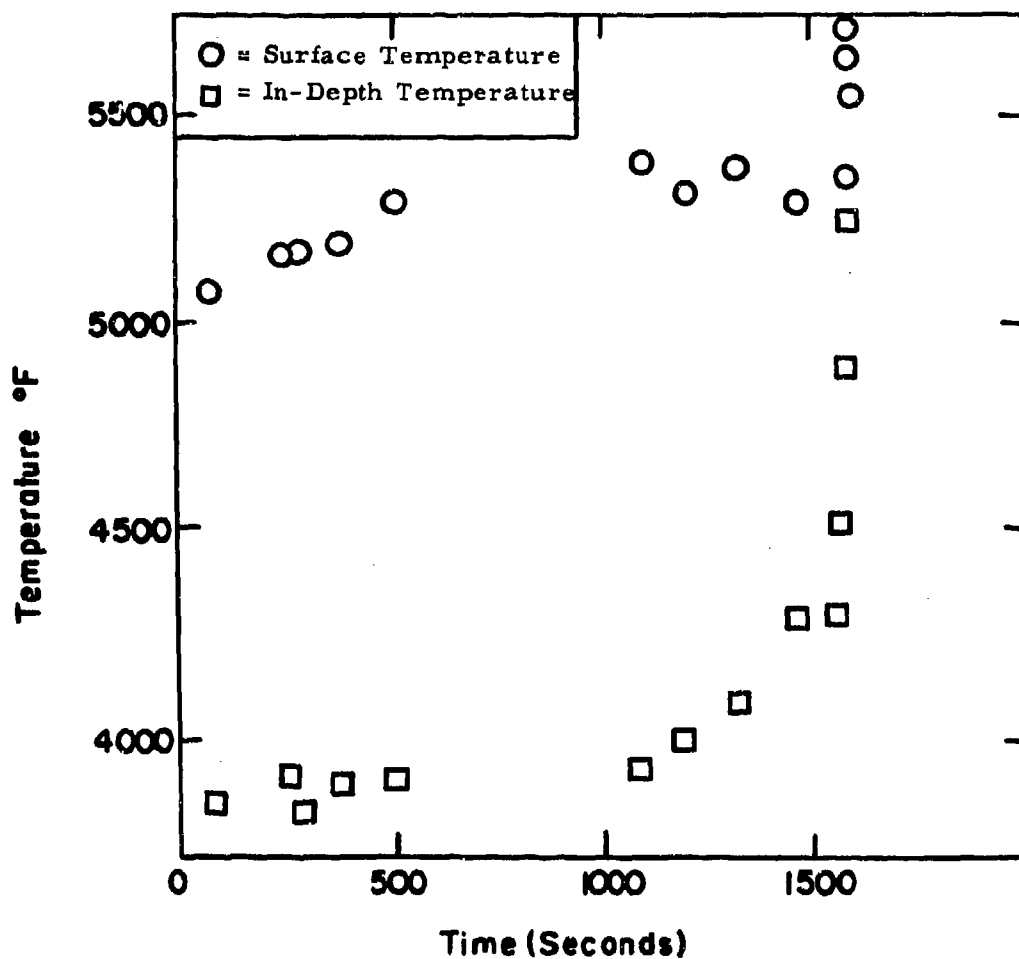


Figure 36. Time-Temperature History for Surface Temperature and In-Depth Temperature (100 mils From Surface) for Sample Hf-Ta-Mo (I-23-3MC),  $P = 1$  atm,  $i_s = 3380$  BTU/lb,  $q = 510$  BTU/ft<sup>2</sup>sec Exposed in the Model 500 Arc.

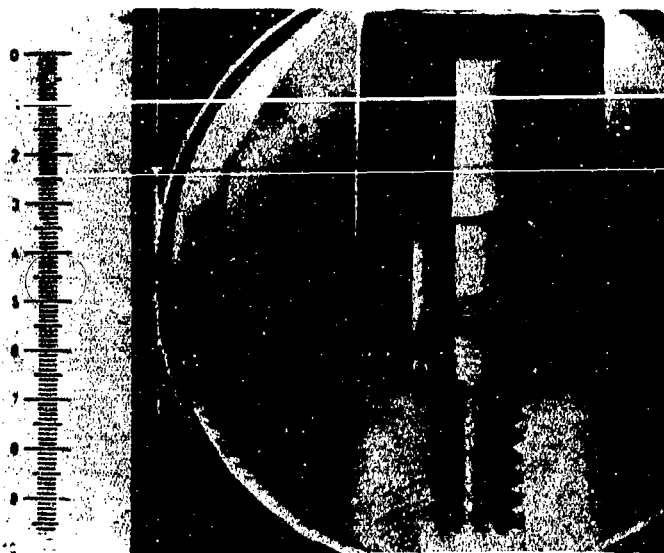


Plate No.  
1-9213

X3.00

Figure 37. Arc Plasma Test  $\text{ZrB}_2(\text{A-3})\text{-2MC}$ , Surface Temperature  $4470^\circ\text{F}$ , Internal Temperature  $2850^\circ\text{F}$ , Exposure Time 1800 Seconds, Stagnation Pressure 1.05 atm., Stagnation Enthalpy 3230 BTU/lb, Cold Wall Heat Flux  $365 \text{ BTU/ft}^2\text{sec}$ , 33 Mil Recession. Hot Face Up. One Inch Scale.

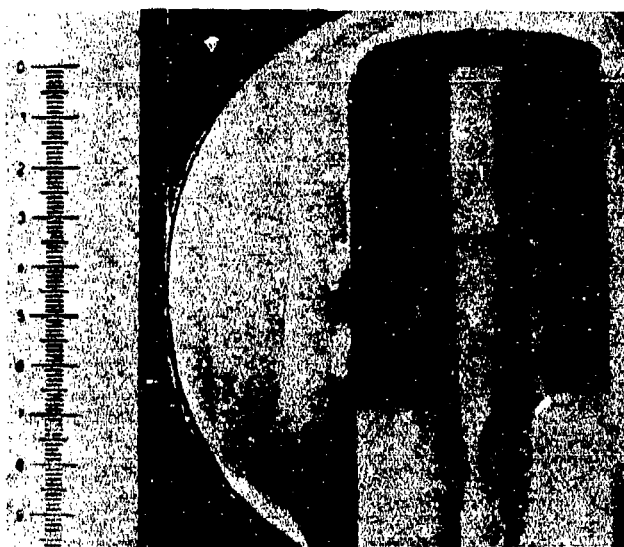


Plate No.  
1-9224

X3.00

Figure 38. Arc Plasma Test  $\text{Hf-20Ta-2Mo(I-23)-1MC}$ , Surface Temperature  $4760^\circ\text{F}$ , Internal Temperature  $3500^\circ\text{F}$ , Exposure Time 1800 Seconds, Stagnation Pressure 1.05 atm., Stagnation Enthalpy 3220 BTU/lb, Cold Wall Heat Flux  $425 \text{ BTU/ft}^2\text{sec}$ , 46 Mil Recession. Hot Face Up. One Inch Scale.



Figure 39. Hemispherical Tip Transient Calorimeter (Photo #19856B).



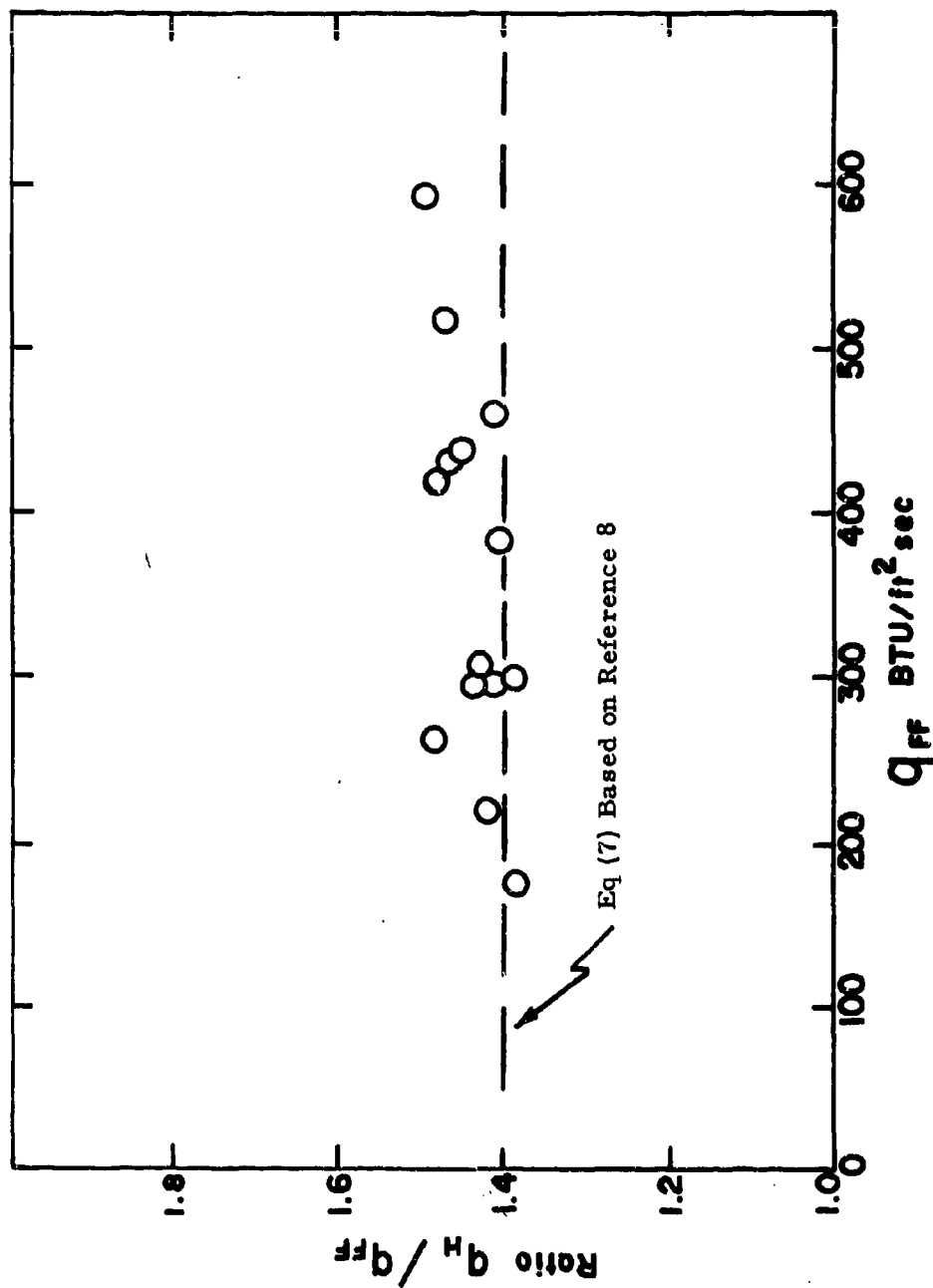
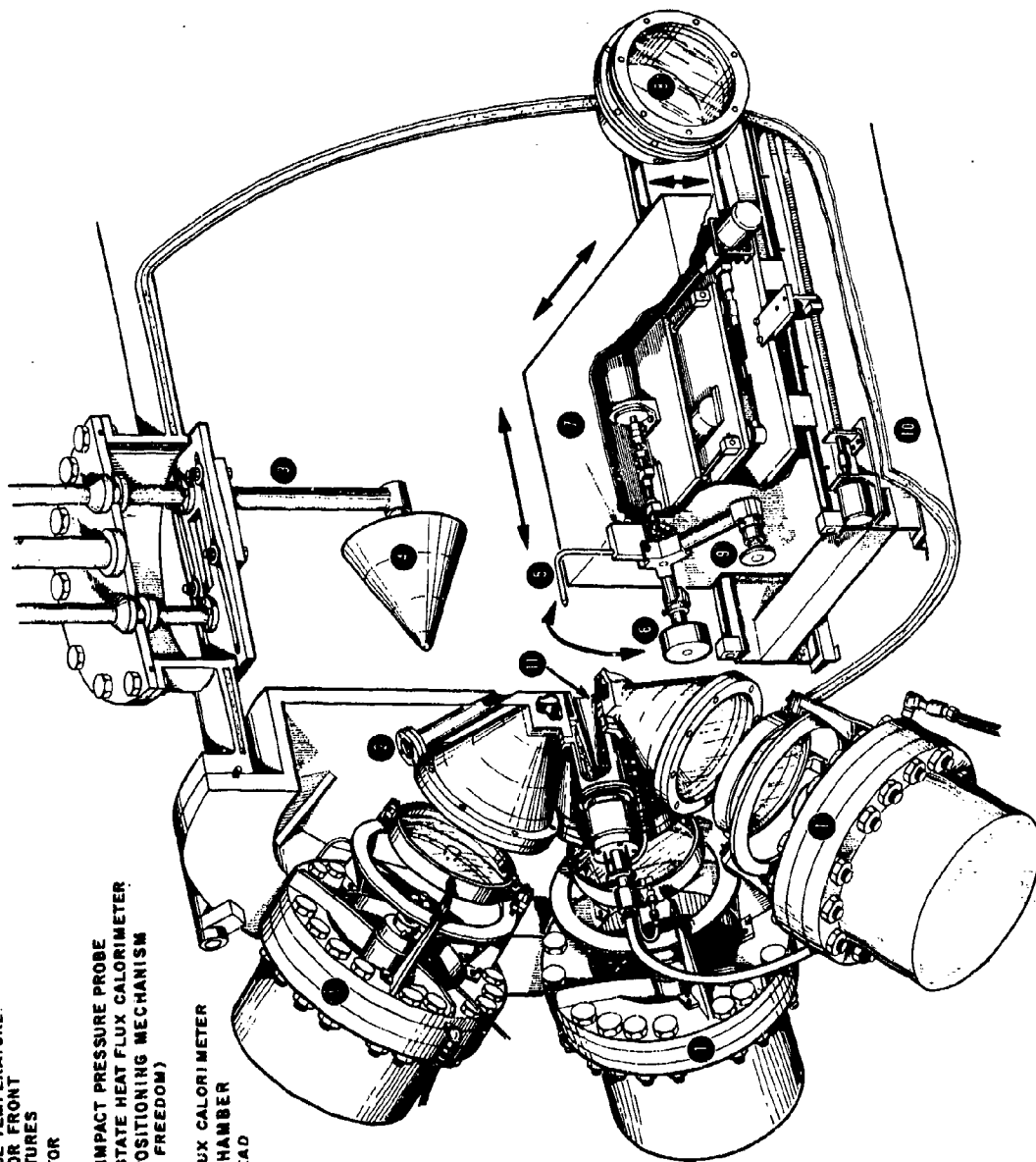


Figure 40. Comparison of Heat Flux Measurements with a 0.125 inch diameter calorimeter in a 0.500 inch diameter hemispherical shroud ( $q_H$ ) and a 0.500 inch diameter calorimeter in a 1.500 inch diameter flat faced shroud ( $q_{FF}$ ) in the Model 500 Facility. Stream Diameter = 0.60 inches.

- 1 RADIANT LAMP ( RADIATION SOURCE)
- 2 VIEW PORT FOR SURFACE TEMPERATURE MEASUREMENT AND / OR FRONT SURFACE MOTION PICTURES
- 3 LARGE MODEL INJECTOR
- 4 LARGE TEST MODEL
- 5 ENTHALPY PROBE & IMPACT PRESSURE PROBE
- 6 MODEL OR STEADY- STATE HEAT FLUX CALORIMETER
- 7 PROBE AND SAMPLE POSITIONING MECHANISM ( THREE DEGREES OF FREEDOM)
- 8 OBSERVATION PORT
- 9 TRANSIENT HEAT FLUX CALORIMETER
- 10 ENVIRONMENTAL CHAMBER
- 11 CONVECTIVE ARC HEAD



SECTIONAL VIEW OF ROVERS FACILITY

Figure 41.

26-2500

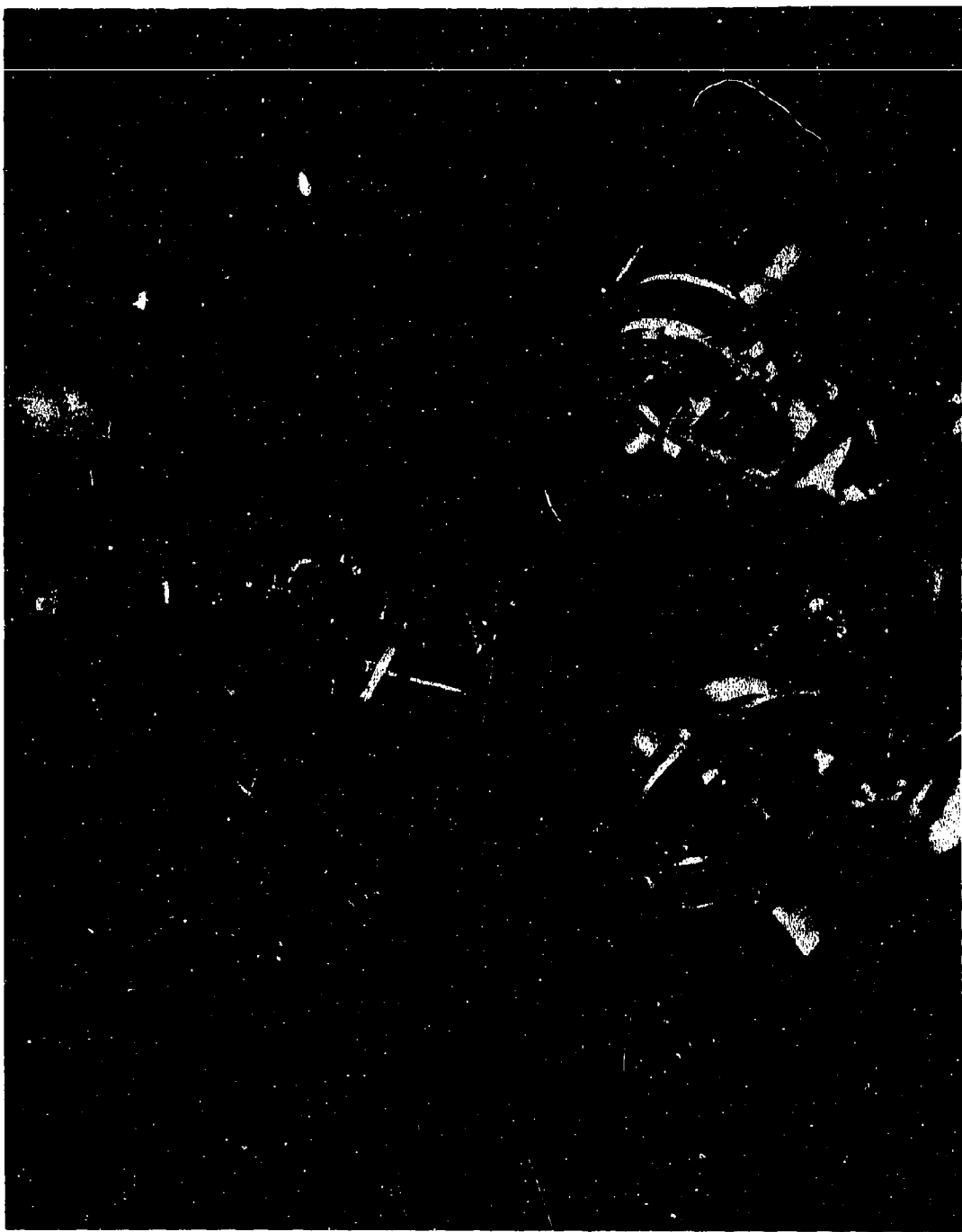


Figure 42. ROVERS Arc Facility (#14951E).

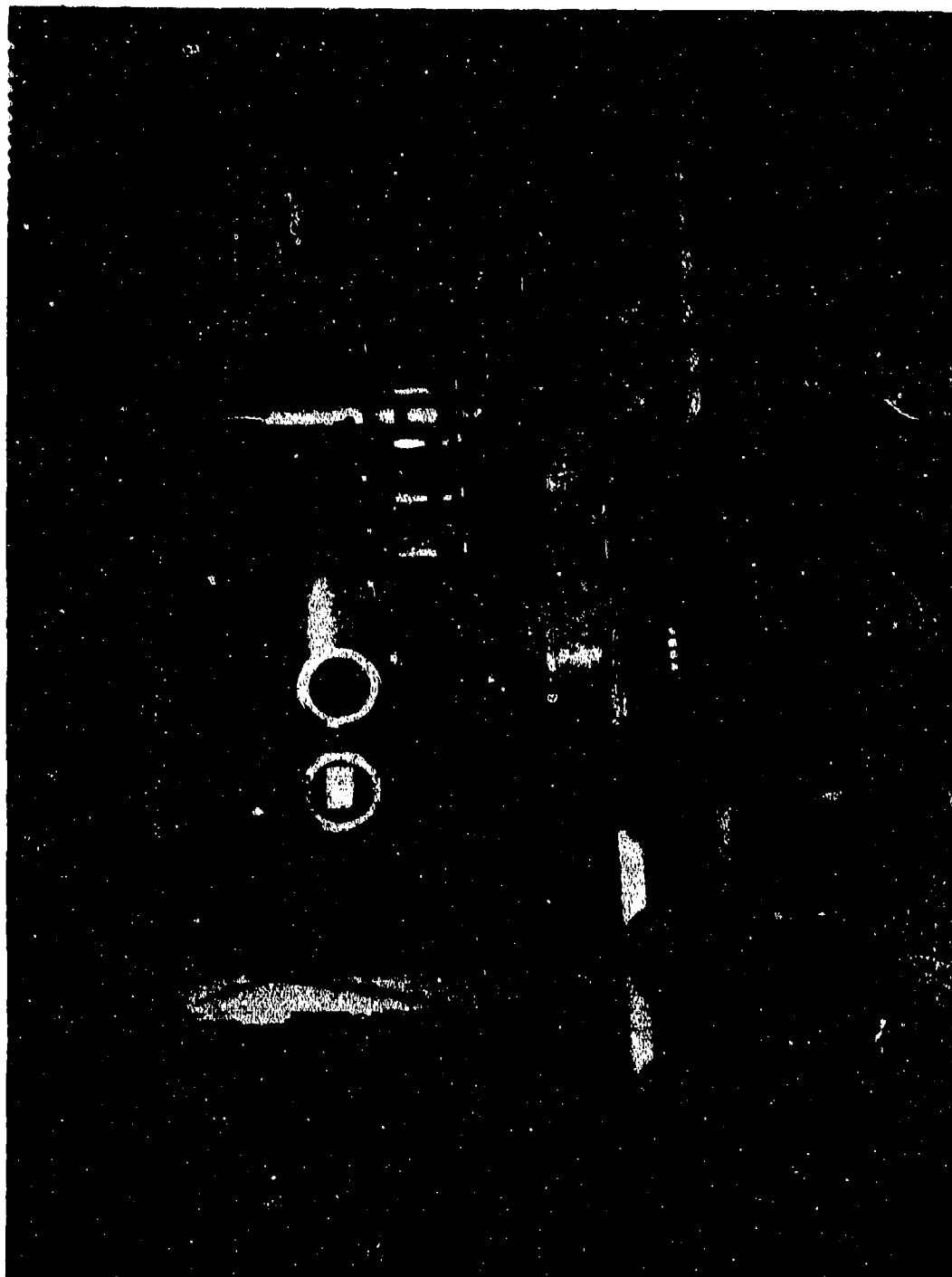


Figure 43. ROVERS Arc Facility Operating (View from Control Room) (#14951B).



Figure 44. RVA Graphite Cylinder Prior to Exposure in the Avco-SSD ROVERS Facility.



Figure 45. RVA Graphite Cylinder During Exposure in the Avco-SSD ROVERS Facility.

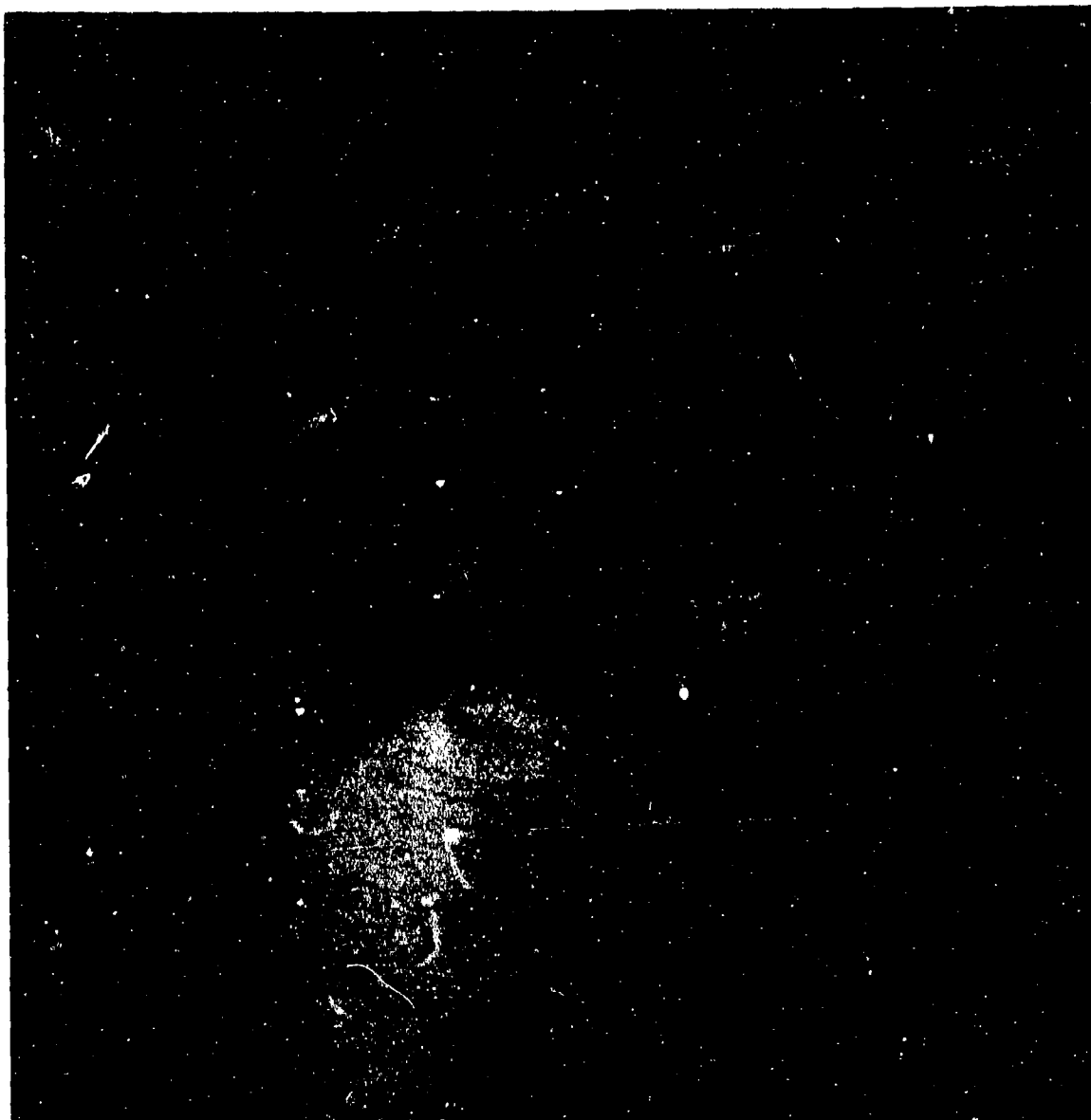


Figure 46. Water Calorimeter Mounted in Test Position in ROVERS Arc (#18156).

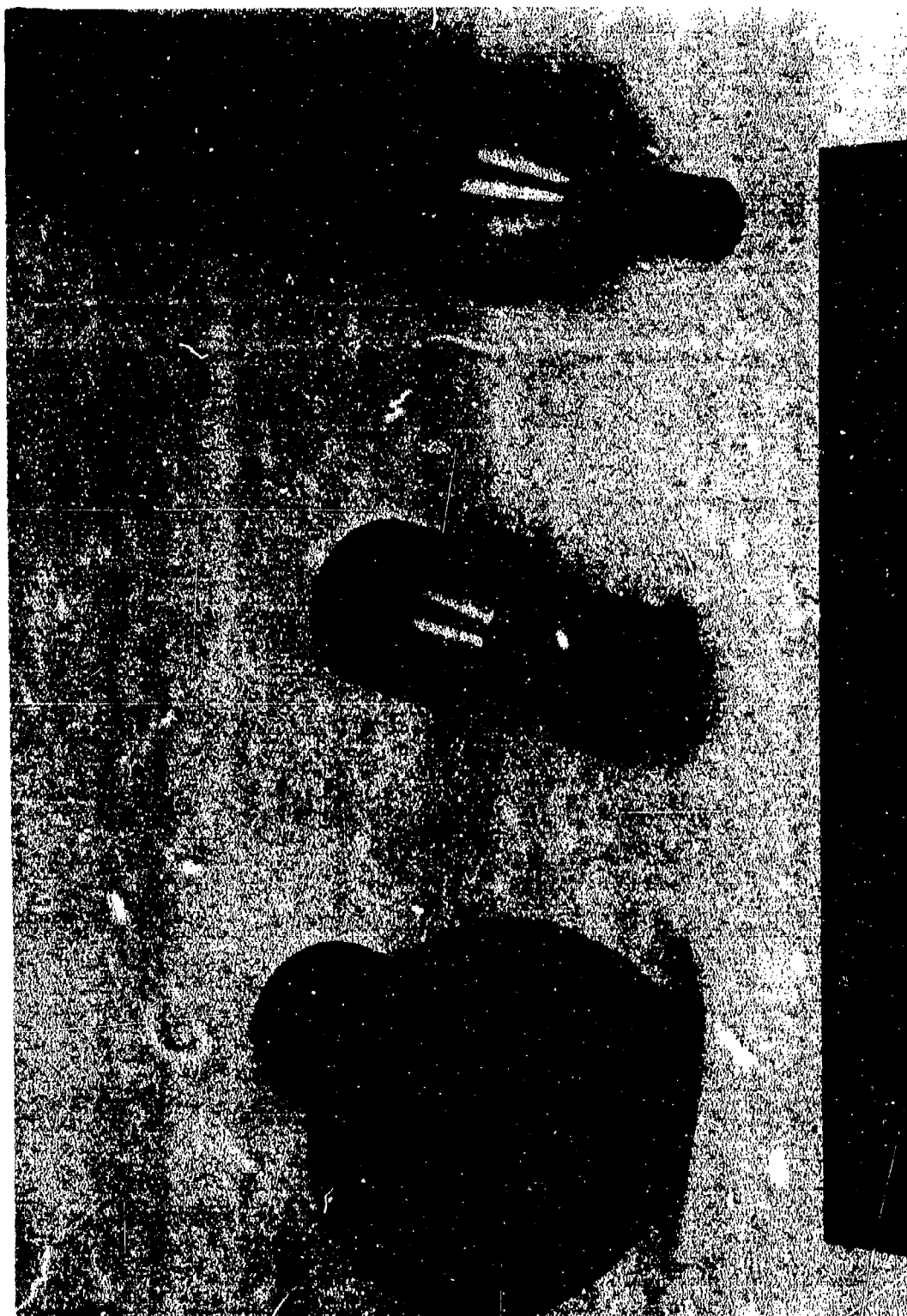
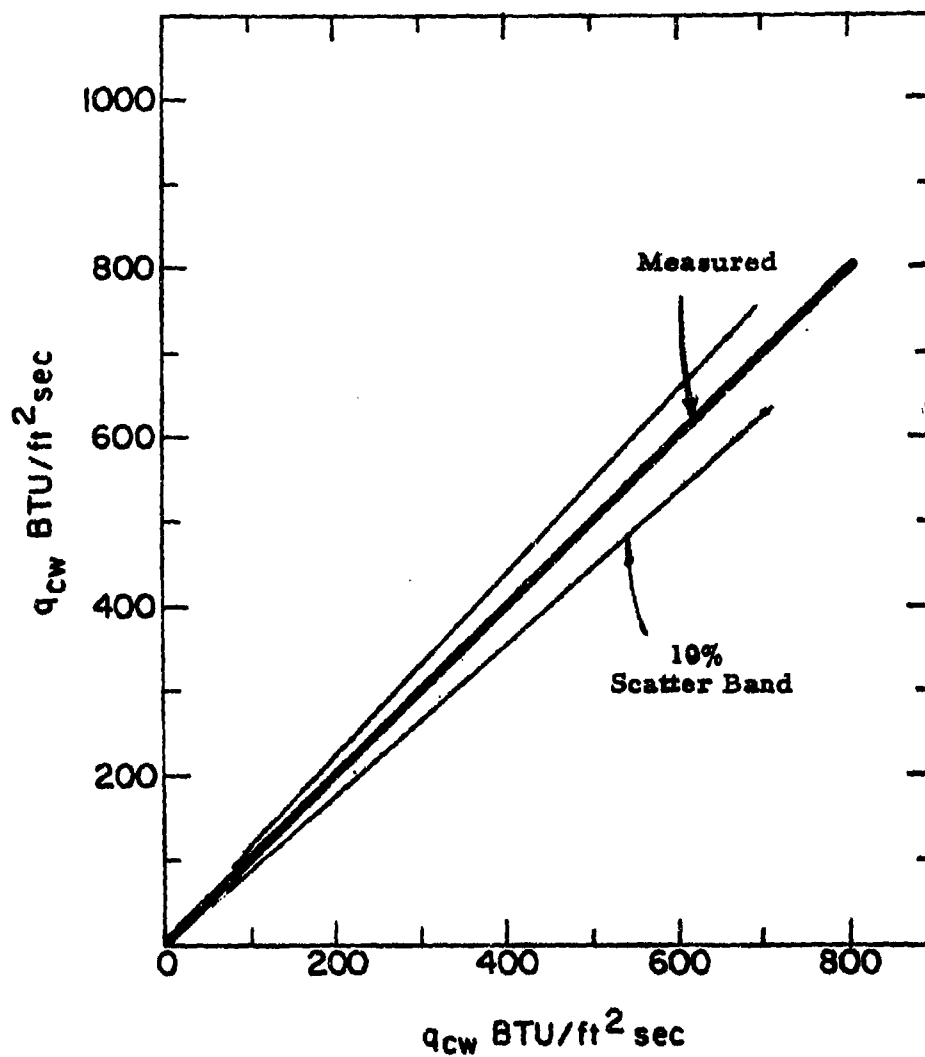


Figure 47. Transient Calorimeter with 3.5, 1.0 and 0.5 Inch Shields (#18166A).



Heat Flux to a 3/8 Inch Diameter Transient Calorimeter in a  
1/2 Inch Shroud



Heat Flux to a 5/8 Inch Diameter Water Calorimeter in a  
1-1/2 Inch Shroud

Figure 48. Comparison of Cold Wall Heat Fluxes to a 3/8 Inch Diameter Transient Calorimeter in a 1/2 Inch Shroud and a 5/8 Inch Diameter Water Calorimeter in a 1-1/2 Inch Shroud in the Avco ROVERS Facility.



Figure 49  
Transient Calorimeters Mounted on Remote  
Controlled Stings in the ROVERS Arc.

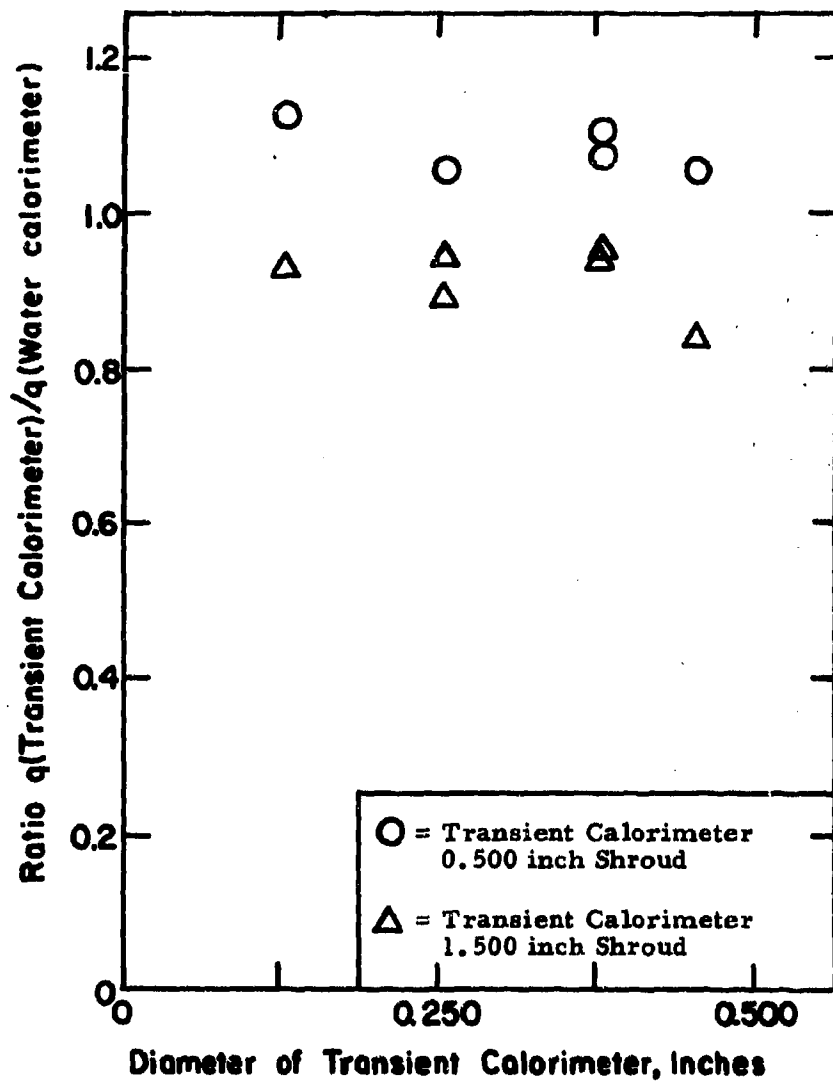


Figure 50. Ratio of Transient Calorimeter Heat Flux to Water Calorimeter Heat Flux (0.625 inch Diameter - 1.500 inch Shroud) as a Function of Transient Calorimeter Diameter in the Low Pressure ROVERS Arc at Mach 3.2.

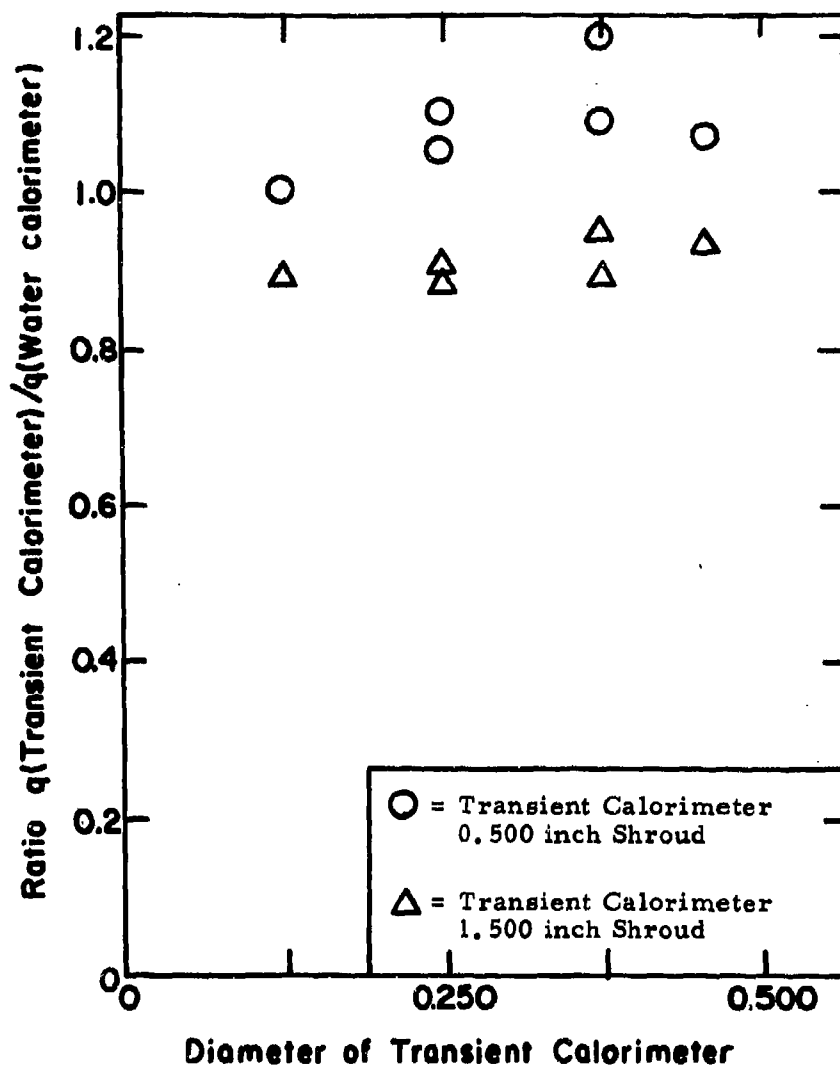


Figure 51. Ratio of Transient Calorimeter Heat Flux to Water Calorimeter Heat Flux (0.625 Inch Diameter - 1.500 Inch Shroud) as a Function of Transient Calorimeter Diameter in the High Pressure ROVERS Arc at Mach 3.2.

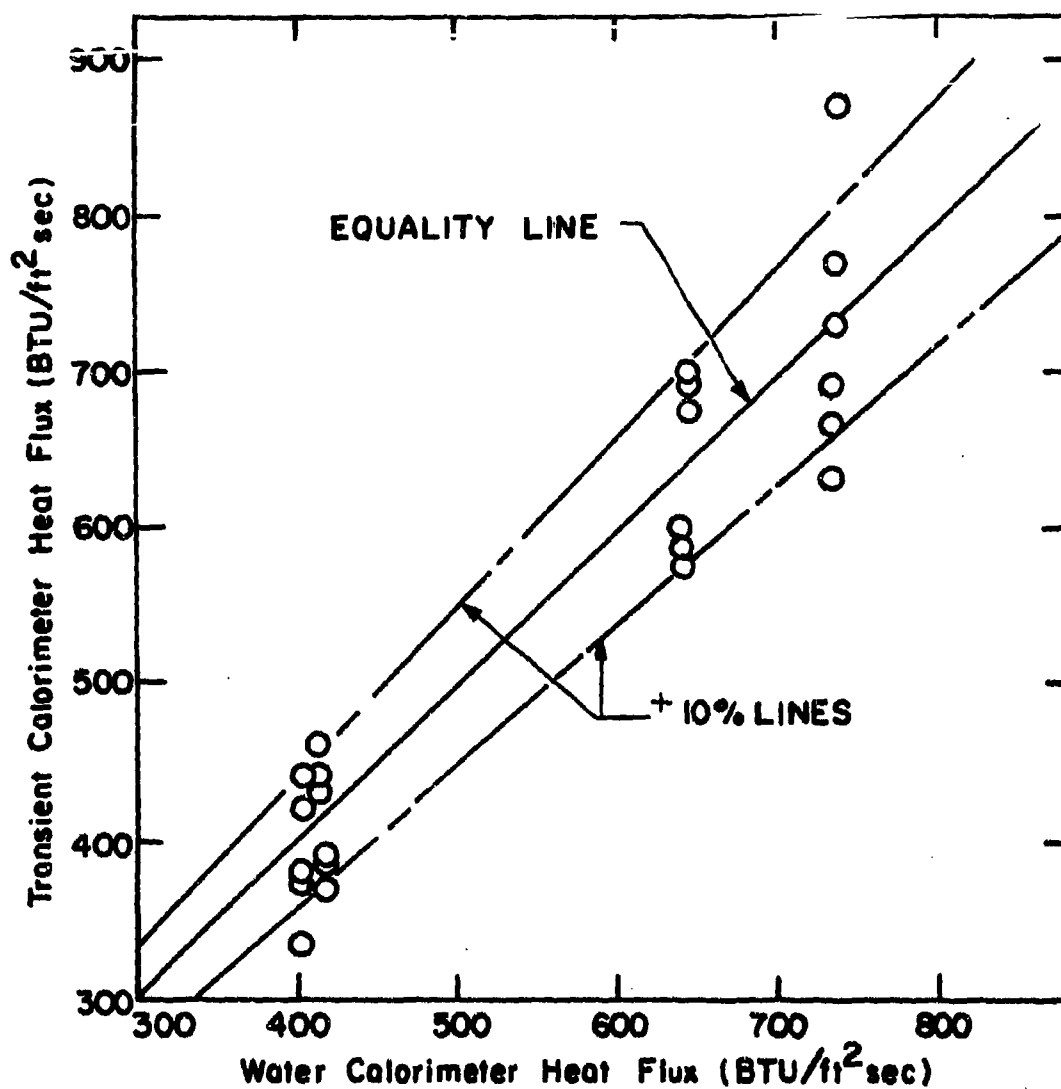


Figure 52. Comparison of Transient and Water Calorimeter Measurements of Heat Flux in the ROVERS Arc at Mach 3.2.



Figure 53. ManLabs Hemispherical Model in Testing Position (ROVERS Facility) (Photo # 20046A).



Figure 54. ManLabs Specimen Being Tested with Holder for Observing Backface Temperatures  
(Photo #20055).

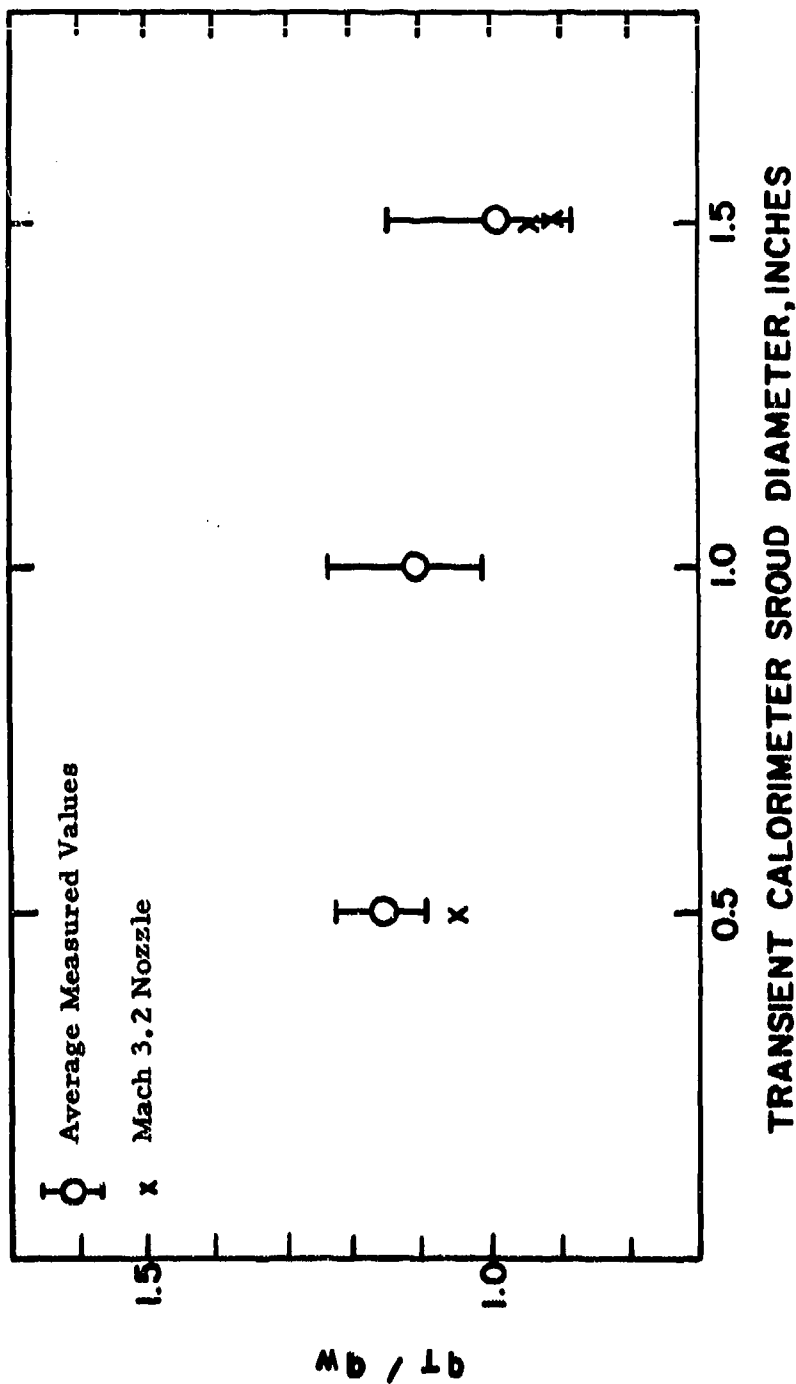


Figure 55. Comparison of the Ratio  $q_t$  (Heat Flux Measured with a 0.250 Inch Diameter Transient Calorimeter) to  $q_w$  (Heat Flux Measured with a 0.625 Inch Water Calorimeter in a 1.50 Inch Diameter Shroud) as a Function of Transient Calorimeter Shroud Size in the ROVERS Arc at Mach 2.2 for Flat Faced Calorimeters. Stream Diameter 0.750 Inches.





Figure 56. The 1.0 and Unassembled 0.5 Inch Hemispherical Calorimeter (Photo #19856A).

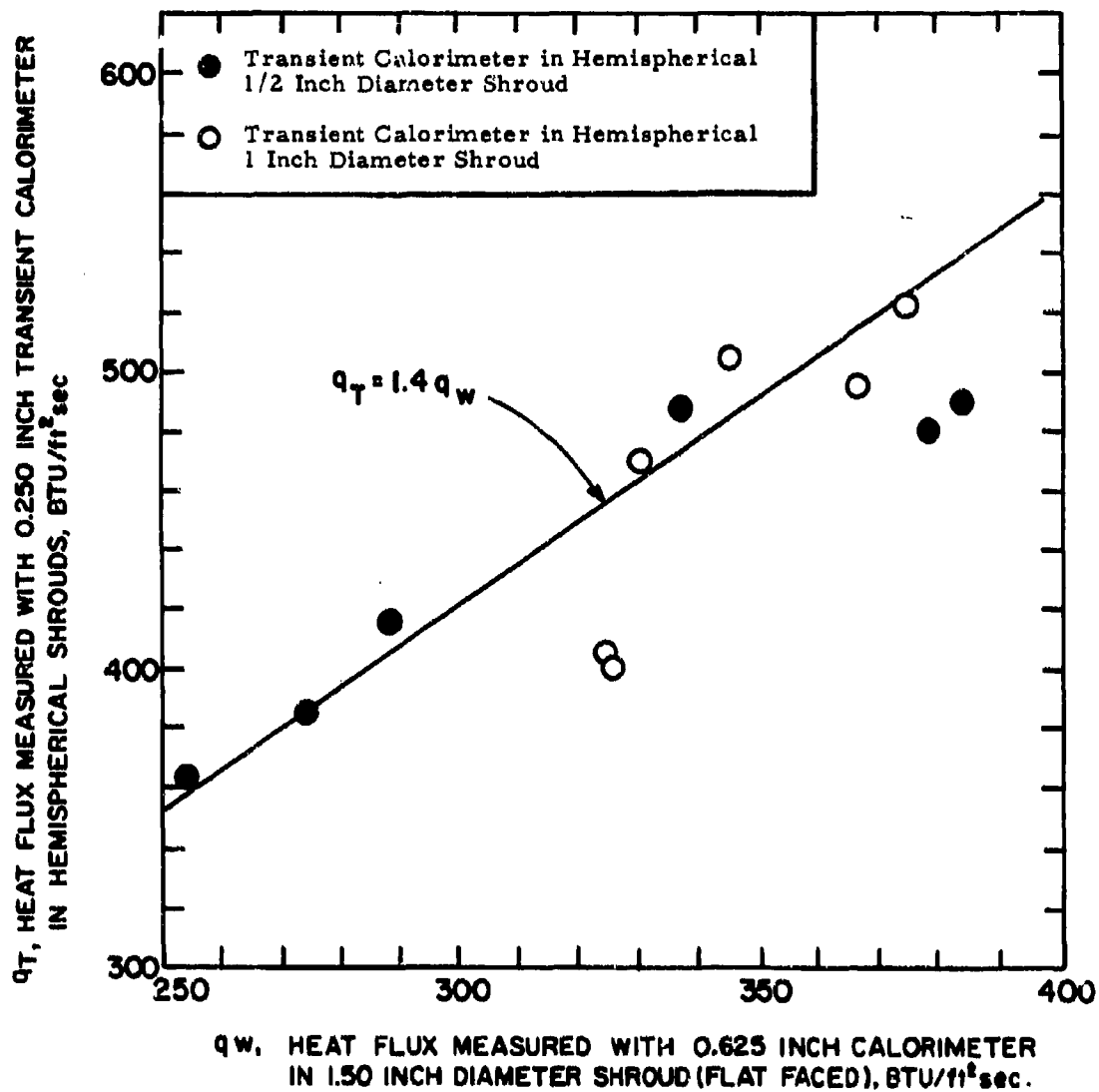


Figure 57. Comparison of Heat Flux Measurements Performed in ROVERS Arc at Mach 2.2 (Stream Diameter 0.750 Inches) Employing Flat Faced and Hemispherical Models.



Figure 58. Overall View of the Ten Megawatt Arc Test Cell (#14213C).

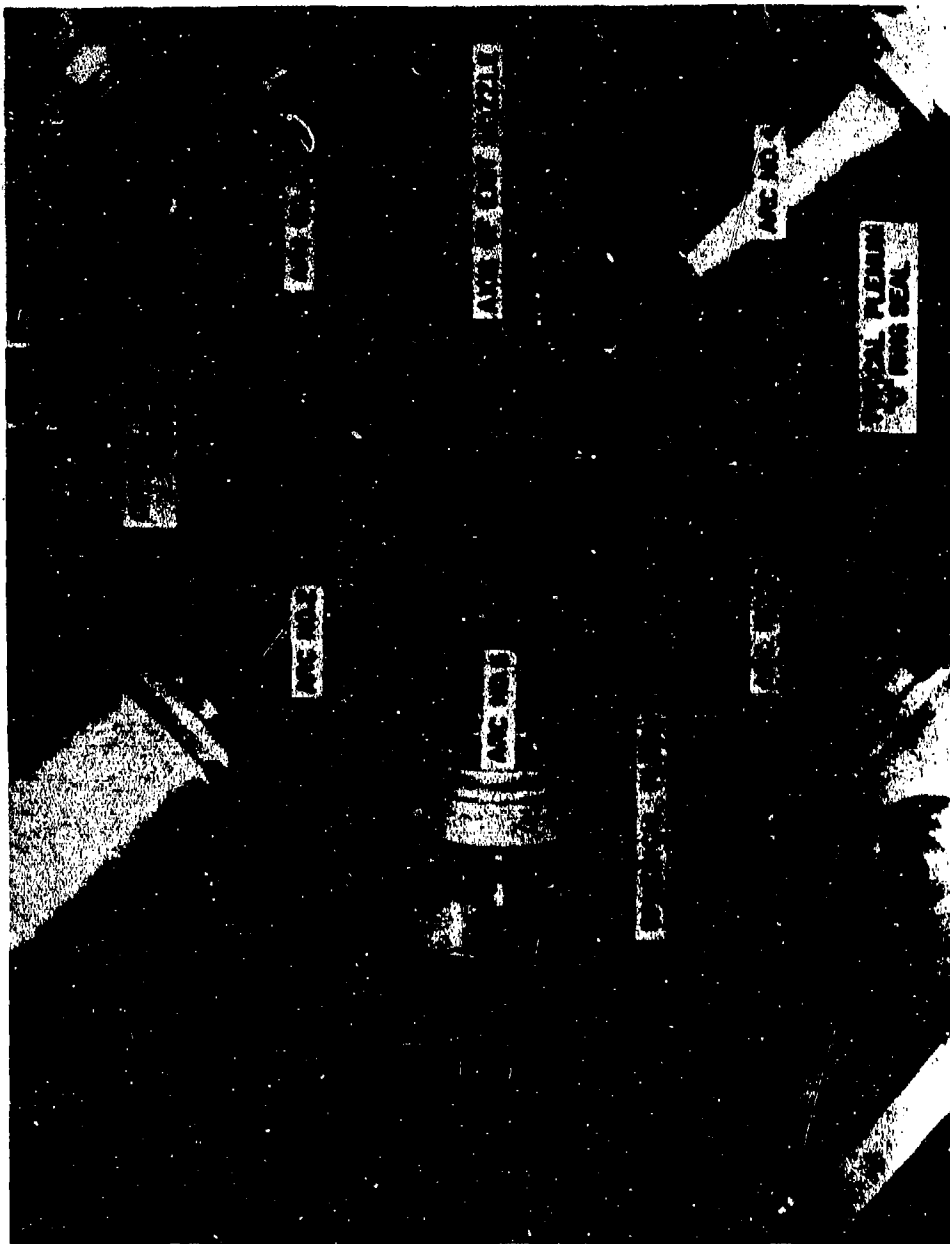


Figure 59. AVCO-SSD Ten-Megawatt Arc Plenum Chamber and Arc Head Configuration.

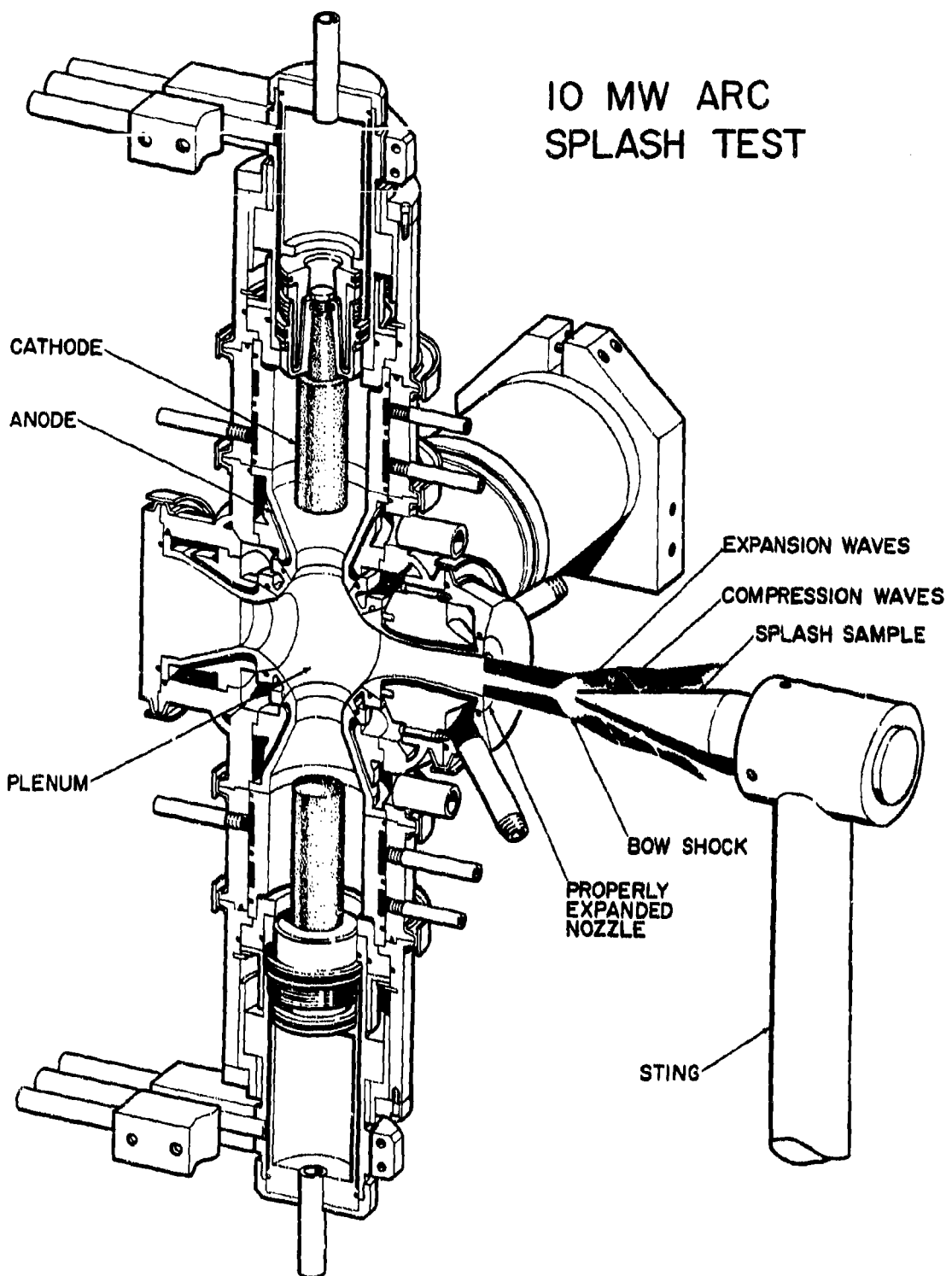


Figure 60. Schematic View of Ten Megawatt Arc Splash Test.

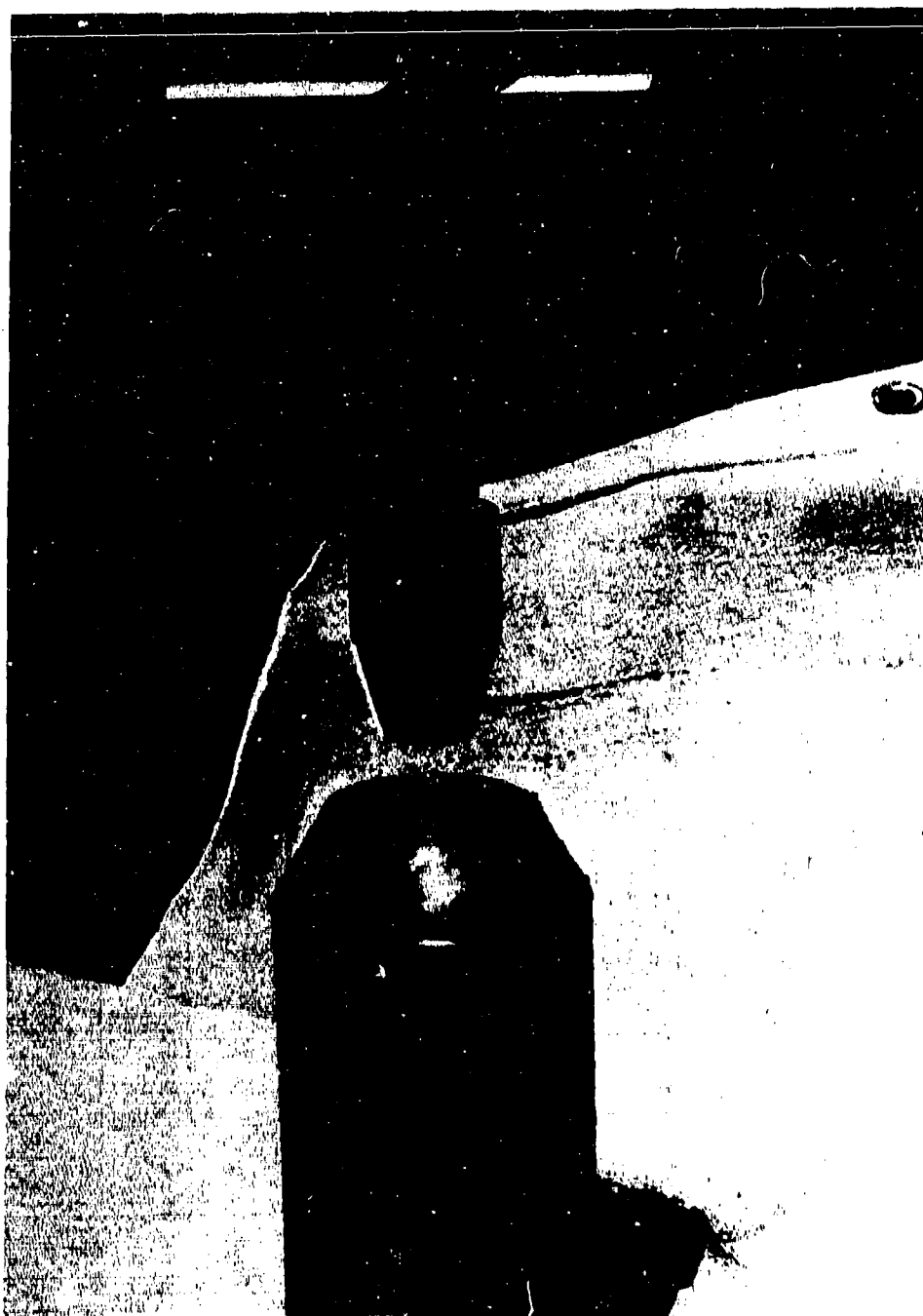


Figure 61. Pre-Test View of ManLabs Test Sample in Ten Megawatt Arc (#18420A).

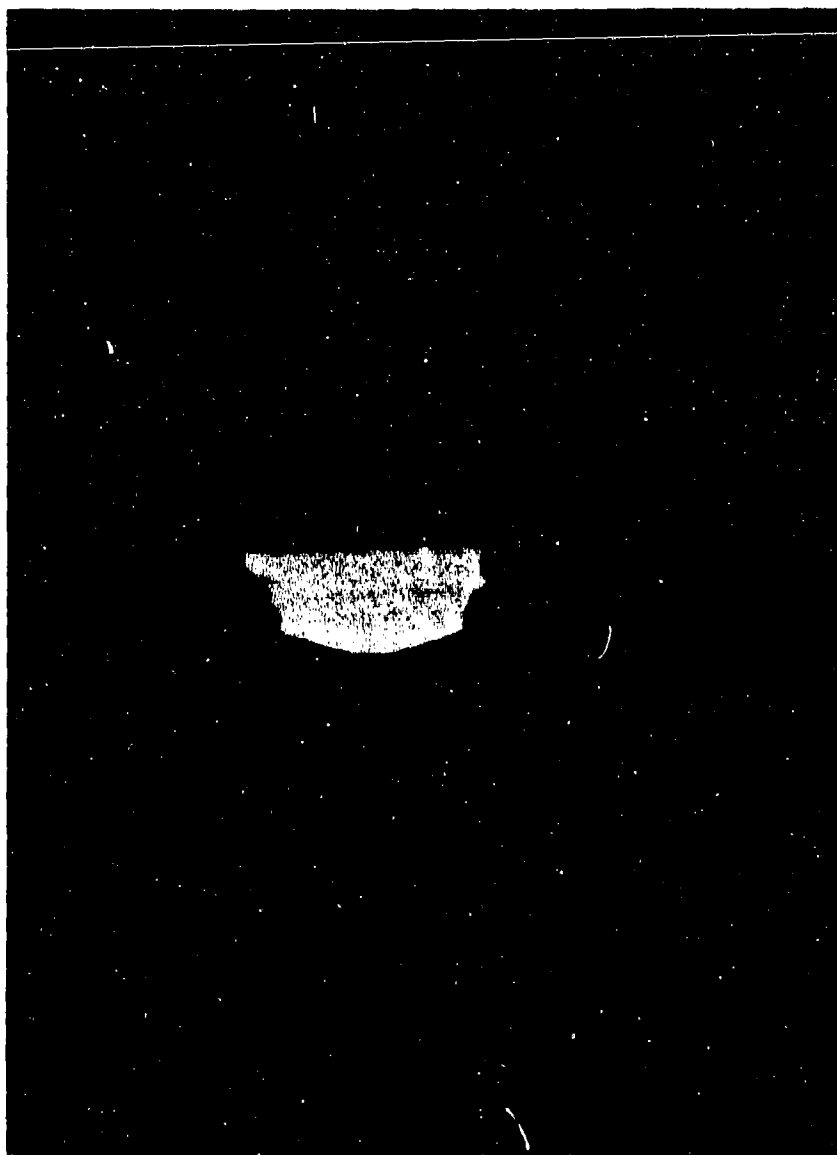


Figure 62. ManLabs Test Sample During Exposure in Ten Megawatt Arc Facility (#18420E).

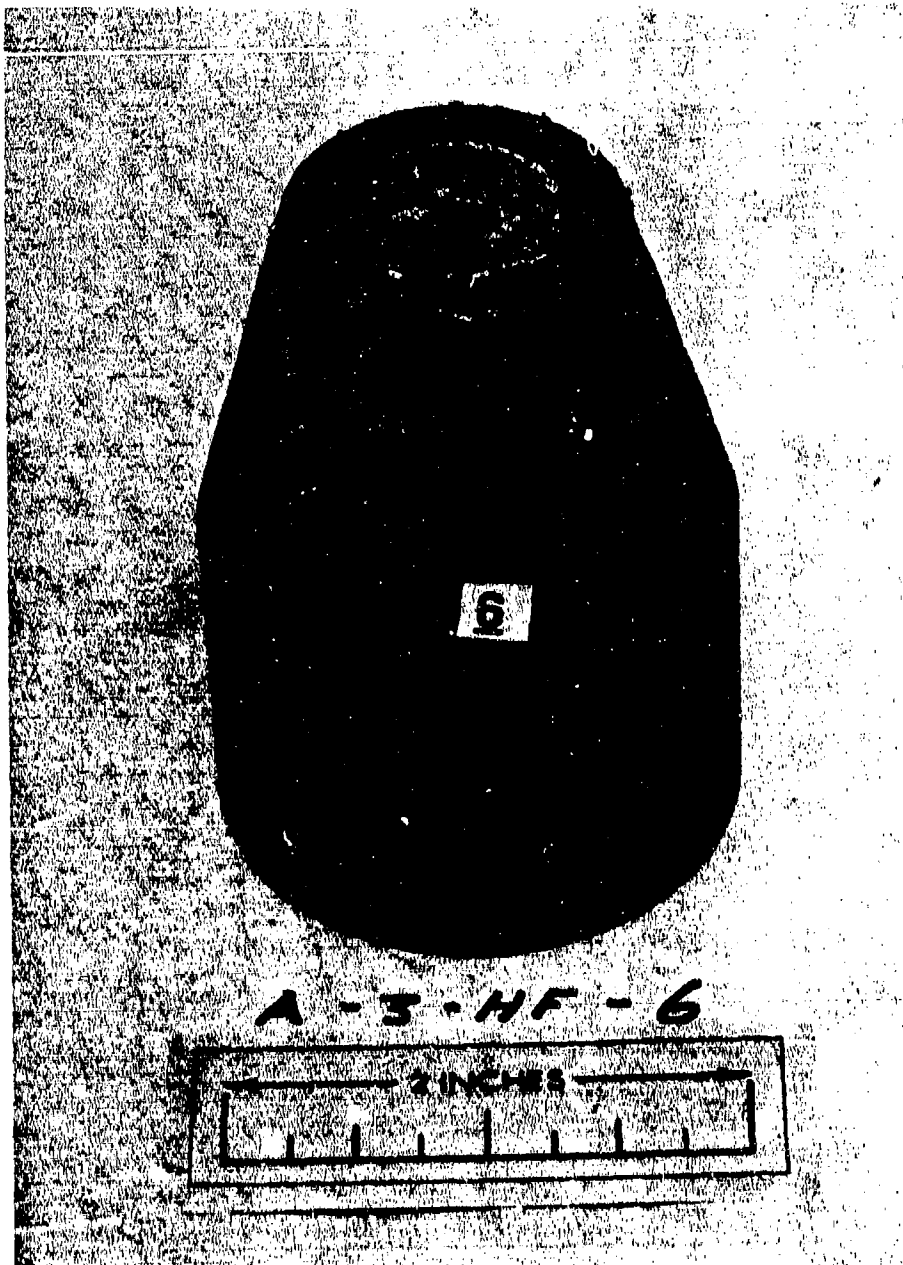
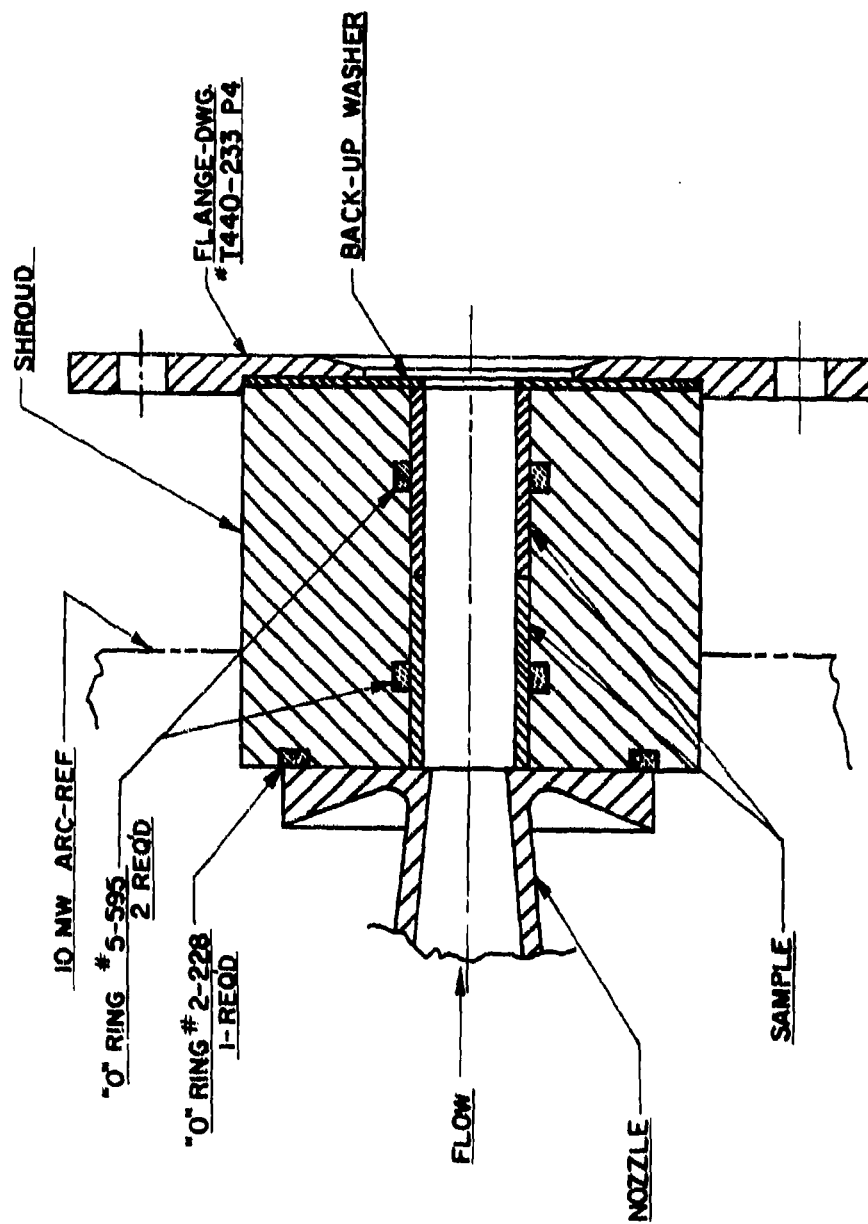


Figure 63. Post Test View of Sample Tested in Ten Megawatt Arc Facility (#18420C).





(G1) SAMPLE TEST ASSEMBLY

Figure 64. Supersonic Pipe Test Configuration.

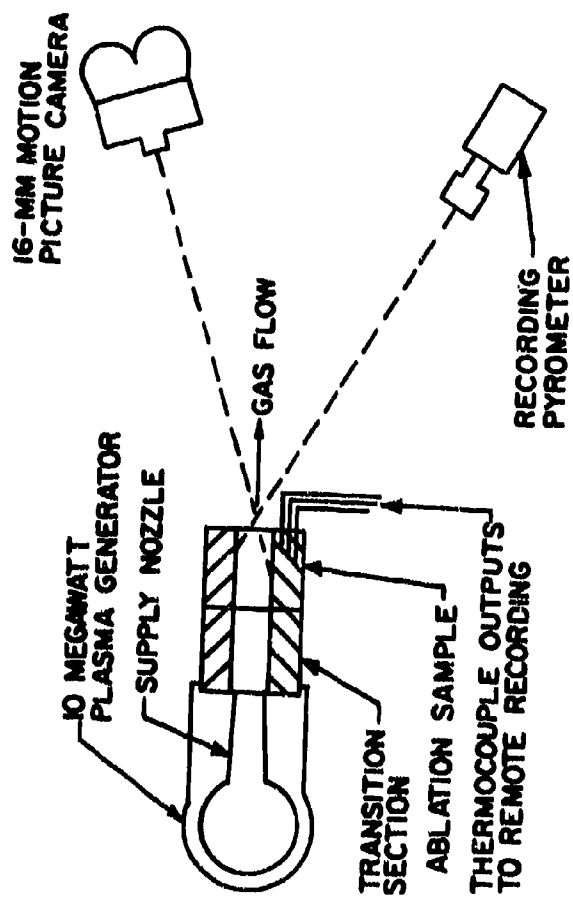


Figure 65. Experimental Configuration for Supersonic Pipe Ablation Tests.

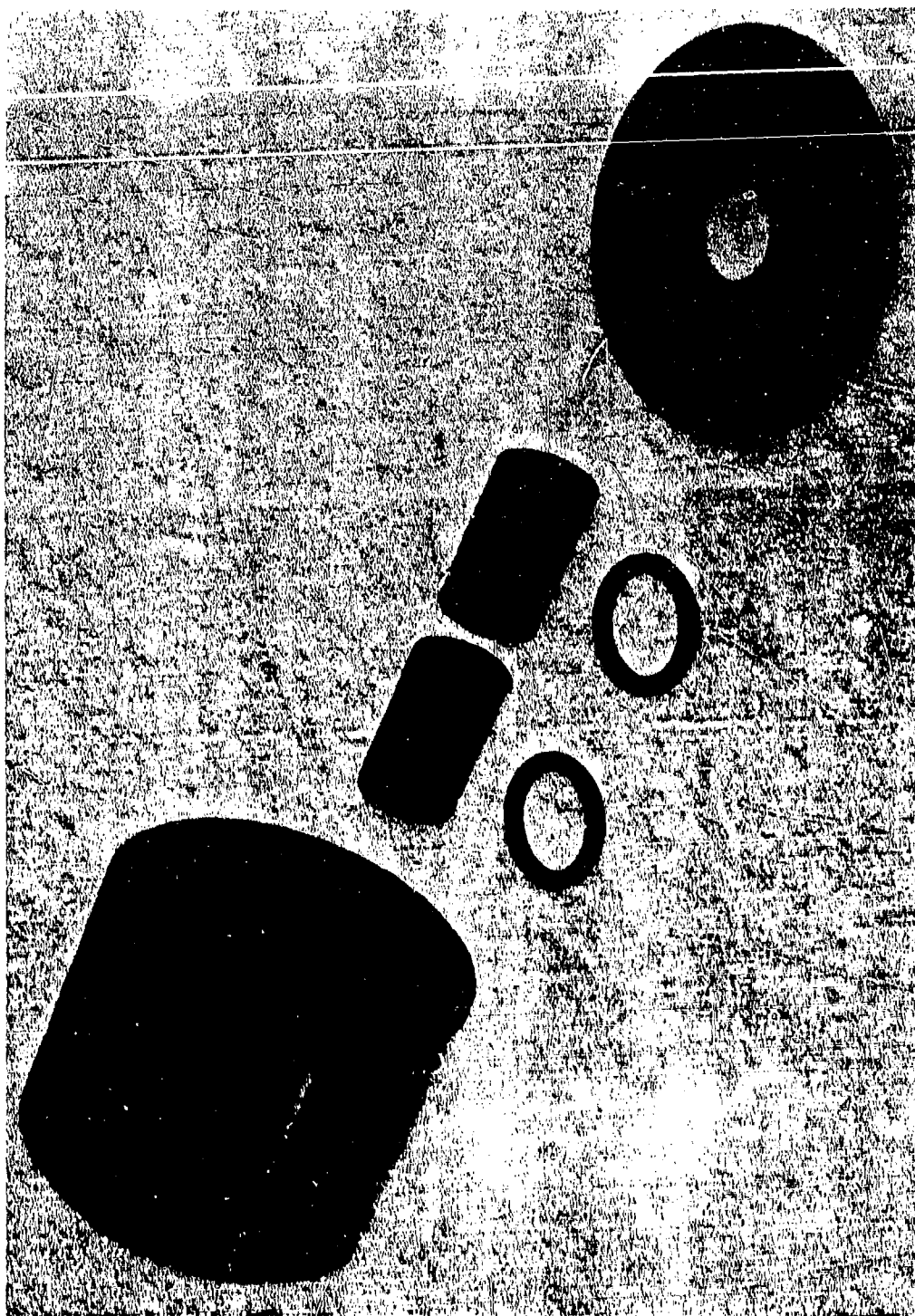


Figure 66. Supersonic Pipe Holder and Test Samples Prior to Assembly (Photo #20057B).

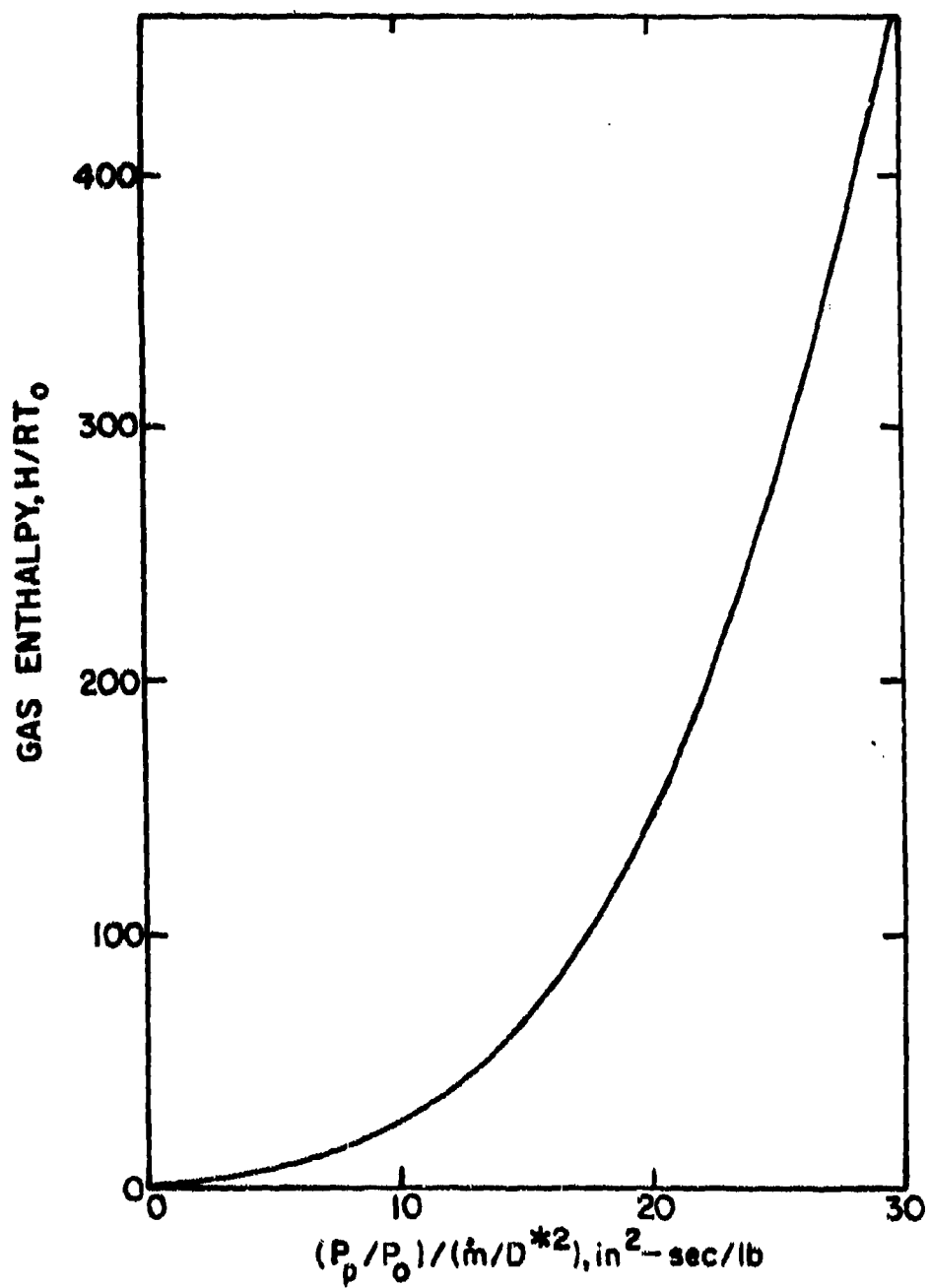


Figure 67. Ten Megawatt Arc Facility Flow Parameters.



Figure 68. Supersonic Pipe Calorimeter Containing Two (2) Pressure Sensors and Two (2) Heat Flux Calorimeters (Photo #20057A).

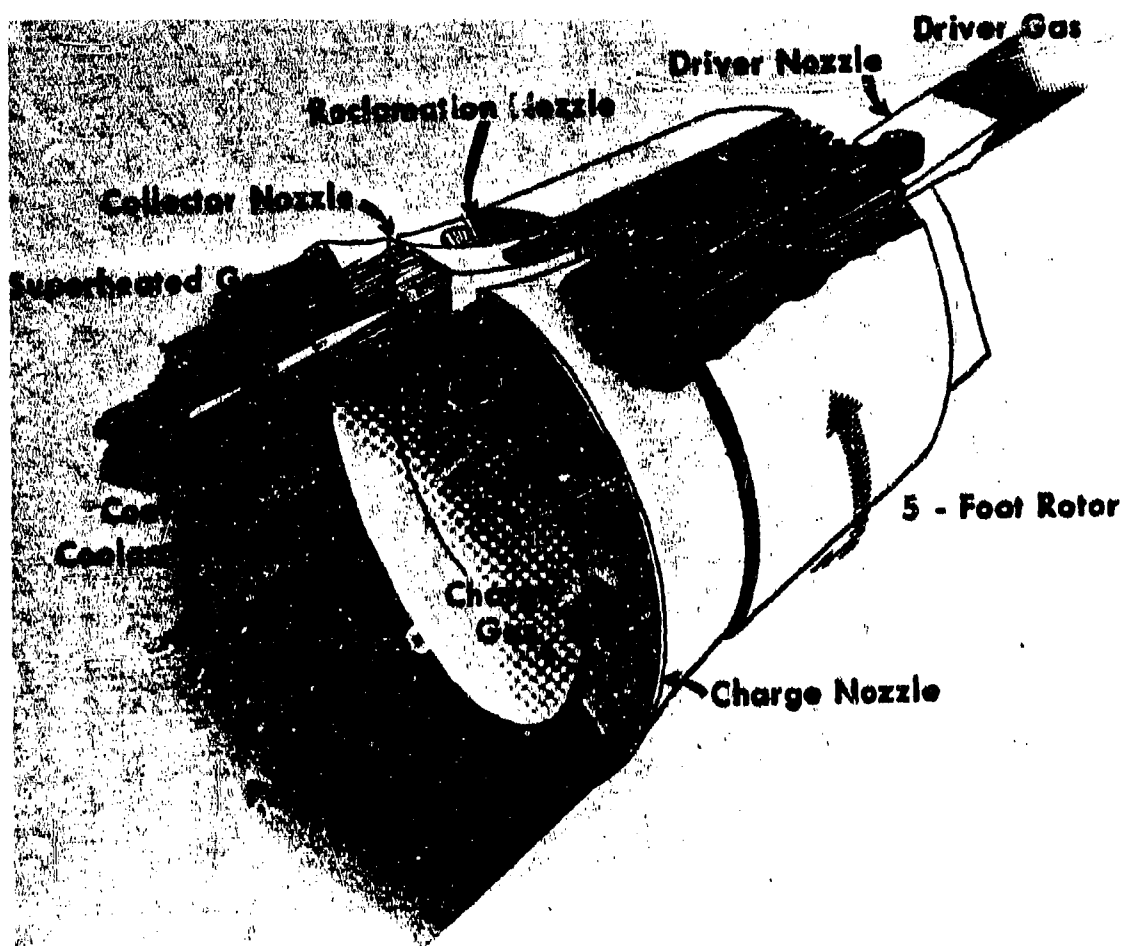


Figure 69. CAL Wave Superheater Rotor and Nozzle.

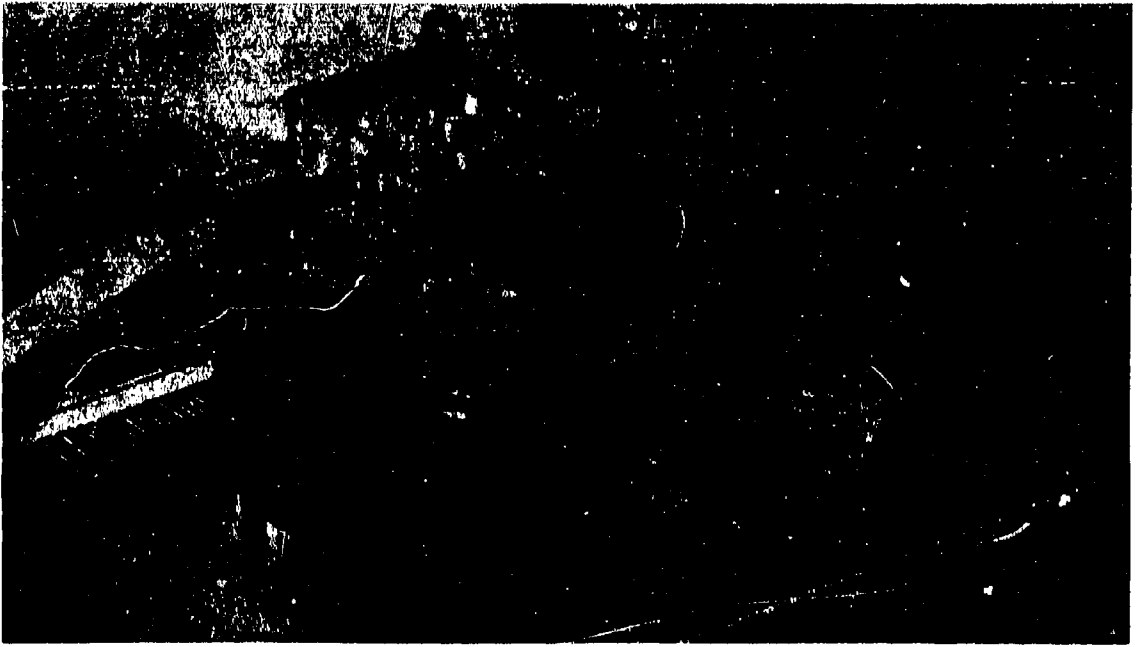


Figure 70. CAL Wave Superheater Hypersonic Tunnel.

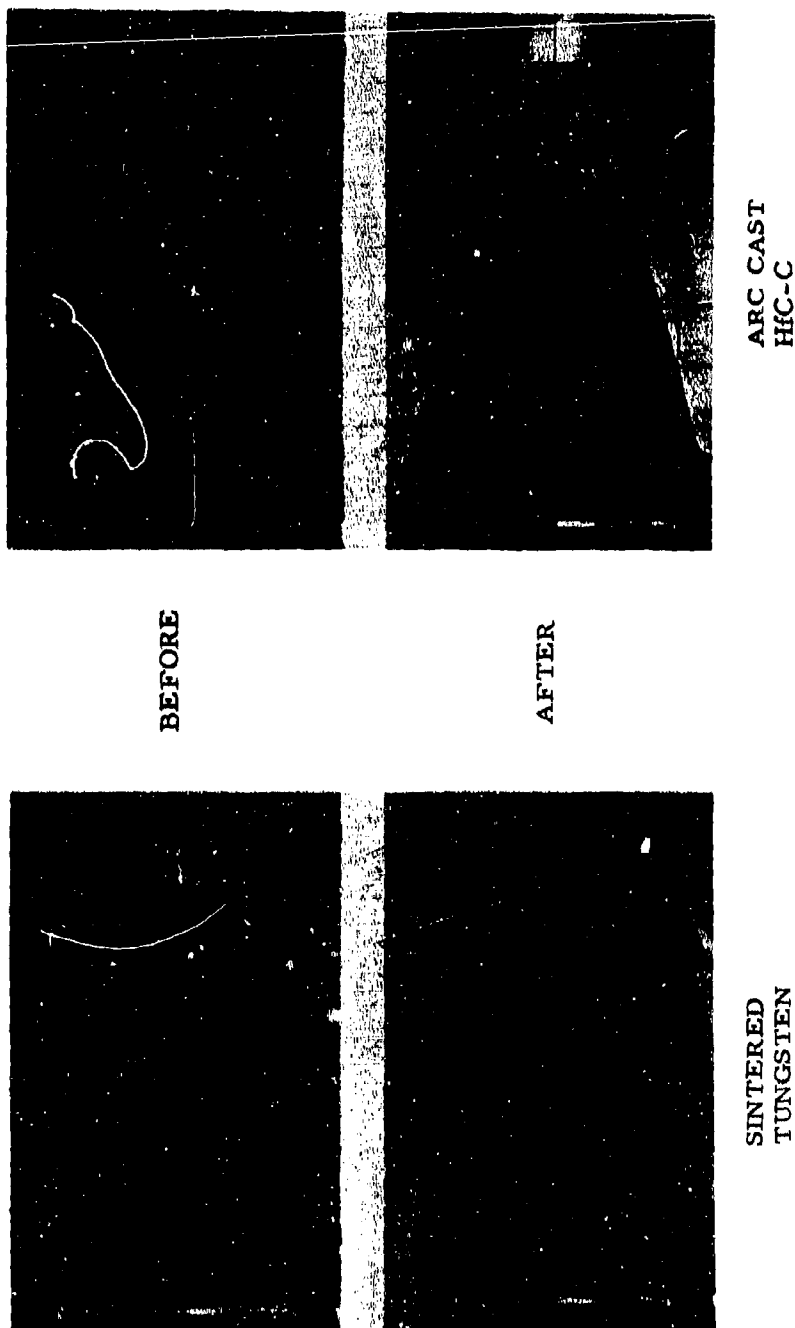
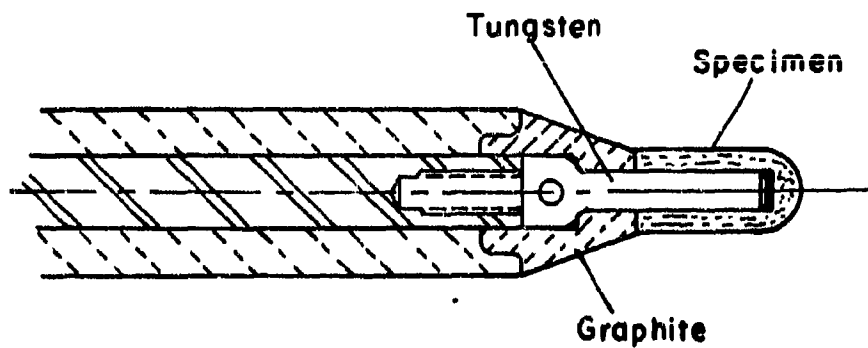
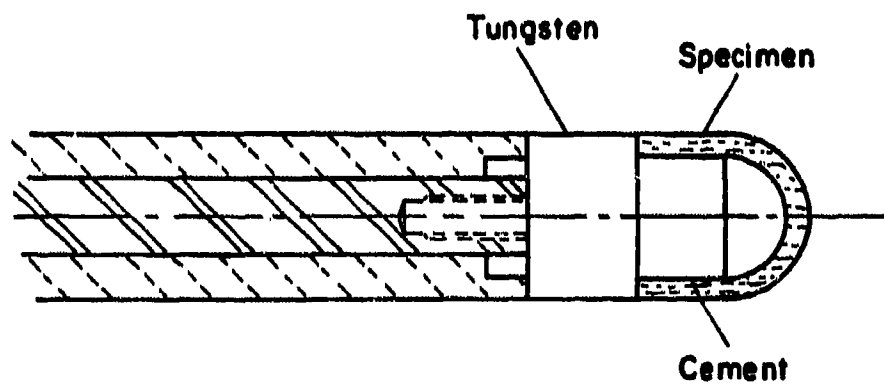


Figure 71. Tungsten and HfC-C 15° Cone Models Tested in Cornell Wave Superheater for 6 Seconds at a Cold Wall Heat Flux of 4080 BTU/ft<sup>2</sup>/sec and Stagnation Pressure of 50 Atmospheres (after E.G. Kendall, J.I. Slaughter and W.C. Riley, Aerospace Corp. [27]) (one box = 1/2" x 1/2").



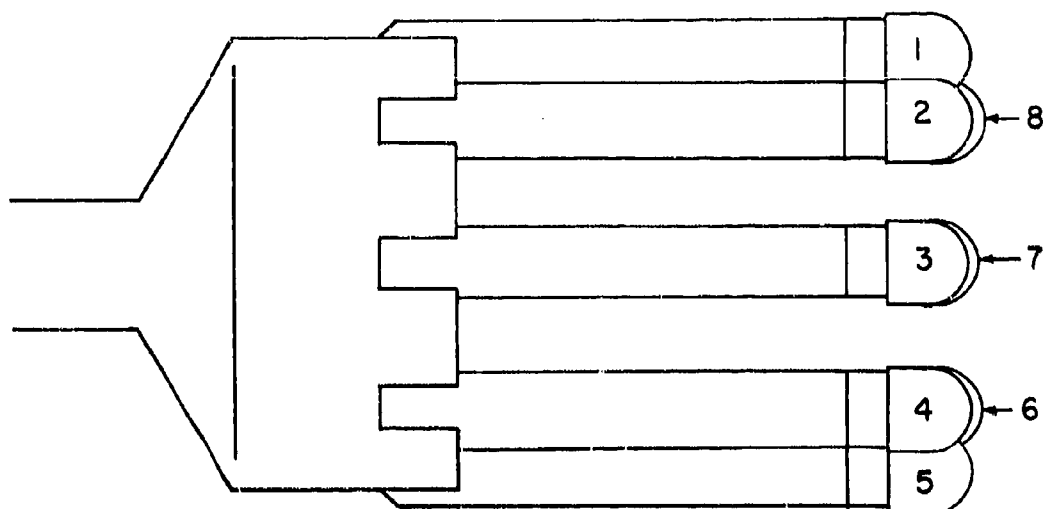


**One Half Inch Diameter Specimens**

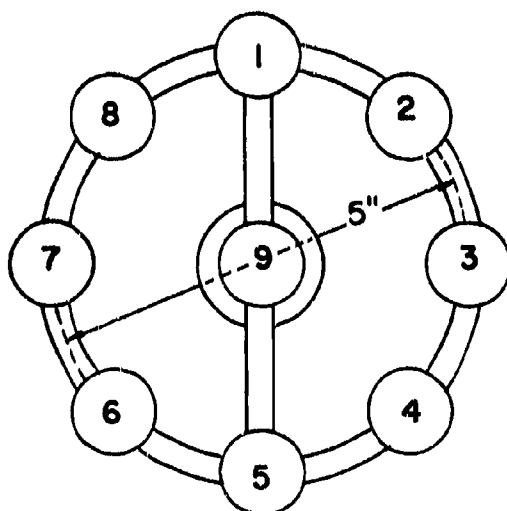


**One Inch Diameter Specimens**

**Figure 72. Details of Specimen Holders Employed in Wave Superheater Tests.**



(a) View From Right Side  
(Camera View)



Motion  
Picture  
Camera

(b) Pilot's View (Looking Upstream)

Figure 73. Orientation of Calorimeter and Models in Wave Superheater Exposures.

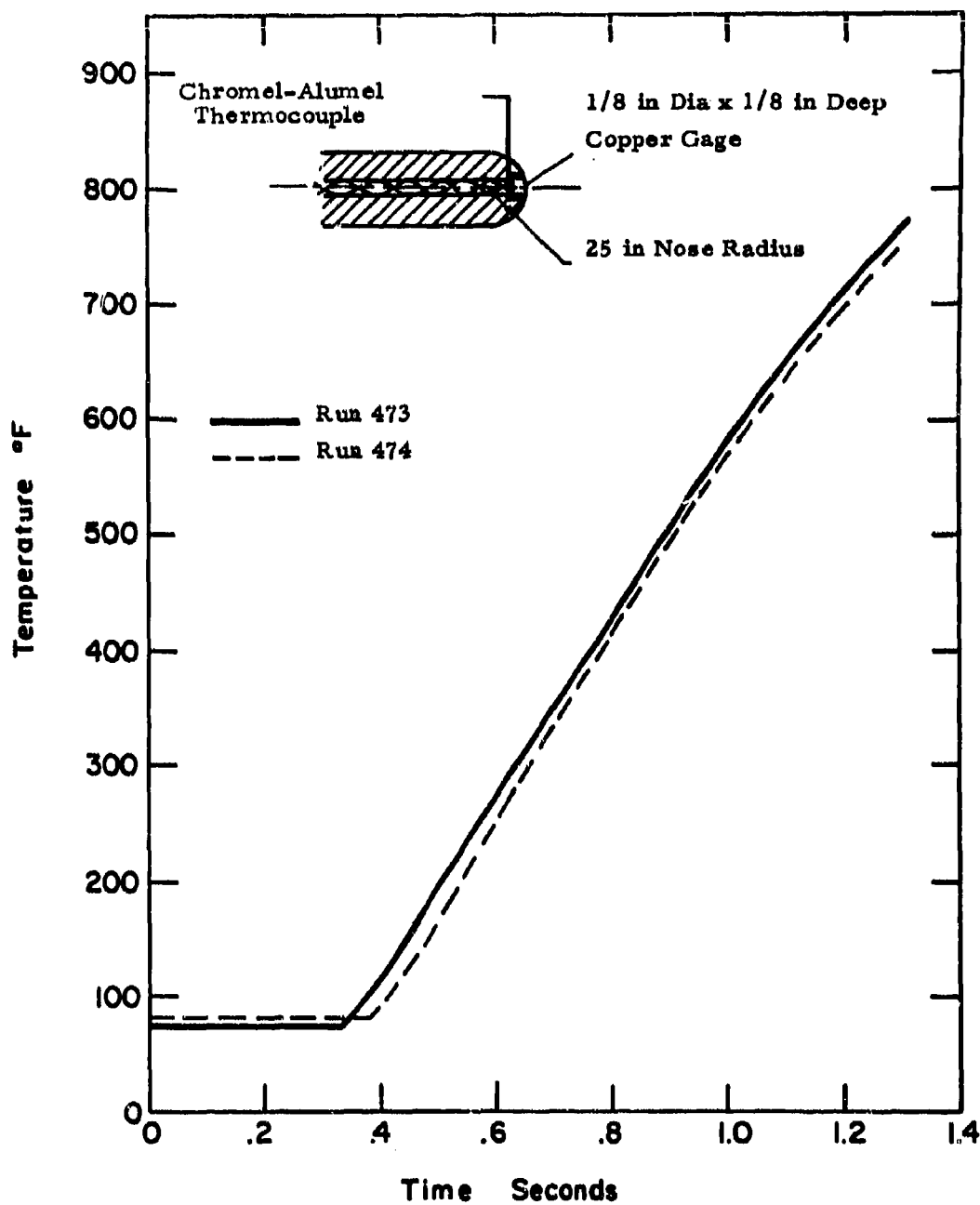


Figure 74. Calorimeter Time-Temperature History.

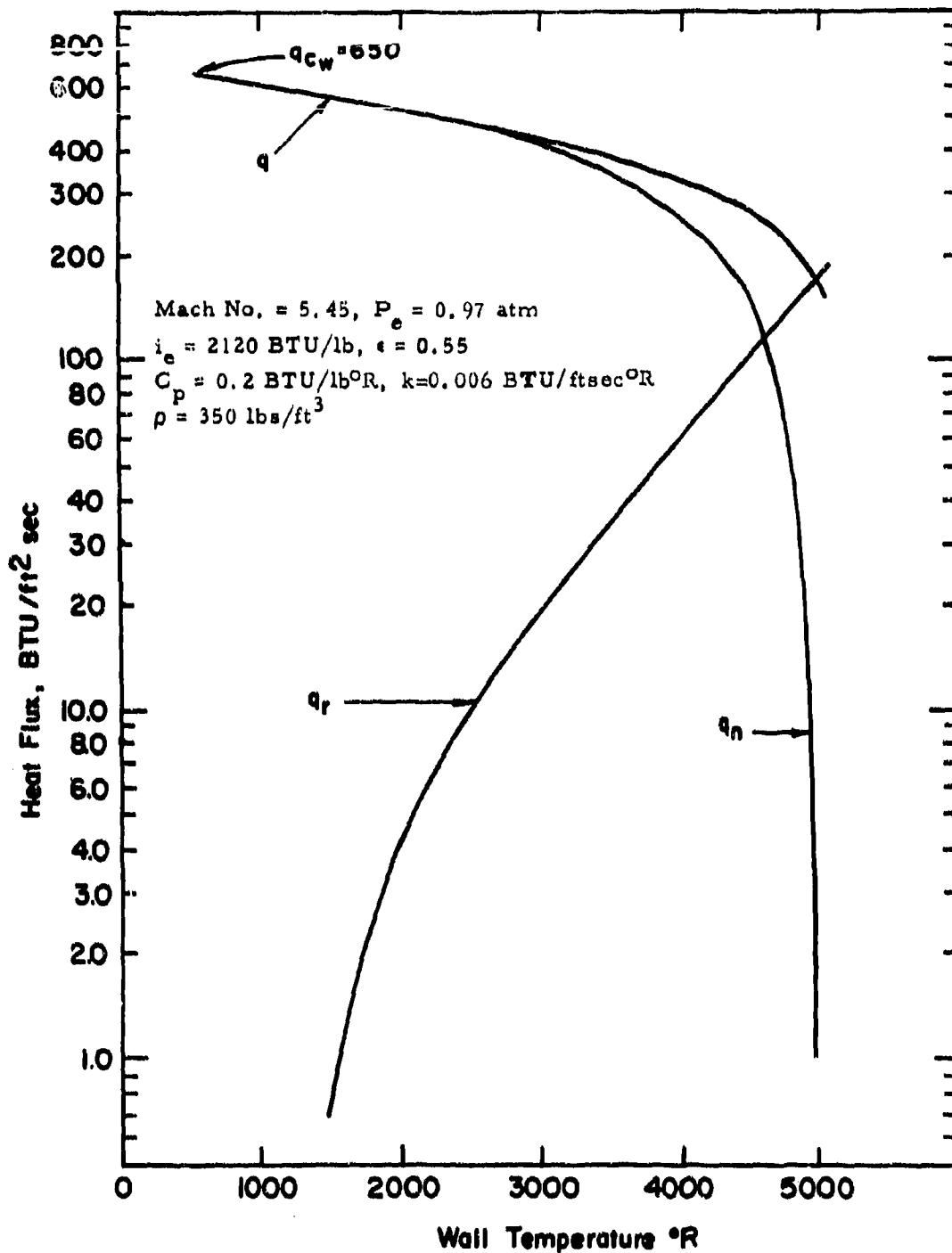


Figure 75. Calculated Heat Flux As A Function of Wall Temperature for A One-Half Inch Diameter Hemispherical Cap Shell of Zirconium Diboride One-Eighth Inch Thick in the Mach 6 Test Section of the Cornell Wave Superheater.

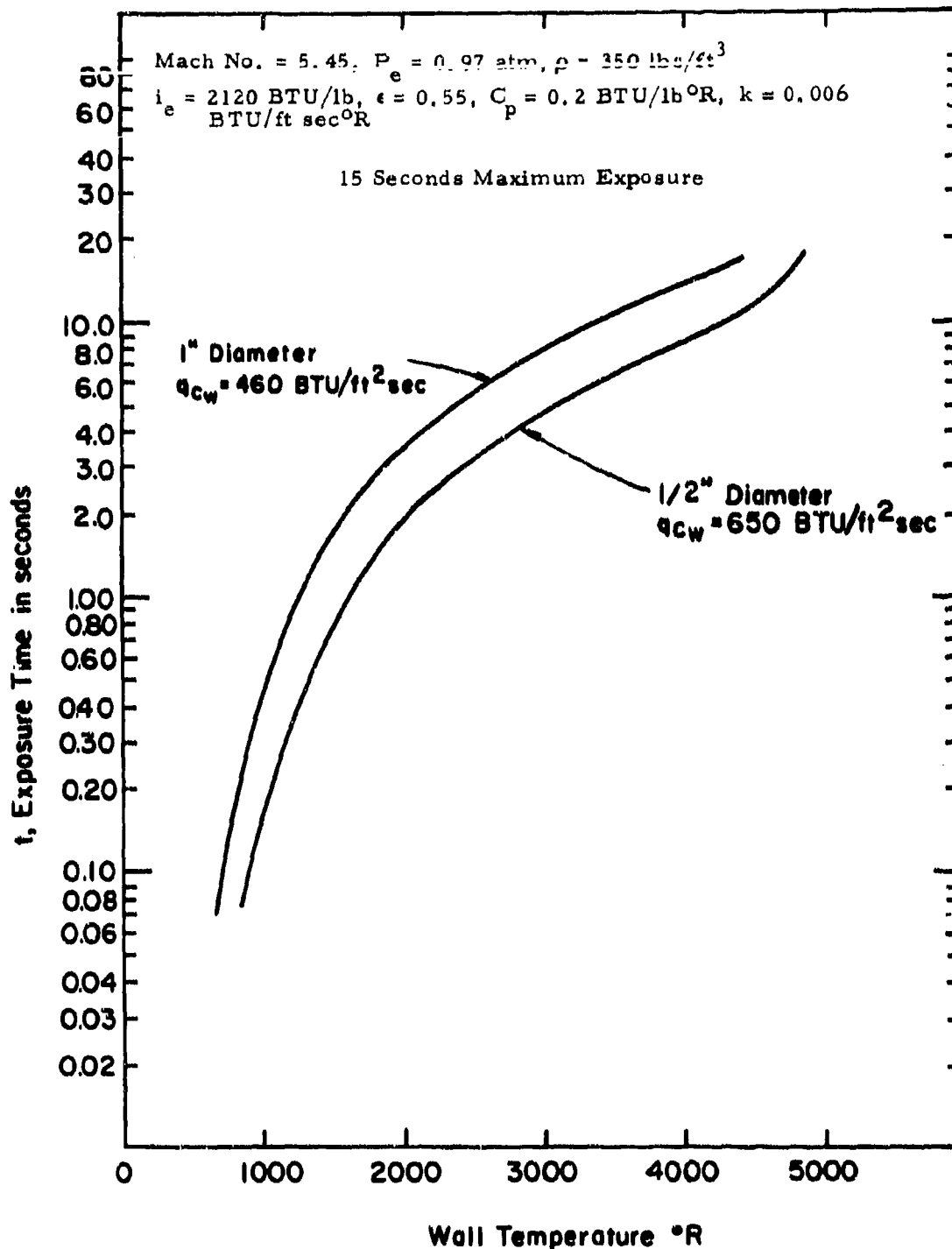


Figure 76. Calculated Wall Temperature As A Function of Time for A One Inch and a One-Half Inch Diameter Hemispherical Cap Shell of Zirconium Diboride One-Eighth Inch Thick in the Mach 6 Test Section of the Cornell Wave Superheater.

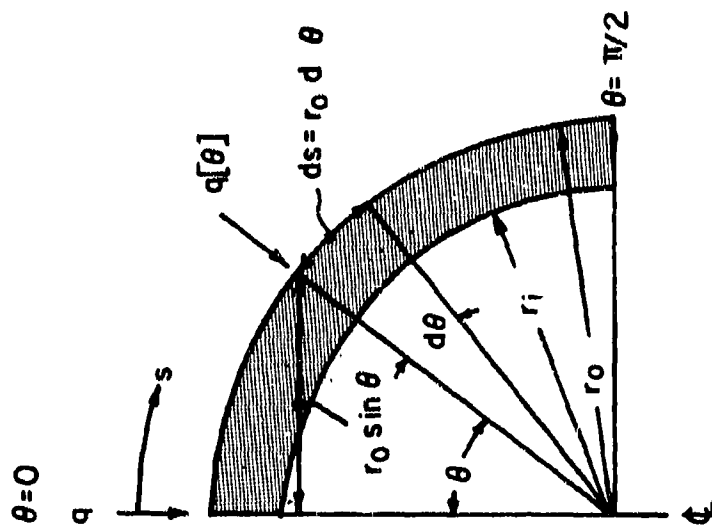


Figure 77. Geometrical Definitions for Analysis of Conduction Losses Through a Hemispherical Shell.

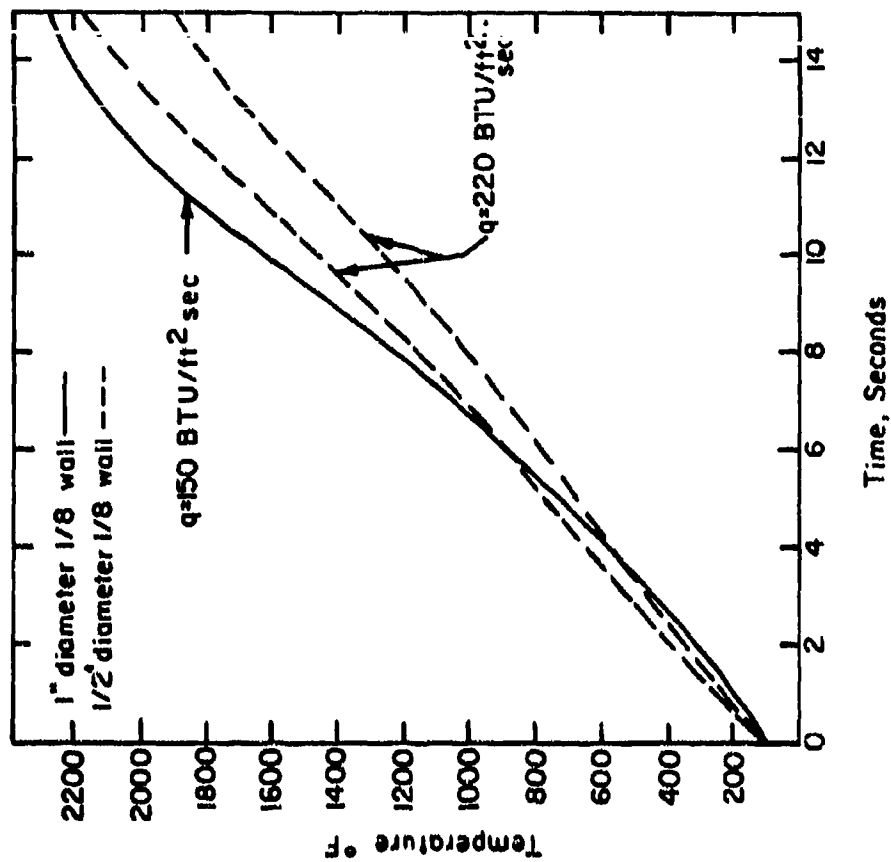


Figure 78. Temperature Response for Hemispherical Shells of 1020 Steel Exposed under Flux-Conductivity Conditions to Simulated Wave Superheater Tests.

TABLE 1  
TEST CONDITIONS AND HEAT FLUX MEASUREMENTS\*

Test No.	Enthalpy (BTU/lb)	Arc Current (amps)	Arc Voltage (volts)	Air Flow Rate (lb/sec)	Plasma Temp. (°F)	Stagnation Pressure (atm)	Mach No.
1	3670	500	159	0.008	7220	1.060	0.31
2	5320	998	152	0.008	9540	1.079	0.36
3	3290	440	162	0.008	6690	1.053	0.30
4	5440	1000	153	0.008	9640	1.079	0.36
5	3350	440	158	0.008	6760	1.053	0.30
6	5280	1056	146	0.008	9500	1.079	0.36

Steady-State Calorimeter  
1.500 Inch  
Diameter Shroud

Test No.	0.500 Inch Dia. Cal.	0.750 Inch Dia. Cal.
1	475	390
2	705	640
3	420	340
4	735	615
5	370	300
6	685	605

Heat Flux (BTU/ft<sup>2</sup>-sec)

Transient Calorimeter

Test No.	0.500 Inch Diameter Shroud				1.500 Inch Diameter Shroud		
	0.125 Inch Dia. Cal.	0.250 Inch Dia. Cal.	0.375 Inch Dia. Cal.	0.450 Inch Dia. Cal.	0.125 Inch Dia. Cal.	0.450 Inch Dia. Cal.	0.500 Inch Dia. Cal.
1	420	455	490				
2	650	710	770				
3	365			395			
4	670			680			
5					315	330	350
6					615	615	700

\*No data was obtained for the 0.500 inch diameter transient calorimeter without the shroud attachment since side heating was significant without the shroud.

TABLE 2  
NORMALIZED COMPARISON OF RADIAL HEAT FLUX DISTRIBUTION  
IN THE MODEL 500 FACILITY

Normalizing Factor (4400/i <sub>e</sub> )	Shroud Diam. (in.) Calorimeter Diam. (in.)	Normalized Heat Flux (BTU/ft <sup>2</sup> sec)									
		Steady State Calorimeter		Transient Calorimeter							
		1.500	1.500	0.500	0.500	0.500	0.500	0.500	1.500	1.500	1.500
		0.500	0.750	0.125	0.250	0.375	0.450	0.125	0.450	0.450	0.500
1.205		572	470	506	549	590					
0.825		581	528	536	585	635					
1.345		565	457	491			531				
0.807		593	496	540			549				
1.321		489	396					416	436	436	432
0.830		568	502					510	510	510	531
Average Normalized Flux		561	475	518	567	612	540	463	473	473	531
Ratio of Average Normalized Flux Divided by Average Normalized Flux for 0.125 Calorimeter in 0.500 inch Shroud		1.083	0.918	1.000	1.095	1.181	1.041	0.895	0.914	0.914	1.006



TABLE 3

SUMMARY OF TEST CONDITIONS FOR SAMPLES USED FOR  
TEMPERATURE GRADIENT STUDIES

Material Sample No. Assumed Emittance at $\lambda = 0.65\mu$	Mach No.	P e atm	i e BTU lb	D (in)	q cw BTU ft <sup>2</sup> sec	T °R obs	q <sub>r</sub> Surface Radiation BTU ft <sup>2</sup> sec	ε <sub>N</sub> Computed Normal Emittance
<b>ZrB<sub>2</sub> (A-3)</b>								
ε = 0.57								
-1MC	0.31	1.06	4540	0.491	475	5150	113	0.34
-2MC	0.29	1.05	3230	0.491	365	4930	176	0.63
-3MC	0.31	1.06	3380	0.491	460	5170	236	0.70
-4MC	0.33	1.07	4560	0.491	610	6340	404	0.53
<b>Hf-20Ta-2Mo(I-23)</b>								
ε = 0.55								
-1MC	0.29	1.05	3220	0.501	425	5220	233	0.67
-2MC	0.30	1.05	3350	0.503	505	5310	206	0.55
-3MCA	0.31	1.06	3380	0.499	510	5415	193	0.48
-3MCB	0.31	1.06	3380	0.499	510	5795	214	0.40
-4MC	0.31	1.06	3560	0.503	480	5395	212	0.53

TABLE 4

## SUMMARY OF IN DEPTH TEMPERATURE MEASUREMENTS

SUMMARY OF TEST DATA FOR  $ZrO_2(A-N)-1MC$ 

Time (sec)	Surface Temperature (°F)		In Depth Temperature (°F)	Surface Radiation (BTU/ft <sup>2</sup> -sec)
	T <sub>SR</sub>	T <sub>TRUE</sub>		
200	4230	4000	---	72
300	4610	4710	---	81
400	4530	4660	---	96
500	4670	4920	---	96
600	4700	5040	---	106
700	4700	5080	---	107
1200	4700	5110	---	111
1300	4680	5150	---	113
1400	4680	5150	---	113

Mach No. = 0.31  
 Supersonic Enthalpy = 4040 BTU/lb  
 Cold Wall Heat Flux = 475 BTU/ft<sup>2</sup>-sec  
 Stagnation Pressure = 1.06 atm.  
 \* = 0.57 (Surface)  
 \* = 1.00 (In Depth)

\* Data not given due to improper filter selection.

SUMMARY OF TEST DATA FOR  $ZrO_2(A-N)-2MC$ 

Time (sec)	Surface Temperature (°F)		In Depth Temperature (°F)	Surface Radiation (BTU/ft <sup>2</sup> -sec)
	T <sub>SR</sub>	T <sub>TRUE</sub>		
100	4300	4590	3160	66
200	4300	4640	3160	99
300	4310	4370	3130	111
400	4320	4490	3160	111
500	4350	4700	3220	141
600	4400	4770	3300	141
1000	4600	4810	3340	156
1200	4600	4790	3250	146
1400	4600	4910	3310	174
1600	4610	4930	3400	176

Mach No. = 0.39  
 Supersonic Enthalpy = 3230 BTU/lb  
 Cold Wall Heat Flux = 545 BTU/ft<sup>2</sup>-sec  
 Stagnation Pressure = 1.06 atm.  
 \* = 0.57 (Surface)  
 \* = 1.00 (In Depth)

SUMMARY OF TEST DATA FOR  $ZrO_2(A-N)-3MC$ 

Time (sec)	Surface Temperature (°F)		In Depth Temperature (°F)	Surface Radiation (BTU/ft <sup>2</sup> -sec)
	T <sub>SR</sub>	T <sub>TRUE</sub>		
50	4440	4770	---	112
100	4430	4940	---	154
200	4490	5030	3010	210
300	4480	5020	3700	207
400	4480	5010	3700	204
500	4720	5040	3700	210
600	4600	5150	3740	220
1000	4630	5170	3760	236

Mach No. = 0.31  
 Supersonic Enthalpy = 1300 BTU/lb  
 Cold Wall Heat Flux = 440 BTU/ft<sup>2</sup>-sec  
 Stagnation Pressure = 1.06 atm.  
 \* = 0.57 (Surface)  
 \* = 1.00 (In Depth)

SUMMARY OF TEST DATA FOR  $ZrO_2(A-N)-4MC$ 

Time (sec)	Surface Temperature (°F)		In Depth Temperature (°F)	Surface Radiation (BTU/ft <sup>2</sup> -sec)
	T <sub>SR</sub>	T <sub>TRUE</sub>		
20	5020	5340	4420	484
33.3	5020	5340	---	484

Mach No. = 0.33  
 Supersonic Enthalpy = 4040 BTU/lb  
 Cold Wall Heat Flux = 610 BTU/ft<sup>2</sup>-sec  
 Stagnation Pressure = 1.07 atm.  
 \* = 0.57 (Surface)  
 \* = 1.00 (In Depth)

\* Temperature and radiation remained at steady-state values throughout test. At 33.3 seconds, sample melted through to hole.

SUMMARY OF TEST DATA FOR  $Mo-SiO_2-1Mc(I-1)-1MC$ 

Time (sec)	Surface Temperature (°F)		In Depth Temperature (°F)	Surface Radiation (BTU/ft <sup>2</sup> -sec)
	T <sub>SR</sub>	T <sub>TRUE</sub>		
40	3600	3090	3160	75
100	3600	3090	3600	78
200	3700	3940	3640	81
300	3900	4320	3600	100
400	4225	4600	3740	122
500	4300	4640	3795	132
600	4370	4910	3640	167
700	4700	5005	3990	203
1200	4760	5115	3990	214
1400	4800	5170	3920	232
1600	4800	5170	3900	230
1700	4840	5220	3975	230
1800	4840	5230	3990	230

Mach No. = 0.27  
 Supersonic Enthalpy = 3230 BTU/lb  
 Cold Wall Heat Flux = 425 BTU/ft<sup>2</sup>-sec  
 Stagnation Pressure = 1.06 atm.  
 \* = 0.57 (Surface)  
 \* = 1.00 (In Depth)

SUMMARY OF TEST DATA FOR  $Mo-SiO_2-1Mc(I-1)-2MC$ 

Time (sec)	Surface Temperature (°F)		In Depth Temperature (°F)	Surface Radiation (BTU/ft <sup>2</sup> -sec)
	T <sub>SR</sub>	T <sub>TRUE</sub>		
100	4110	4300	3625	117
200	4340	4545	3700	139
275	4400	4605	3740	160
300	4500	4970	3640	182
400	4500	4970	3740	174
500	4710	5040	3825	196
600	4870	5175	3900	222
700	4900	5110	3740	204
800	4940	5335	3810	204
1000	4840	5240	3760	200
1700	4920	5310	3760	204
1800	4920	5310	3600	204

Mach No. = 0.30  
 Supersonic Enthalpy = 1360 BTU/lb  
 Cold Wall Heat Flux = 505 BTU/ft<sup>2</sup>-sec  
 Stagnation Pressure = 1.06 atm.  
 \* = 0.57 (Surface)  
 \* = 1.00 (In Depth)

SUMMARY OF TEST DATA FOR  $Mo-SiO_2-1Mc(I-1)-3MC$ 

Time (sec)	Surface Temperature (°F)		In Depth Temperature (°F)	Surface Radiation (BTU/ft <sup>2</sup> -sec)
	T <sub>SR</sub>	T <sub>TRUE</sub>		
50	4600	5030	3040	204
200	4800	5170	3040	216
300	4820	5195	3010	222
400	4830	5205	3000	226
500	4940	5325	3000	236
1000*	5010	5410	3000	192
1200	4940	5335	3000	192
1300	5010	5415	4075	195
1400	4940	5335	4200	170
1500*	4900	5340	4200	190
1600	5130	5600	4000	190
1670	5240	5670	4000	203
1670**	5330	5795	5340**	216

Mach No. = 0.31  
 Supersonic Enthalpy = 1300 BTU/lb  
 Cold Wall Heat Flux = 510 BTU/ft<sup>2</sup>-sec  
 Stagnation Pressure = 1.06 atm.  
 \* = 0.57 (Surface)  
 \* = 1.00 (In Depth)

\* A sudden increase in temperatures and radiation accompanied by melting was observed at 1560 seconds.

\*\* Estimated values.

\*\*\* Minimum values used on data for I-23-14CA.

\*\*\*\* Minimum values used on data for I-23-14CB.

SUMMARY OF TEST DATA FOR  $Mo-SiO_2-1Mc(I-1)-4MC$ 

Time (sec)	Surface Temperature (°F)		In Depth Temperature (°F)	Surface Radiation (BTU/ft <sup>2</sup> -sec)
	T <sub>SR</sub>	T <sub>TRUE</sub>		
115	4450	4770	3400	160
200	4720	4970	3400	194
300	4940	5130	3400	230
400	4830	5195	3720	203
500	4940	5305	3630	227
600	4900	5305	3640	226
1000	4970	5395	3810	212
1200	4800	5345	3810	221
1300	4790	5310	3810	220
1710	4830	5475	3810	215
1800	4830	5475	3810	216

Mach No. = 0.31  
 Supersonic Enthalpy = 1640 BTU/lb  
 Cold Wall Heat Flux = 480 BTU/ft<sup>2</sup>-sec  
 Stagnation Pressure = 1.06 atm.  
 \* = 0.57 (Surface)  
 \* = 1.00 (In Depth)

TABLE 5

## ROVERS ARC FACILITY - CALORIMETER DATA AT MACH 3.2

TEST	ARC	ARC CURRENT (amps)	ARC VOLTAGE (volts)	ENTHALPY (BTU/lb)	AIR FLOW RATE (lb/sec)	PLENUM PRESSURE (mm Hg)	STATIC PRESSURE (mm Hg)
1	L.P.	1900	61.5	13800	0.0030	42	1.2
2	L.P.	2000	62.5	15100	0.0030	42	1.2
3	L.P.	2000	62.0	14700	0.0030	42	1.2
4	L.P.	2100	61.5	13800	0.0030	42	1.2
5	H.P.	1500	240.0	9600	0.0160	485	7.0
6	H.P.	1500	240.0	9200	0.0160	480	7.0
7	H.P.	1700	192.0	7300	0.0170	476	7.0
8	H.P.	1700	192.0	7300	0.0170	476	7.0

TEST	TRANSIENT CALORIMETER SHROUD DIAMETER (inch)	WATER CALORIMETER* 1.5 INCH SHROUD (BTU/ft <sup>2</sup> sec)	TRANSIENT, BTU/ft <sup>2</sup> sec CALORIMETER DIAMETER, inch			
			0.125	0.250	0.375	0.450
1	0.500	410	460	430	440	---
2	1.500	410	385	370	390	---
3	1.500	400	---	375	380	335
4	0.500	400	---	420	440	420
5	0.500	733	730	770	870	---
6	1.500	728	650	640	640	---
7	1.500	637	---	574	598	587
8	0.500	640	---	700	692	675

\*Diameter of water calorimeter equals 0.625 inches.

TABLE 6  
CHARACTERISTIC OPERATING CONDITIONS IN THE  
CAL WAVE SUPERHEATER

Gas Temperature = 7000°R

Pressure = 100 Atmospheres

Mach Number	2.0	3.0	6.0	12.0
Stagnation Pressure (atm)	60.0	12.0	0.9	0.04
Flux Product $(q(s)R)^{1/2}$ (BTU/ft $3/2$ sec)	800.0	400.0	100.0	18.0

TABLE 7  
HEAT TRANSFER RESULTS

	<u>Run No.</u>	<u>473</u>	<u>474</u>
$\frac{\Delta T}{\Delta t}$	Rate of Temperature Rise - deg. F/sec	780	880
$\delta$	Gage Thickness - in	0.1260	0.1265
T	Average Thermocouple Temp at Time of Reading - °F	360	350
c	Corresponding Specific Heat to T of Copper - BTU/lb - °F	0.096	0.096
$q_w$	Indicated Heat Transfer Rate - BTU/ft <sup>2</sup> -sec	440	485
$T_w$	Gage Surface Temp - °F	410	395
$i_w$	Gage Surface Enthalpy - BTU/lb	210	205
$i_s$	Total Enthalpy of Stream at Time of Reading - BTU/lb	1880	1870
$q_{cw}$	Cold Wall Heat Transfer Rate - BTU/ft <sup>2</sup> sec	495	545
$i_e$	Run Enthalpy - BTU/lb	2200	2180
$q_{cw}$	Cold Wall Heat Transfer Rate Corrected to Run Enthalpy - BTU/ft <sup>2</sup> sec	580	635

TABLE 8  
TEST CONDITIONS

<u>Run No.</u>	<u>473</u>	<u>474</u>
Rotor Total Pressure - atm	98.2	96.9
Total Temperature - °R	6740	6700
Total Enthalpy - BTU/lb	2200	2180
Tunnel Reservoir Pressure - atm	56.0	55.0
Test Section Stagnation Pressure on Model Nose - atm	1.15	1.15
Free Stream Mach Number	5.45	5.45
Free Stream Density - lbs/ft <sup>3</sup>	$8 \times 10^{-5}$	$8 \times 10^{-5}$
Free Stream Pressure - psi	0.65	0.64
Free Stream Velocity - fps	9700	9700

TABLE 9

WALL TEMPERATURE AND HEAT FLUX HISTORY FOR THE STAGNATION  
POINT OF A 0.500-INCH RADIUS HEMISPHERICAL NOSE WITH  
A THICKNESS OF 0.125 INCH

<u>Time</u>	<u>T<sub>w</sub> (°R)</u>	<u>q<sub>AERO</sub></u>	<u>-q<sub>RAD</sub></u>	<u>q<sub>NET</sub></u>
0	560	464.1	0.026	464.1
0.5	1090	431.8	0.370	431.4
1.0	1302	418.9	0.753	418.1
1.5	1481	408.0	1.26	406.7
2.0	1650	397.7	1.94	395.7
2.5	1814	387.7	2.83	384.9
3.0	1972	378.0	3.96	374.1
3.5	2126	368.6	5.35	363.3
4.0	2274	358.4	7.01	351.4
4.5	2417	348.3	8.93	339.3
5.0	2554	338.5	11.14	327.3
6.0	2813	320.0	16.39	303.6
7.0	3051	303.0	22.7	280.3
8.0	3269	287.4	29.9	257.5
9.0	3468	273.3	37.9	235.4
10.0	3648	259.8	46.4	213.4
11.0	3808	246.3	55.0	191.3
13.0	(4146)*			(146)*
15.0	(4405)*			(96)*

\* Estimated by hand calculations.

TABLE 10

WALL TEMPERATURE AND HEAT FLUX HISTORY FOR THE STAGNATION  
POINT OF A 0.250-INCH RADIUS HEMISPHERICAL NOSE WITH  
A THICKNESS OF 0.125 INCH

<u>Time</u>	<u>T<sub>w</sub>(°R)</u>	<u>q<sub>AERO</sub></u>	<u>-q<sub>RAD</sub></u>	<u>q<sub>NET</sub></u>
0	560	653.0	0.026	653.0
0.5	1293	593.1	0.732	592.4
1.0	1576	568.7	1.62	567.1
1.5	1812	548.4	2.82	545.6
2.0	2032	529.4	4.47	524.9
3.0	2441	490.1	9.29	480.8
3.5	2629	471.0	12.5	458.5
4.0	2808	453.0	16.3	436.7
4.5	2978	435.8	20.6	415.2
5.0	3139	419.6	25.4	394.2
6.0	3434	389.8	36.4	353.4
7.0	3695	361.8	48.8	313.0
8.0	3919	335.0	61.8	273.3
9.0	4113	311.9	74.9	237.0
10.0	4279	292.1	87.8	204.3
11.0	4421	275.2	100.0	175.2
12.0	(4576)*			(140)*
13.0	(4700)*			(112)*
14.0	(4800)*			(82)*
15.0	(4872)*			(67)*

\* Estimated by hand calculation.



UNCLASSIFIED

Security Classification

## DOCUMENT CONTROL DATA - R &amp; D

(Security classification of title, body of abstract and indexing annotation must be entered when the overall report is classified)

1. ORIGINATING ACTIVITY (Corporate author)		2a. REPORT SECURITY CLASSIFICATION	
ManLabs, Inc. 21 Erie Street Cambridge, Massachusetts 02139		UNCLASSIFIED	
2. REPORT TITLE		2b. GROUP	
Stability Characterization of Refractory Materials under High Velocity Atmospheric Flight Conditions, Part II Volume III: Facilities and Techniques Employed for Hot Gas/Cold Wall Tests		N/A	
3. DESCRIPTIVE NOTES (Type of report and inclusive dates)			
Technical Documentary Report, April 1966 to July 1969			
4. AUTHOR(S) (First name, middle initial, last name)			
Larry Kaufman Harvey Nesor			
5. REPORT DATE		7a. TOTAL NO. OF PAGES	7b. NO. OF REFS
September 1969		122	27
6a. CONTRACT OR GRANT NO.		6b. ORIGINATOR'S REPORT NUMBER (if)	
AF33(615)-3859		N/A	
6c. PROJECT NO.		6d. OTHER REPORT NO(S) (Any other numbers that may be assigned this report)	
7312 Task 731201 7350 Tasks 735001 and 735002		AFML-TR-69-84, Part II Volume III	
10. DISTRIBUTION STATEMENT			
This document is subject to special export controls and each transmittal to foreign governments or foreign nationals may be made only with prior approval of the Air Force Materials Laboratory (MAMC), WPAFB, Ohio 45433.			
11. SUPPLEMENTARY NOTES		12. SPONSORING MILITARY ACTIVITY	
N/A		Air Force Materials Laboratory (MAMC) Air Force Systems Command Wright-Patterson Air Force Base, Ohio	
13. ABSTRACT			
<p>This report deals with facilities and techniques employed for performing HG/CW tests in the Model 500, ROVERS and Ten Megawatt Arc installations at Avco and the Wave Superheater at Cornell. Stagnation pressures between 0.002 and 4.0 atm, stagnation enthalpy between 2000 and 16,000 BTU/lb, cold wall heat flux between 100 and 1500 BTU/ft<sup>2</sup>sec and exposure times between 20 and 23,000 seconds were employed. Diagnostic measurements included continuous recording of surface temperature and radiated heat flux. Color motion picture coverage was also provided. Although most of the testing was performed on flat faced right circular cylinders some hemispherical capped samples and some pipes were also tested.</p> <p>In depth temperature measurements were performed in the Model 500 and ROVERS facilities. A micro-optical pyrometer was employed to measure the temperature at the base of a cavity drilled from the rear of the model to within 0.100 inch of the heated face. For oxide forming materials like ZrB<sub>2</sub> and Hf-Ta-Mo, the temperature at the in-depth station was found to range from 500° to 1900°R lower than the surface temperature.</p> <p>This abstract is subject to special export controls and each transmittal to foreign governments or foreign nationals may be made only with prior approval of the Air Force Materials Laboratory (MAMC), Wright-Patterson Air Force Base, Ohio 45433.</p>			

DD FORM 1473

REPLACES DD FORM 1473, 1 JAN 60, WHICH IS OBSOLETE FOR ARMY USE.

UNCLASSIFIED

Security Classification

UNCLASSIFIED

Security Classification

14. KEY WORDS	LINK A		LINK B		LINK C	
	ROLE	WT	ROLE	WT	ROLE	WT
oxidation						
refractory borides						
graphites						
JT composites						
hypereutectic carbide-graphite composites						
refractory metals						
coated refractory metals						
metal oxide composites						
iridium coated graphites						
high velocity atmospheric flight						
facilities						
techniques						
Model 500						
ROVERS						
Ten Megawatt Arc						
Wave Superheater						

UNCLASSIFIED

Security Classification